Ingredients for blocking in a dry dynamical atmospheric model

Master's thesis

to obtain the Master of Science degree in *Climate Physics: Meteorology and Physical Oceanography*

Faculty of Mathematics and Natural Sciences
Christian-Albrechts-Universität zu Kiel

submitted by
Swantje Bastin
Matriculation number: 1005538

Supervisor: Prof. Dr. Richard J. Greatbatch
Second assessor: Dr. Gereon Gollan

April 30, 2018

Abstract

Using the Portable University Model of the Atmosphere (PUMA), a dry, spectral, primitive equation atmospheric model, the influence of idealised orography and tropospheric heating anomalies on Northern Hemisphere winter blocking is investigated. By means of sensitivity experiments, the impact of several atmospheric features and phenomena on blocking is separately examined, which is difficult to achieve with, for example, reanalysis data. The analysis is carried out in two parts: first, the contributions of mid-latitude orography and continent-ocean heat contrasts to blocking are studied, followed by an investigation of blocking changes due to tropical heating anomalies, including idealised tropical heating based on the El Niño/Southern Oscillation (ENSO), the Madden-Julian Oscillation (MJO) and the tropical precipitation bias of the Coupled Model Intercomparison Project Phase 5 (CMIP5) models.

Orography is found to be necessary for mid-latitude blocking in the model to occur, because it forces stationary planetary waves that disrupt the westerly mean flow and form jet exit regions where blocking can be maintained against zonal advection. A mid-latitude continent-ocean heating dipole causes a strengthening of the synoptic-scale activity in the jet stream, which does not lead to blocking on its own, but can, in combination with orography, strongly enhance mid-latitude blocking downstream of its location.

Generally, a negative tropical heating anomaly is found to impact mid-latitude blocking more than a positive heating anomaly of the same amplitude. The negative heating leads to reduced mid-latitude blocking at the longitude of the heating and increased mid-latitude blocking west of the longitude of the heating. For El Niño, increased high-latitude blocking over Siberia and Greenland and slightly reduced mid-latitude blocking over the Pacific and Europe is found; whereas La Niña is associated with reduced high-latitude blocking over Siberia and increased (decreased) mid-latitude blocking over the Atlantic and Europe (the Pacific). MJO phase 2 leads to a weak increase (decrease) of high-latitude blocking over Greenland (Siberia), and MJO phase 6 is associated with strongly increased high-latitude blocking over Siberia and Greenland as well as strongly increased European-Atlantic mid-latitude blocking. Tropical heating based on the CMIP5 multi-model mean precipitation bias leads to reduced (increased) high-latitude blocking over Greenland (Siberia), and to strongly reduced mid-latitude blocking over Europe, Atlantic and Pacific, offering a possible explanation for the tendency to find reduced blocking in these models compared to observations, especially over the Atlantic and Europe.

Zusammenfassung

Mit dem *Portable University Model of the Atmosphere* (PUMA), einem spektralen Atmosphärenmodell ohne Feuchtigkeit, wird der Einfluss von idealisierten Orografie- und Wärmeanomalien auf atmosphärische Blockierung im borealen Winter auf der Nordhalbkugel untersucht. Anhand von Sensitivitätsexperimenten wird die Auswirkung verschiedener atmosphärischer Merkmale und Phänomene auf atmosphärische Blockierung getrennt voneinander analysiert, was etwa mit Reanalysedaten schwierig ist. Die Arbeit beinhaltet zwei Teile: Zunächst wird die Bedeutung von Orografie und Kontinent-Ozean-Wärmekontrasten in mittleren Breiten für Blockierung untersucht, gefolgt von einer Analyse des Einflusses tropischer Wärmeanomalien, angelehnt an ENSO, die MJO und den tropischen Niederschlagsfehler der CMIP5-Modelle.

Orografie erweist sich als notwendig für das Auftreten von Blockierung in mittleren Breiten, denn durch Erhebungen werden stationäre planetare Wellen angeregt, die die mittlere westliche Strömung schwächen oder unterbrechen können. In Regionen mit schwacher westlicher Strömung kann dann Blockierung auftreten und gegen zonale Advektion aufrechterhalten werden. Ein Kontinent-Ozean-Wärmedipol führt zu verstärkter synoptischer Aktivität im Jetstream, was für sich allein keine Blockierung ermöglicht, allerdings in Kombination mit Orografie für deutlich vermehrtes Auftreten von Blockierung in mittleren Breiten sorgen kann.

Allgemein ist der Einfluss einer negativen tropischen Wärmeanomalie auf atmosphärische Blockierung in mittleren Breiten deutlicher ausgeprägt als der einer gleich starken positiven Wärmeanomalie. Die negative Anomalie führt zu einer Verringerung der Blockierung in mittleren Breiten direkt nördlich von ihrer Position, und nordwestlich zu einem Anstieg. El Niño geht mit vermehrter Blockierung in hohen Breiten und leicht verringerter Blockierung in mittleren Breiten einher, während La Niña zu verringerter Blockierung in hohen Breiten über Sibirien und zu vermehrter (verringerter) Blockierung in mittleren Breiten über dem Atlantik und Europa (dem Pazifik) führt. Die 2. Phase der MJO ist verbunden mit einem schwachen Anstieg (Abfall) der Blockierung in hohen Breiten über Grönland (Sibirien), die 6. Phase der MJO dagegen mit stark vermehrter Blockierung in hohen Breiten sowie über dem Atlantik und Europa in mittleren Breiten. Tropische Erwärmung angelehnt an den mittleren Niederschlagsfehler der CMIP5-Modelle führt zu verringerter (vermehrter) Blockierung in hohen Breiten über Grönland (Sibirien) und zu stark verringerter Blockierung in mittleren Breiten über Europa, dem Atlantik und dem Pazifik, was eine Erklärungsmöglichkeit für die Tendenz dieser Modelle zu verringerter Blockierung aufzeigt.

Contents

1. Introduction

Atmospheric blocking is an important feature of mid-latitude circulation, because of its influence on the jet stream path and its thus potentially severe impact on surface weather conditions. The phenomenon arises from a complex system of dynamical interactions between the westerly mean flow, stationary planetary waves and transient baroclinic eddies. Since there are many parameters that have an influence on the occurrence and persistence of blocking, it is not trivial to simulate blocking correctly: climate models still exhibit biases in blocking frequencies. In this thesis, the response of Northern Hemisphere winter atmospheric blocking to changes in different parameters is investigated in the framework of a simplified dry dynamical atmospheric model.

The following sections comprise a portrayal of the blocking phenomenon (Section 1.1) including a qualitative description, a review of theories concerning blocking dynamics, and an overview of the impact of blocking on surface weather; a description of how blocking is influenced by the circulation and mean state in the tropics (Section 1.2); and, finally, a section about the questions to be investigated in this thesis (Section 1.3).

1.1. Atmospheric blocking

The circulation in the mid-latitudes is, in both hemispheres, characterised by westerly winds that become stronger with height until they reach a maximum at about 200 hPa. These westerly wind maxima, called jet streams, are located on average around 30–35°N/S in the winter hemisphere and shifted to 40–45°N/S in the summer hemisphere. Their location and strength is a direct consequence of the thermal wind balance and the vertical distribution of the temperature difference between equator and poles (cf. e. g. Gill, 1982, p. 587; Holton, 1992, pp. 142–148). However, especially in the Northern Hemisphere, the climatological path of the jet stream exhibits large deviations from zonal symmetry, due to stationary planetary waves forced by orography (particularly the Himalayas and the Rocky Mountains) and continent-ocean heat contrasts (Holton, 1992, pp. 142, 220, 346). The latter are particularly important in Northern Hemisphere winter, when the meridional temperature gradients between land and ocean become very strong and lead to large vertical shear in the jet stream over the eastern coasts of Asia and North America (Holton, 1992, p. 346).

There are two main regions where the Northern Hemisphere climatological jet stream is intensified due to the orography and heat contrasts: above the east coast of the Asian continent extending over the western Pacific, and above the east coast of the North American continent extending over the western Atlantic (cf. e. g. Holton, 1992, p. 146).

Embedded in the westerly jet stream are travelling, baroclinically unstable storm systems whose growth and decay are closely related to the jet stream path and intensity. Their growth is sustained by available potential energy from the background flow through the process of baroclinic instability, and they are responsible for a significant fraction of the mid-latitude poleward heat transport, comparable in magnitude to the heat transport due to the stationary waves (cf. Lau, 1979; and Gill, 1982, p. 588). The storm systems usually develop in the regions where the jet stream intensifies, grow while being advected along the intense jet cores over the western Pacific and Atlantic oceans, and decay in the jet exit regions where the jet stream broadens and weakens (Gill, 1982, p. 591; and Holton, 1992, p. 347). Thus, the typical paths of the travelling cyclones, the Northern Hemisphere storm tracks, closely follow the location of the intensified jets over the Pacific and Atlantic oceans. Due to the prevailing westerly winds, the synoptic-scale storm systems cause mild temperatures at the western coasts of Europe and North America. Additionally, they are associated with moisture transport and convective motions leading to regions of enhanced precipitation along the storm tracks (Lohmann et al., 2016, p. 278).

The term *atmospheric blocking* describes a situation in which the usual mid-latitude westerly flow and the westerly progression of the embedded synoptic-scale weather systems is blocked by a large-scale quasi-stationary high pressure anomaly poleward of the climatological location of the jet stream, often accompanied by a split in the jet stream and a region of reversed zonal flow. Due to its large impact on the mid-latitude circulation and surface weather, atmospheric blocking has been an object of interest for meteorologists since the mid-1940s, when e. g. Namias (1947) investigated atmospheric blocking leading to the anomalies in Northern Hemisphere surface weather during the winter of 1946/1947, Berggren et al. (1949) attempted to give a characteristic description of the process of blocking development and Rex (1950a,b) gave the first blocking definition and climatology.

In the following sections, an overview of the current knowledge on atmospheric blocking is given, starting with a qualitative description of the phenomenon and its variety in appearance in Section 1.1.1. The dynamics of blocking onset, maintenance and decay are discussed in Section 1.1.2, followed by a description of the impact that atmospheric blocking can have on surface weather in Section 1.1.3.

1.1.1. Description and observation of blocking

Although atmospheric blocking occurs in both hemispheres, it is much more frequent and also more persistent in the Northern Hemisphere. There, in turn, the blocking frequency (i. e. fraction of the time when a blocking event is present) is highest in boreal winter and early spring (Tibaldi and Molteni, 2018). In all seasons, the Northern Hemisphere blocking frequency exhibits strong interannual variability on time scales between five and ten years (D'Andrea et al., 1998). In Figure 1.1, the winter blocking frequency climatology in the Northern Hemisphere is shown, calculated from combined data from the ERA-40 and the ERA-Interim reanalysis datasets (for details see Gollan and Greatbatch, 2017). Four regions of enhanced blocking frequency stand out – two at higher latitudes over Siberia and Greenland, and two regions at mid-latitudes over the eastern Atlantic/Europe and, though not so clear, over the eastern Pacific. The high-latitude blocking diverts the westerly flow from its usual climatological path rather than actually blocking the westerly flow and the embedded storm systems, because it is not located in the jet stream path (Woollings et al., 2008).

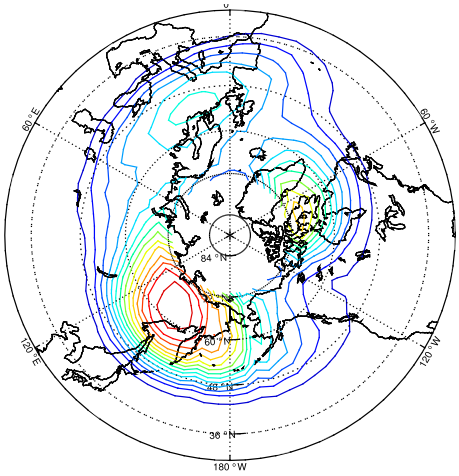

Figure 1.1.: Northern Hemisphere DJF (December, January, February; for a list of abbreviations see Table A.2 in the appendix) blocking frequency climatology from a combined ERA-40/ERA-Interim reanalysis dataset. Contours are drawn every 5 %. The figure is taken from Gollan and Greatbatch (2017).

Mid-latitude blocking episodes are generally characterised by a large-scale quasi-stationary anticyclone north of the climatological position of the jet stream that either divides the jet stream into two branches or diverts its path towards the north around the region of anomalously high pressure. In the first case, the blocking anticyclone is often accompanied by a smaller cyclone to the south, which is often described as a *dipole block*. In the second case, the resulting characteristic shape of the jet stream flowing northward around the high pressure anomaly and then southward again has given rise to the term *omega block* (Pelly and Hoskins, 2003; Barriopedro et al., 2006; Tibaldi and Molteni, 2018). Interestingly, the two mid-latitude blocking regions over

the eastern Pacific and the eastern Atlantic differ in their relative frequency of occurrence of dipole and omega blocks: Atlantic blocking preferably shows the dipole form, whereas Pacific blocking more often resembles an omega block (Pelly and Hoskins, 2003). The region of the high pressure anomaly usually experiences stagnant winds, to the south the flow can even become easterly (Tibaldi and Molteni, 2018). On both sides of the blocking anticyclone, the circulation is forced into a strongly meridional state, which leads to anomalous exchange of warm air from lower latitudes and cold air from higher latitudes (cf. e. g. Antokhina et al., 2018).

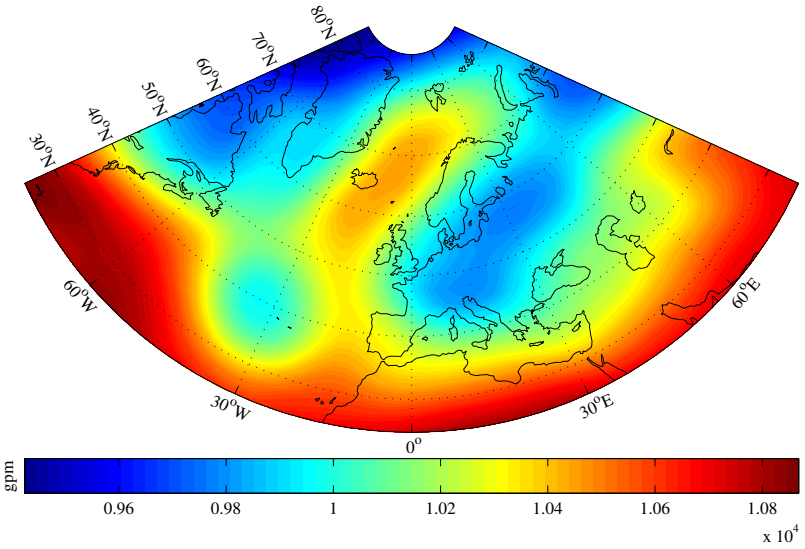

Figure 1.2.: Geopotential height field at 250 hPa from February 27, 2018, 00:00 UTC. The data shown is from the National Centers for Environmental Prediction/National Center for Atmospheric Research (NCEP/NCAR) reanalysis, taken from *https://www.esrl.noaa.gov/psd/* (Kalnay et al., 1996; Kistler et al., 2001).

In Figures 1.2 and 1.3, a recent blocking event over the Atlantic and western Europe can be seen. Figure 1.2 shows the geopotential height on the 250 hPa isobaric surface, Figure 1.3 the 250 hPa wind field on February 27, 00:00 UTC. Both fields clearly show the blocking anticyclone over the eastern North Atlantic that extends from north of Norway to northern Spain. South of the high pressure anomaly, centred at approximately 40°N and 30°W, there is a smaller cyclonic structure visible, making this blocking event a typical Atlantic/European dipole blocking as described above. The wind field clearly shows the division of the jet stream into a northern and a southern part, with stagnant winds in the region of the blocking anticyclone. This blocking event was accompanied by very cold temperatures in large parts of northern and central Europe (see Figure 1.4), due to the persistent north-easterly inflow of cold arctic air, which is also typical for an Atlantic/European blocking in winter or early spring (see Section 1.1.3 for more details on the influence of blocking on the surface weather).

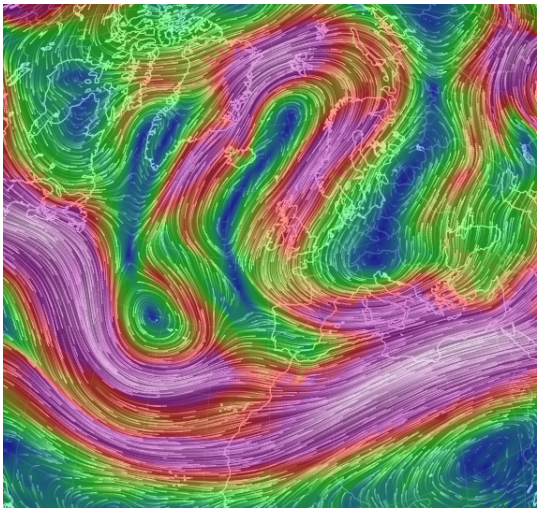

Figure 1.3.: Wind field at 250 hPa from February 27, 2018, 00:00 UTC. Blue colour shading indicates lowest wind speed, higher wind speeds are represented by green, red and pink in ascending order. (The graphics is taken from *https://earth.nullschool.net*, the wind data orginates from the Global Forecast System (GFS) of the National Oceanic and Atmospheric Administration (NOAA).)

There is some variation in the temporal persistence as well as the spatial extent of blocking episodes. However, there is general agreement that blocking exceeds the typical dimensions of synoptic-scale disturbances both temporally and spatially, hence the often used terminology 'large-scale quasi-stationary' when blocking is described (e. g. Tibaldi and Molteni, 2018). Blocking indices that are used to identify blocking episodes (see Section 2.3 for more details) mostly require a minimum longitudinal extent between 12° and 20° and a minimum duration of four to five days in order for an anomalous high pressure region poleward of the jet stream to be classified as blocking (Barnes et al., 2012). The number of blocking episodes decreases approximately exponentially with increasing persistence (D'Andrea et al., 1998; Barriopedro et al., 2006). The average persistence time of a blocking episode is about one week, whereas the longest episodes can reach a duration of three to four weeks (e. g. Barriopedro et al., 2006; Davini and D'Andrea, 2016; and Tibaldi and Molteni, 2018).

1.1.2. Blocking dynamics

The fixed location of regions where blocking preferably occurs suggests a strong dependence of blocking on the stationary planetary wave structure that develops in the Northern Hemisphere as a response to orography and land-ocean temperature contrasts (cf. Section 1.1). Therefore, some theories of blocking dynamics have tried to explain blocking occurrence, stationarity and persistence as a result of stationary planetary wave amplification (Tibaldi and Molteni, 2018).

However, there is often no coincidence between Atlantic and Pacific blocking episodes. This indicates that blocking cannot simply be due to occasional hemispheric amplifications of the stationary wave pattern, but that a dynamical explanation of blocking must account for the regional independence of the phenomenon (Tibaldi and Molteni, 2018). Rossby (1950) connected the development of blocking to a hydraulic jump in the jet stream, i. e. a sudden transition from westerly wind speeds faster than the gravity wave speed to wind speeds below the gravity wave speed. He calculated that the cross section of the jet stream must at least double in order to produce a hydraulic jump with vanishing or even eastward propagation velocity, thus giving rise to a 'retrograde blocking wave'. A widening of the jet and associated decrease of westerly wind speed is indeed present in the jet exit regions over the Atlantic and Pacific oceans, where the blocking regions are located. The theory is also consistent with the enhanced blocking frequency in Northern Hemisphere winter, when the temperature contrasts between continents and oceans become larger and cause a further intensification of the two jet stream maxima upstream of the blocking regions (cf. Section 1.1).

There is more to blocking, however, than Rossby's idealised theory can explain. Vautard and Legras (1988) also showed that blocking can occur wherever the jet stream has a local intensification and a following weakening, but that a large contribution to blocking in those regions comes from the non-linear feedback of baroclinic eddies which acts to maintain blocking structures against dissipation. The importance of baroclinic eddies for blocking amplification and maintenance has also been shown by several other studies (e. g. Illari and Marshall, 1983; Shutts, 1983; Haines and Marshall, 1987). Blocking and the maintaining feedbacks with baroclinic eddies become very accessible when described in a potential vorticity (PV) framework, as proposed by e. g. Hoskins et al. (1985). As Pelly and Hoskins (2003) put it, 'the essence of the formation of a block is that a substantial mass of subtropical air, with its low PV on a θ [potential temperature] surface, is advected poleward ahead of a large amplitude slow moving cyclone. As a PV anomaly, this air develops its own anticyclonic circulation and cuts off from its region of origin. It then influences the upstream weather systems to elongate meridionally and deposit more low PV air on the poleward side and high PV air on the equatorward side, thereby acting to reinforce the block.'

More recently, some studies have connected the poleward advection of low PV air that is responsible for blocking onset with upper tropospheric Rossby wave breaking that occurs north or south of the jet stream due to the strong meridional shear of zonal velocity. Altenhoff et al. (2008) demonstrated that Northern Hemisphere winter blocking events are associated with enhanced synoptic-scale Rossby wave breaking before their onset and during their entire lifetime. According to Tyrlis and Hoskins (2008) and Weijenborg et al. (2012), mid-latitude Atlantic/European blocking is (in boreal winter) preferentially associated with anticyclonic Rossby wave breaking, whereas mid-latitude Pacific blocking is more often preceded by cyclonic wave breaking. Woollings et al. (2008) also established a connection between high-latitude Northern Hemisphere

winter blocking and upper tropospheric Rossby wave breaking.

Despite the number of studies on different aspects of blocking dynamics, no unified dynamical description of blocking has been agreed on so far (cf. e. g. Weijenborg et al., 2012; and Tibaldi and Molteni, 2018). This is probably due to the complexity of the blocking phenomenon because of its many interactions, some of them highly non-linear, with atmospheric processes on a broad range of temporal and spatial scales. Nonetheless, the importance of some features of the Northern Hemisphere circulation for blocking is reasonably certain. The shape of the jet stream, which is determined by stationary planetary scale waves, sets the regions where blocking is possible; this is especially true for mid-latitude blocking that preferably occurs in regions where the jet stream broadens and weakens after an intense maximum. Blocking onset can then be initiated by poleward advection of low potential vorticity air, in many cases due to upper tropospheric Rossby wave breaking. The non-linear interaction of the blocking structure and the surrounding flow field with synoptic-scale baroclinic eddies acts to maintain the block against dissipation and downstream advection, leading to the long time scales of blocking compared to synoptic-scale storm systems (cf. Tibaldi and Molteni, 2018).

1.1.3. Influence of blocking on surface weather

Through its blocking of the westerly flow and the obstruction of the usual progression of synoptic-scale weather systems, atmospheric blocking can have a large impact on surface weather. Blocking events affect temperature and precipitation as well as air quality, and since their lifetime can in extreme cases be as long as several weeks, those anomalies can become quite severe, resulting in 'catastrophic impacts on society' (Barnes et al., 2012). The sign and intensity of the weather anomalies depend on both the location of the affected region relative to the blocking anticyclone and the season (e. g. Tibaldi and Molteni, 2018). In the case of a summer European blocking, for example, the 'massive high covering [Europe] deflects the extratropical frontal systems northward and suppresses the local convective instabilities, leading to light winds, dryness, clear skies, and warming' (Cassou et al., 2005). Regions to the north or south of the blocking anticyclone, however, suddenly lie in the path of the shifted jet stream and the storm systems and thus experience rather opposite anomalies.

In Northern Hemisphere summer, it has been shown that blocking has contributed to or been responsible for several heat waves, for example the European heat wave in the summer of 2003 (Black et al., 2004) and the heat wave in eastern Europe and western Russia in the summer of 2010 (Dole et al., 2011; Matsueda, 2011), both of which caused anomalously high death rates in the impacted regions. Cassou et al. (2005) showed that European summer blocking is associated with an anomalously high number of extreme warm days in station-based temperature and reanalysis data from 1950–2003.

In Northern Hemisphere winter, the deflection of weather systems and lack of convective instabilities due to a blocking anticyclone lead to dry and unusually cold conditions in the region of the stationary high pressure system, because the clear skies allow for radiative cooling. Additionally, regions to the east of the blocking anticyclone experience inflow of cold air from the northeast (Sillmann et al., 2011). Two examples for large negative temperature anomalies associated with winter blocking events are the winter of 1946/1947, described by Namias (1947), and the winter of 1962/1963 with very cold temperatures over western Europe, described by Dent (2013) and Greatbatch et al. (2015). Buehler et al. (2011) analysed ERA-40 reanalysis data, showing that winter blocking over the Atlantic-European region is associated with colder and drier conditions than usual in central and eastern Europe, but warmer and wetter conditions in southern Europe. As described in Section 1.1.1, Atlantic/European blocking often exhibits a dipole structure with a cyclone south of the blocking anticyclone, causing these reversed weather anomalies to the south of the blocking region. Confirming the results of Buehler et al. (2011), Sillmann et al. (2011) also showed that North Atlantic winter blocking is connected to extreme minimum temperatures over Europe in ERA-40 reanalysis data and additionally in ECHAM5/MPI-OM global climate model simulations. The very recent Atlantic/European winter blocking from February 2018 shown in Figures 1.2 and 1.3 was also accompanied by unusually cold temperatures in large parts of Europe, as can be seen in Figure 1.4.

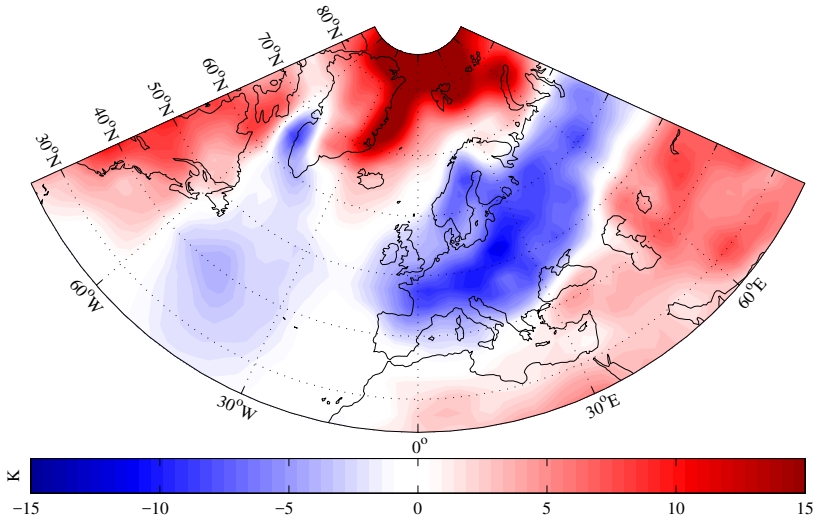

Figure 1.4.: Surface temperature anomaly from February 23 to February 28, 2018, relative to climatological February surface temperature between 1948 and present. The data shown is from the NCEP/NCAR reanalysis, taken from *https://www.esrl.noaa.gov/psd/* (Kalnay et al., 1996; Kistler et al., 2001).

Beside surface temperature and precipitation anomalies, atmospheric blocking can also lead to the accumulation of pollutants, e. g. tropospheric ozone in summer and particulate matter in winter (Tibaldi and Molteni, 2018), because of low wind speeds

in the blocking region and, in winter, very stable temperature stratification due to the strong surface cooling associated with winter blocking. For example, Gangoiti et al. (2002) described the connection between high tropospheric ozone concentrations in the Basque Country in June 1996 and a European blocking event.

1.2. Tropical influence on blocking

Since the circulation in the tropics influences the mid-latitude circulation, it is little surprising that also blocking is affected by tropical variability. Gollan et al. (2015), for example, demonstrated that interannual to decadal mid-latitude blocking frequency variability in the European Centre for Medium Range Weather Forecasts' (ECMWF) global forecast model (IFS) is substantially improved when the model is relaxed towards ERA-40 reanalysis data between 20°S and 20°N.

Two very important modes of tropical variability are the El Niño/Southern Oscillation (ENSO) that varies on an interannual time scale of two to five years (described extensively by Philander, 1990), and the Madden-Julian Oscillation (MJO) that is the dominant tropical mode of variability on intraseasonal time scales with a period of 30 to 80 days (e. g. Wheeler and Hendon, 2004). Especially ENSO, but also the MJO, are important for seasonal predictability, because they globally impact the circulation through large-scale teleconnection patterns.

The influence of ENSO on Northern Hemisphere winter blocking over the Pacific has been investigated by several studies. According to Renwick and Wallace (1996), blocking occurs less frequently over the North Pacific in El Niño winters and more frequently in La Niña winters. They connect this at least partially to the impact of the ENSO phase on the Pacific North American (PNA) pattern – El Niño is associated with a positive PNA (characterised by negative height anomalies over the North Pacific, positive over North America) which in turn is connected to stronger zonal flow over the Pacific and thus less favourable for North Pacific blocking. The inverse relation applies for La Niña, although the response is not exactly linear. Barriopedro et al. (2006) confirmed the results of Renwick and Wallace (1996), but stated that the changes in North Pacific blocking frequencies are due to changes in persistence of the blocking rather than changes in the number of blocking episodes. They also found a westward displacement of North Pacific blocking during La Niña and an eastward displacement during El Niño.

As also noted by Gollan and Greatbatch (2017), the results of Renwick and Wallace (1996) and Barriopedro et al. (2006) are somewhat contradicted by results from Hinton et al. (2009) who examined the connection between tropical sea surface temperatures (SSTs), tropical rainfall and winter North Pacific blocking in the Met Office's coupled climate model (HadGEM1) and observations. They found that a negative

SST bias in the eastern equatorial Pacific leads to a decrease in Pacific blocking frequency, contrary to the increase in Pacific blocking found by the earlier studies in La Niña winters. However, Hinton et al. (2009) also found that a positive bias in Indonesian rainfall and a positive SST bias around the Maritime Continent both lead to an increase in Pacific blocking. Since these anomalies are also associated with La Niña, Hinton et al. (2009) concluded that the overall impact of the ENSO phase on Pacific blocking depends on the relative magnitude of the anomalies in the two regions. Interestingly, Gollan and Greatbatch (2017) also found increased high-latitude North Pacific blocking frequencies associated with El Niño (decreased blocking frequencies with La Niña) in both reanalysis data and model experiments, which is more in line with the findings of Hinton et al. (2009) than those of Renwick and Wallace (1996). Additionally to the increase in blocking in the central and eastern Pacific, there is a decrease of blocking over East Asia and the western Pacific during El Niño in the results of Gollan and Greatbatch (2017). The pattern indicates an eastward shift of the blocking region, which is consistent with Barriopedro et al. (2006).

Whereas Renwick and Wallace (1996) and Barriopedro et al. (2006) only examined the response of North Pacific blocking to ENSO, Gollan and Greatbatch (2017) analysed ENSO related winter blocking frequency changes for the entire Northern Hemisphere. For El Niño, they found strongly decreased blocking freqencies at high latitudes over northern Canada and Greenland, and decreased blocking over the Asian continent. No clear signal is found over Europe. For La Niña, their results showed slightly enhanced blocking over northern Canada and Greenland, reduced blocking over northern Europe and the Atlantic and a small increase of blocking frequency over central Europe.

The influence of the MJO on Northern Hemisphere winter blocking has only recently been explored in some detail. Cassou (2008) found an increase in Scandinavian blocking directly after MJO phase 6 (MJO phases 1–4 are characterised by increased convection over the Indian Ocean and decreased convection over the western Pacific, phases 5–8 by the reversed pattern; for a more detailed definition of the eight MJO phases see Wheeler and Hendon, 2004). Henderson et al. (2016) examined the influence of all MJO phases on Northern Hemisphere winter blocking in reanalysis data. They found decreased blocking over the Pacific, the Atlantic and Europe during and after phase 1–4. Following phase 6–8, they detected a strong increase in Atlantic and European blocking. The strongest increase in European blocking was found by Henderson et al. (2016) after MJO phase 6, which is consistent with the earlier results of Cassou (2008). Gollan and Greatbatch (2017) carried out a similar analysis as Henderson et al. (2016), but extended it by using model simulations as well as reanalysis data. They also found decreased blocking frequencies, especially over the Pacific and northern Canada, after early MJO phases (1–4) and increased blocking frequencies, especially over the Atlantic and Europe, after late MJO phases (5–8).

1.3. Motivation and research question

As discussed in the previous sections, atmospheric blocking is an important part of the mid-latitude circulation variability, because, first, it can have such a large impact on surface weather conditions and thus on society, and second, its relatively long time scales might provide valuable prediction skill on those time scales, given that blocking could be adequately well simulated by forecast models. This is not always the case, though – especially coupled climate models still exhibit significant biases in blocking frequency and persistence. There have been several studies on the representation of Northern Hemisphere blocking in the coupled general circulation models (CGCMs) participating in the latest phase of the Coupled Model Intercomparison Project (CMIP, see Meehl et al., 2000). Although some individual models simulate blocking quite realistically, the majority of the tested models still underestimate blocking frequency and duration in most blocking regions in the Northern Hemisphere (cf. Anstey et al., 2013; Dunn-Sigouin and Son, 2013; Masato et al., 2013; and Davini and D'Andrea, 2016).

It has been found that blocking biases can be reduced by increasing the horizontal resolution (e. g. Jung et al., 2012; and Berckmans et al., 2013) or by removing biases in the mean state (Scaife et al., 2010). Both Scaife et al. (2010) and Berckmans et al. (2013) note, though, that an increase in resolution leads to improved blocking simulations partly because of the improvement of the mean state that is associated with the resolution increase. Errors in the mean state thus seem to be a rather large contributor to the blocking bias. However, especially over Europe increased horizontal resolution also reduces the blocking bias by allowing for a higher contribution of transient eddy momentum forcing to blocking (Berckmans et al., 2013).

The work that is presented in this thesis provides some insight into the essential ingredients that are necessary to simulate blocking in a simplified dry atmospheric model. Beside this general investigation, special focus is laid onto the influence of tropical heating on blocking in middle and high latitudes, since it has been found that the tropical circulation and mean state are important for a realistic simulation of blocking frequencies. The impact of different parameters and different tropical heating regions on Northern Hemisphere winter blocking is separately analysed in several sensitivity experiments. These separate experiments, done in a simplified model setup, help to clarify connections between blocking and individual phenomena that can be difficult to disentangle in observations and coupled climate model simulations due to the large amount of processes and non-linear interactions that contribute to blocking. Experiments include setups based on important modes of tropical variability (ENSO and MJO) as well as tropical rainfall biases in CMIP5 models.

The remaining parts of the thesis are organised as follows: in Chapter 2 a description of the PUMA model used in the thesis is given, followed by an account of all model

experiments and their setups, as well as a section on the methods used for the analysis. In Chapter 3 the results are presented in three parts. The general performance of PUMA in the aqua planet configuration that is used as a basis for all further experiments is assessed in Section 3.1. Section 3.2 contains the results from a series of sensitivity experiments indicating the necessity of orography and mid-latitude continent-ocean heat contrasts for blocking simulation with PUMA. Section 3.3 covers the results of a second series of sensitivity experiments dealing with the influence of tropical heating on blocking frequencies. The results are then discussed in Chapter 4, and summarised in Chapter 5.

2. Model, experiment setup and methods

2.1. Model description

The model used to conduct the experiments described in this thesis is the *Portable University Model of the Atmosphere* (PUMA) which has been developed at the University of Hamburg as a tool for idealised modelling of the atmosphere and training of junior scientists (Fraedrich et al., 1998).

PUMA is based on the multi-layer spectral model by Hoskins and Simmons (1975), that is also nicely described in a study about the influence of surface drag on a baroclinic atmosphere by James and Gray (1986). The multi-layer spectral model of Hoskins and Simmons (1975), as well as PUMA, integrates the primitive equations in their vorticity and divergence form on a sphere, which can, assuming that the atmosphere is an inviscid, adiabatic, hydrostatic, perfect gas, be written in non-dimensional form as (Hoskins and Simmons, 1975):

$$\frac{\partial \zeta}{\partial t} = \frac{1}{1-\mu^2}\frac{\partial}{\partial \lambda}\mathcal{F}_V - \frac{\partial}{\partial \mu}\mathcal{F}_U \tag{2.1}$$

$$\frac{\partial D}{\partial t} = \frac{1}{1-\mu^2}\frac{\partial}{\partial \lambda}\mathcal{F}_U + \frac{\partial}{\partial \mu}\mathcal{F}_V - \nabla^2\left(\frac{U^2+V^2}{2(1-\mu^2)} + \Phi + \overline{T}\ ln(p_*)\right) \tag{2.2}$$

$$\frac{\partial T'}{\partial t} = -\frac{1}{1-\mu^2}\frac{\partial}{\partial \lambda}(UT') - \frac{\partial}{\partial \mu}(VT') + DT' - \dot{\sigma}\frac{\partial T}{\partial \sigma} + \kappa\frac{Tw}{p} \tag{2.3}$$

$$\frac{\partial ln(p_*)}{\partial t} = -\frac{U}{1-\mu^2}\frac{\partial ln(p_*)}{\partial \lambda} + V\frac{\partial ln(p_*)}{\partial \mu} - D - \frac{\partial \dot{\sigma}}{\partial \sigma} \tag{2.4}$$

$$\frac{\partial \Phi}{\partial ln(\sigma)} = -T \tag{2.5}$$

with

$$\mathcal{F}_U = V\zeta - \dot{\sigma}\frac{\partial U}{\partial \sigma} - T'\frac{\partial ln(p_*)}{\partial \lambda} \quad ; \quad \mathcal{F}_V = -U\zeta - \dot{\sigma}\frac{\partial V}{\partial \sigma} - T'(1-\mu^2)\frac{\partial ln(p_*)}{\partial \mu} \quad ;$$

$$U = u\sqrt{1-\mu^2} \quad ; \quad V = v\sqrt{1-\mu^2}$$

T denotes temperature (split into a constant part $\overline{T}$ and a variable part T'), κ is the adiabatic coefficient, ζ denotes absolute vorticity, t is time, μ is the sine of latitude,

λ is longitude, D is divergence, Φ is the geopotential, p is pressure and p_* is surface pressure, $\sigma = p/p_*$ is the vertical coordinate, and u, v and w are zonal, meridional and vertical wind velocities respectively (Hoskins and Simmons, 1975). For a list of variables see Table A.1 in the appendix.

The variables have been non-dimensionalised with the following scales: the vorticity ζ and the divergence D with the Earth's angular velocity Ω, the temperature T with $(a^2\Omega^2)/R$ where a is the planetary radius and R the gas constant, the pressure p by the global mean surface pressure of $p_{\text{surf}} = 1013.25\,\text{hPa}$, and the orography with $(a^2\Omega^2)/g$ where g denotes acceleration due to gravity.

There is no moisture included in the model, and consequently a range of processes that are usually incorporated in atmospheric general circulation models (AGCMs) are not present in the model equations. The model thus behaves as a dynamical core of an AGCM including only friction and diabatic heating that are represented, using a simple linear approach, by Rayleigh friction and Newtonian cooling respectively. Rayleigh friction parameterises all large scale dissipation processes in the model, whereas Newtonian cooling represents e. g. the radiative damping of the atmosphere (Hoskins and Simmons, 1975; James and Gray, 1986). The two parameterisations are implemented in the model by adding the following linear relaxation terms to the equations (Fraedrich et al., 1998):

$$-\frac{\xi}{\tau_F} \qquad \text{to the vorticity equation (2.1)} \tag{2.6}$$

$$-\frac{D}{\tau_F} \qquad \text{to the divergence equation (2.2)} \tag{2.7}$$

$$+\frac{T_R - T}{\tau_R} \qquad \text{to the thermodynamic equation (2.3)} \tag{2.8}$$

The Rayleigh friction (Eqs. 2.6 and 2.7) thus draws the momentum fields to zero with the time scale τ_F, whereas the Newtonian cooling (Eq. 2.8) draws the temperature field towards the prescribed restoration temperature T_R with the time scale τ_R. ξ denotes the relative vorticity.

Additionally, subgrid scale dissipation is parameterised by introducing a high-order diffusion operator into the equations. MacVean (1983) showed that this so-called hyperdiffusion is necessary when simulating non-linear baroclinic processes, otherwise the energy will accumulate at the model's truncation limit. The hyperdiffusion is added to the vorticity, divergence and thermodynamic equations (Eqs. 2.1, 2.2 and 2.3) as

$$-K(-1)^h \nabla^{2h} \cdot X \tag{2.9}$$

where the hyperdiffusion operator acts on X that stands for, depending on the equation, respectively vorticity, divergence or temperature. K denotes here the hyperdiffusion coefficient, and h the hyperdiffusion order (Fraedrich et al., 1998).

The model uses a spectral representation of the equations in the horizontal, i. e. the

vorticity ζ, the divergence D, the temperature anomaly T', the geopotential Φ and the logarithm of the surface pressure $ln(p_*)$ are each represented by a series of spherical harmonics (Hoskins and Simmons, 1975) as:

$$X \approx \sum_{m=-M}^{M} \sum_{n=|m|}^{N(m)} X_n^m Y_n^m \tag{2.10}$$

where m is the zonal wave number, $n - m$ is the 'meridional nodal number' and the spherical harmonics Y_n^m are the eigenfunctions of the Laplacian on the sphere. For an exact representation of the function X, the summation limits M and $N(m)$ must equal infinity; the choice of values for M and N sets the number of spherical harmonics included in the representation of X, the *spectral truncation*. There are different forms of truncation, set by the relation of N relative to m and M (Randall, 2015). For the triangular truncation used in the PUMA code, $N = M$ must be satisfied. As with all spectral models, only linear terms are computed in the spectral domain, whereas non-linear terms are computed on a grid and then transformed back into the spectral domain (Hoskins and Simmons, 1975).

Vertically, a finite difference representation is used, with sigma, i. e. terrain-following, model levels (Hoskins and Simmons, 1975).

The time stepping scheme used is the semi-implicit scheme, by which all gravity wave propagation terms are integrated implicitly in time, the remaining terms explicitly (Fraedrich et al., 2017). This allows a larger time step than fully explicit time stepping schemes without becoming numerically unstable (Hoskins and Simmons, 1975). The explicit integration in time is done using a leap-frog scheme, with the application of a Robert-Asselin time filter to avoid decoupling of the two time levels (Fraedrich et al., 2017).

PUMA has been modified from the original spectral primitive equation model by Hoskins and Simmons (1975) in mainly two ways (Fraedrich et al., 1998). The developers from the University of Hamburg have rewritten the model code in Fortran 90, in order to allow for the model to be run on different computer systems. Additionally, the output format has been adjusted to facilitate compatibility with the ECHAM general circulation model (European Centre - HAMburg GCM) developed at the Max Planck Institute for Meteorology in Hamburg (Stevens et al., 2013).

2.2. Experiment setup

2.2.1. Basic setting

The basic settings of the model are mostly inspired by Kunz et al. (2009), who used PUMA to investigate the influence of synoptic-scale wave breaking in the mid-latitude

jet stream on the North Atlantic Oscillation (NAO). Although the aim of this thesis is somewhat different from their topic of research, their model setting seemed to be a good starting point for an investigation of blocking in PUMA. This is because, as described in Section 1.1.2, planetary wave breaking in the jet stream is a contributor to mid-latitude blocking. Kunz et al. (2009), in turn, based their model settings on the proposal of Held and Suarez (1994) for the evaluation of climate models' dynamical cores.

The basic model settings are chosen to be zonally symmetric (i. e. resemble an aqua planet setting) with a sinusoidal restoration temperature distribution as in Held and Suarez (1994). The stratosphere is, as in their setup, relaxed to a constant temperature of 200 K. These basic settings were modified in order to have one winter hemisphere (chosen to be the Northern Hemisphere) as in Kunz et al. (2009), with a temperature difference of 20 K between the South and the North Pole. Figure 2.1 shows the resulting restoration temperature distribution.

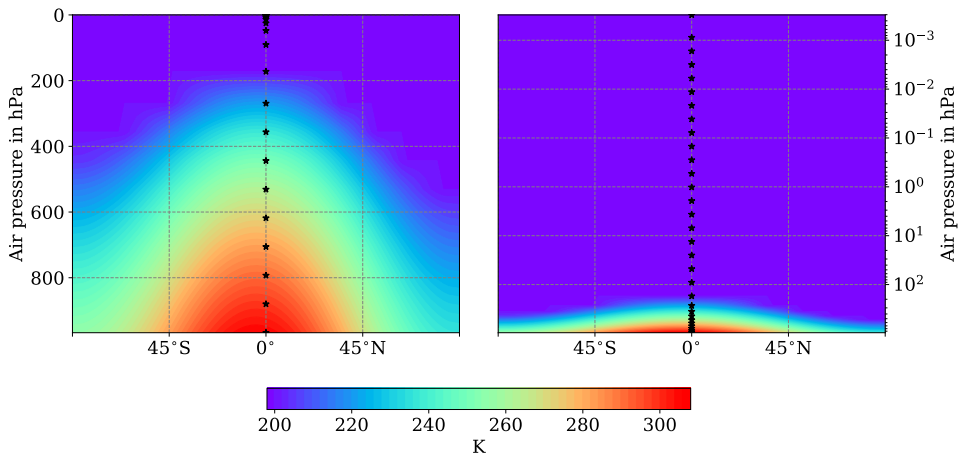

Figure 2.1.: Basic zonally symmetric restoration temperature setup, shown as colour shading, in the troposphere (left panel) and over the entire model height (right panel). The location of the sigma levels is indicated by the black asterisks in each panel.

The spectral truncation used in all model runs presented in this thesis is T42 (approximately corresponding to 64 × 128 gridpoints on a Gaussian grid). The model is run with 30 levels in the vertical as in Scinocca and Haynes (1998) and Kunz et al. (2009), where 9 levels are linearly spaced with respect to air pressure in the troposphere, and 21 levels are logarithmically spaced with respect to air pressure in the stratosphere. The spacing of the sigma levels is indicated with black asterisks in Figure 2.1.

The Newtonian cooling time scale τ_R is set to 40 days at all levels except the lowest five, where the time scale is reduced to 30, 20, 15, 10, and 5 days respectively (cf. Held and Suarez, 1994; Kunz et al., 2009). Rayleigh friction is only applied in the three

lowest model levels, where its time scale τ_F is set to 1.168 days at the surface, 1.759 days at the second level and 3.562 days at the third level (again as in Held and Suarez, 1994; Kunz et al., 2009) and in a sponge layer at levels higher than 0.5 hPa, following Polvani and Kushner (2002) and Kunz et al. (2009), who introduced this sponge layer in order to 'avoid spurious wave reflection at the model top and numerical instability due to large amplitude gravity waves' (Kunz et al., 2009).

For all sensitivity experiments, described in more detail in the following sections, two types of anomalies are introduced into this basic zonally symmetric model setting; orography and heating anomalies. All anomalies used are Gaussian-shaped, and all heating anomalies are vertically centred in the middle troposphere (they are also Gaussian-shaped in the vertical direction). In order to keep the restoration temperature field stable and physically meaningful around the orography anomalies, interpolation of the restoration temperature field (which is defined on sigma levels) to pressure levels is necessary. An example of the resulting temperature field around a mountain range centred at 60°W can be seen in Figure 2.2.

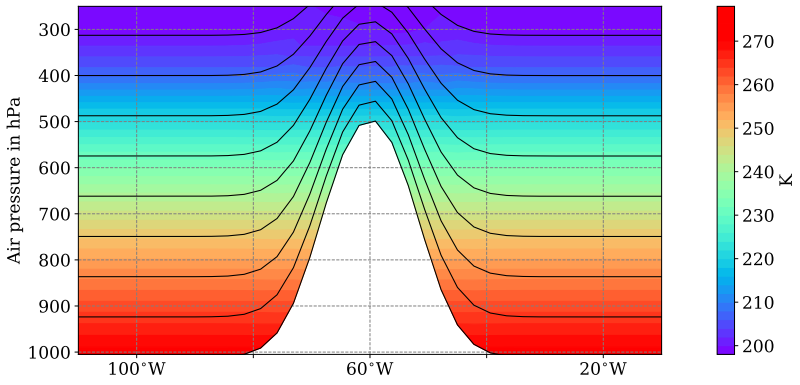

Figure 2.2.: Example of restoration temperature interpolation to pressure levels around orography. The colour shading shows the restoration temperature along 48°N, with a mountain range centred at 60°W. Sigma levels are indicated as black lines.

Due to the semi-implicit scheme that is used in PUMA, the time step could normally be relatively large (e. g. Hoskins and Simmons, 1975; James and Gray, 1986). Kunz et al. (2009), for example, used a time step of 15 minutes in their zonally symmetric setting. However, as soon as orographic anomalies are introduced into the boundary files, PUMA becomes unstable when a comparable time step is used, probably due to the relatively fine vertical resolution and the larger vertical velocities forced by the orography. A smaller time step of one minute is thus used in all PUMA experiments carried out here, to ensure numerical stability throughout the model runs.

The first two years of all model runs are not included in any analysis described in the following chapters, to ensure that the model's spin-up is excluded. Every model run

is at least 22 years long (20 years without the spin-up), because it is found that on shorter time scales the blocking frequency varies too much.

2.2.2. Sensitivity experiments I: mountain range and heating dipole

When PUMA is run with the basic zonally symmetric setup described in Section 2.2.1, there is no blocking detectable in the model output. A first series of sensitivity experiments is therefore carried out in order to identify the 'ingredients' that are necessary to establish blocking in the model.

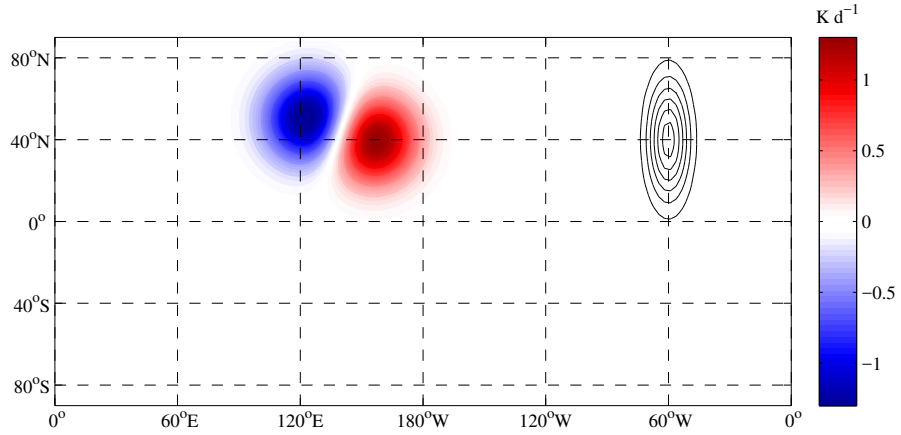

Figure 2.3.: Example setup with heating dipole at 140°E and mountain range at 60°W. Shown in colour are the heating anomalies added to the basic restoration temperature setting (see Figure 2.1). All heating anomalies are centred in the mid-troposphere. The black contours indicate the mountain range added to the basic setting (contours every 1000 m).

As described in Sections 1.1.1 and 1.1.2, blocking occurs preferentially at the end of the northern Pacific and northern Atlantic storm tracks, also referred to as jet exit regions. These are primarily shaped by the Northern Hemisphere orography, but especially in boreal winter also influenced by land-ocean heat contrasts at the east coasts of the Asian and North American continents (cf. Section 1.1 and Holton, 1992, p. 346). Hence, two kinds of anomalies are introduced into PUMA's zonally symmetric fields to disturb the model's jet stream and induce intensifications and jet-exit-like weakenings of the storm track in the model's Northern Hemisphere. First, a mountain range is introduced that is Gaussian-shaped both longitudinally and latitudinally. Second, a heating dipole is introduced into the model's restoration temperature field. The two poles of the heating anomaly are both Gaussian-shaped in all three dimensions. They are centred vertically in the middle troposphere at 500 hPa, where they add baroclinicity to the atmospheric temperature distribution and thus influence the jet stream resulting from the thermal wind balance. Their horizontal position is chosen

so as to resemble the land-ocean contrast at the western boundary of an ocean basin. Franzke et al. (2000) used heating dipoles similar to those described here to generate storm tracks in PUMA. An example of a 6000 m high mountain range and a heating dipole with a maximum amplitude of $1.5\,\mathrm{K\,d^{-1}}$ can be seen in Figure 2.3.

The influence of the following parameters on mid-latitude blocking frequencies in the model is then examined: the location of the heating dipole relative to the mountain range, the height of the mountain range and the amplitude of the heating dipole. All results are shown in Chapter 3.

2.2.3. Sensitivity experiments II: tropical heating anomalies

As mentioned in Section 1.2, the circulation in the tropics exerts an influence on mid- and high-latitude blocking. Therefore, a second series of sensitivity experiments is carried out to examine the tropical influence on blocking in the simplified PUMA setting. First, a general analysis of the influence of tropical heating on blocking depending on the location of the heating is performed, followed by an examination of the influence that dominant features of the tropical variability (ENSO and the MJO) have on blocking. Finally, the impact of a tropical heating anomaly based on the CMIP5 tropical precipitation bias is explored.

Reference run

In order to obtain a reference run for this second series of sensitivity experiments and to allow meaningful comparison of the results to other studies, it is now attempted to make the model setting more realistic than for the first series of sensitivity experiments. The basic setting is kept zonally symmetric except for orography and heating anomalies as described in Section 2.2.2. However, the number and placement of mountain ranges and heating dipoles are now chosen based on the distribution of the major oceans and continents in the real Northern Hemisphere. As shown in Figure 2.4, there are two mountain ranges set to the locations of the Rocky Mountains and the Himalayas, and two heating dipoles set to represent the continent-ocean borders between Asia and the Pacific Ocean, and North America and the Atlantic Ocean respectively.

Note that the continents shown in Figure 2.4 and all other figures showing model fields are only drawn for easier orientation and better comparability to the results of other studies – PUMA is run without realistic continents in all experiments discussed in this thesis.

The reference setup shown in Figure 2.4 is kept unchanged throughout all sensitivity experiments of this second series, except for tropical heating anomalies added to the restoration temperature. All tropical heating anomalies are again Gaussian-shaped in all three dimensions and centred vertically in the middle troposphere. The amplitudes

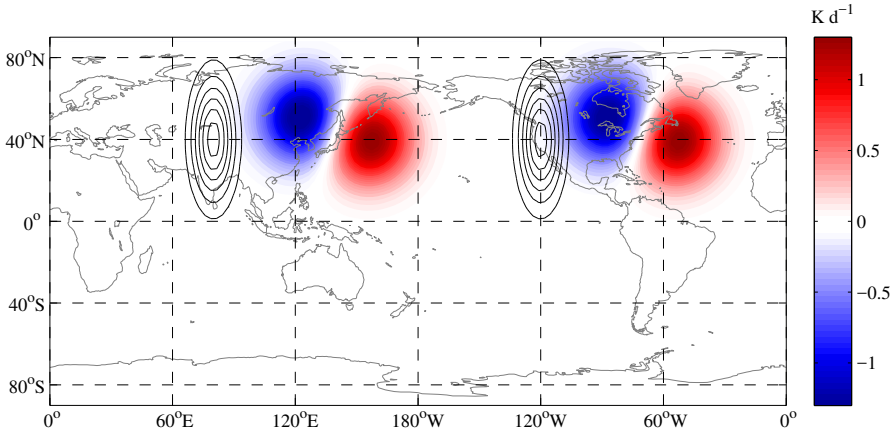

Figure 2.4.: Setup of the reference experiment. Shown in colour are the heating anomalies added to the basic restoration temperature setting (see Figure 2.1). All heating anomalies are centred in the mid-troposphere. The black contours indicate the mountain ranges added to the basic setting (contours every 1000 m). The continents shown in grey are only for orientation; all PUMA runs described here are run without realistic orography.

of the heating anomalies are chosen based on Morita et al. (2006) who nicely connect rainfall, outgoing longwave radiation (OLR) and latent heating due to the MJO. These relations (giving a mid-tropospheric heating of roughly $0.7\,\mathrm{K\,d^{-1}}$ corresponding to a precipitation anomaly of $1\,\mathrm{mm\,d^{-1}}$) are generalised to all other experiments here.

Idealised tropical heating anomaly

To get a general picture of the impact of anomalous tropical heating on mid- and high-latitude blocking frequency, a set of experiments is conducted with a heating anomaly centred at the equator, but at different longitudes. The model is run for 22 years 36 times, for the heating anomaly at every ten degrees of longitude. This is done for both a positive and a negative heating anomaly. The zonal and longitudinal extent of the heating is set to 10°, and the amplitude to $1.25\,\mathrm{K\,d^{-1}}$ (comparable to the amplitudes of the ENSO and MJO anomalies).

ENSO-like heating anomaly

The equatorial Pacific heating anomaly designed to represent El Niño (respectively La Niña) is shown in Figure 2.5. Shape and location are based on the maximum OLR anomaly during Eastern Pacific El Niño events. This is slightly displaced to the west relative to the maximum sea surface temperature (SST) anomaly (Johnson and Kosaka, 2016).

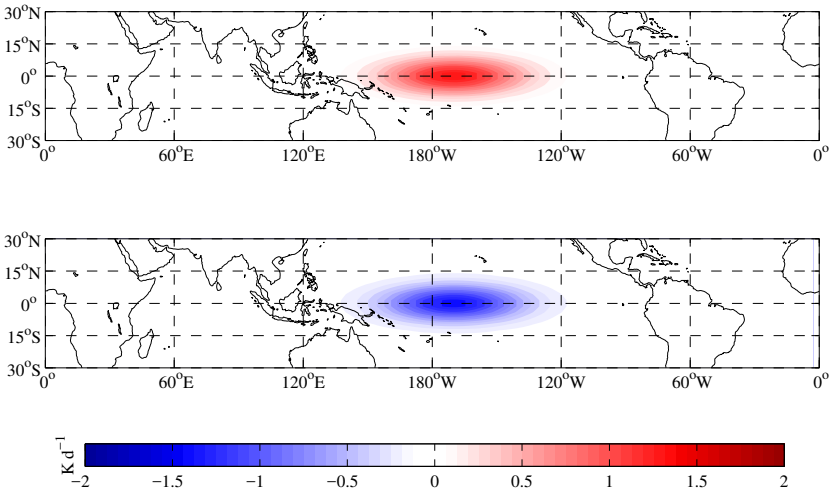

Figure 2.5.: Setup of the ENSO experiment. Displayed as colour shading are diabatic heating anomalies introduced into PUMA's restoration temperature field at their vertical centre in the mid-troposphere. The positive heating anomaly shown in the upper panel corresponds to El Niño, the negative heating anomaly in the lower panel to La Niña. The shape of the anomalies is based on Johnson and Kosaka (2016). Realistic continents are only drawn for better orientation.

MJO-like heating anomaly

The shape of the equatorial heating anomalies chosen to represent the MJO is based on the multi-variate MJO index by Wheeler and Hendon (2004). The two phases whose impact on blocking is examined in this thesis are phase 6, for which both Henderson et al. (2016) and Gollan and Greatbatch (2017) find a strong influence on mid- and high-latitude blocking, and phase 2, for which the heating pattern is approximately opposite to that of phase 6. The anomalies that are added to the PUMA restoration temperature are displayed in Figure 2.6 for both phases.

CMIP5 tropical precipitation bias heating anomaly

Shown in the left panel of Figure 2.7 is the multi-model mean bias in precipitation of all the climate models participating in the CMIP5. Especially in the tropics, the bias is considerable, exceeding e. g. the anomalous precipitation due to the MJO (cf. Morita et al., 2006). In the right panel of Figure 2.7, the heating anomaly is displayed that is added to the PUMA restoration temperature to examine the influence that such a precipitation bias has on the model's blocking frequency.

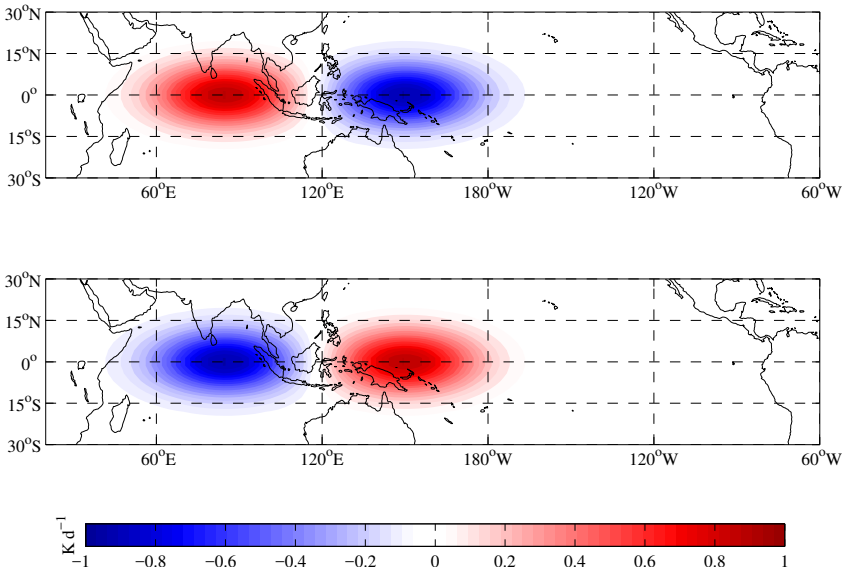

Figure 2.6.: Setup of the MJO experiment. Displayed as colour shading are diabatic heating anomalies introduced into PUMA's restoration temperature field at their vertical centre in the mid-troposphere. The heating anomaly shown in the upper panel corresponds to MJO phase 2, the heating anomaly in the lower panel to MJO phase 6. The shape of the anomalies is based on Wheeler and Hendon (2004). Realistic continents are only drawn for better orientation.

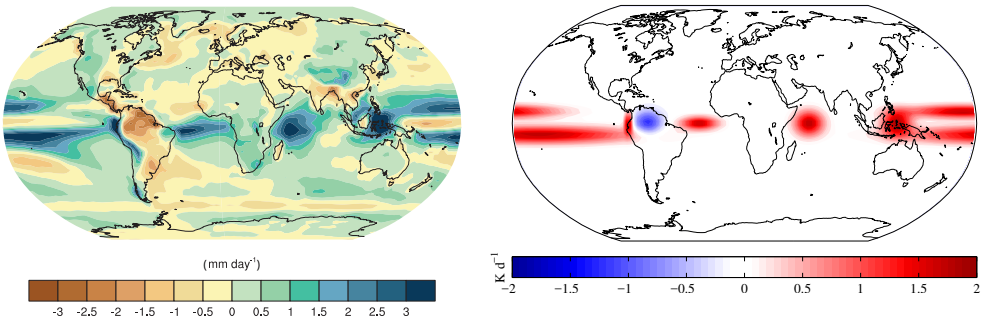

Figure 2.7.: Setup of the CMIP5 precipitation bias experiment. Shown in the left panel is the multi-model mean precipitation bias from the CMIP5 models (figure taken from Flato et al., 2013, p. 763), in the right panel the corresponding mid-tropospheric heating anomalies introduced into PUMA's restoration temperature field. Realistic continents are only drawn for better orientation.

2.3. Methods

2.3.1. Blocking detection

Throughout this thesis, a blocking index is used that identifies reversals of the meridional gradient of geopotential height. This method of blocking detection goes back to the earliest blocking indices defined by Lejenäs and Økland (1983) and Tibaldi and Molteni (1990) who used the 500 hPa geopotential height gradient across a fixed central latitude, e. g. 50°N in Lejenäs and Økland (1983). However, more recently the importance of allowing the central latitude to vary with longitude was shown, e. g. by Pelly and Hoskins (2003) and Barnes et al. (2012), because the region where mid-latitude blocking can occur is largely determined by the location of the mid-latitude westerly jet stream and the preferred path of propagating mid-latitude weather systems. Pelly and Hoskins (2003) showed that if this is not taken into account, geopotential height gradient reversals north of the jet stream can be falsely identified as blocking, leading to spuriously high blocking frequencies. This is especially prone to happen over the western Pacific where the climatological position of the storm track lies relatively far south (Pelly and Hoskins, 2003). In order to avoid this, Pelly and Hoskins (2003) suggested calculating blocking indices across a variable *Central Blocking Latitude* (CBL) located at the climatological position of the storm track.

Apart from the geopotential height field, blocking indices can also be based on potential temperature on a potential vorticity surface (e. g. Pelly and Hoskins, 2003) or zonal winds, because all these fields clearly show the large scale reversal of the mean flow in a case of blocking. Barnes et al. (2012) showed that all three variables (i. e. geopotential height, potential vorticity and zonal wind) give very similar blocking climatologies.

Instead of choosing one particular latitude across which the gradient used to detect blocking is calculated, it is of course possible to calculate a two-dimensional blocking index across several latitudes. Barnes et al. (2012) stated that 'these indices have the advantage of being robust to changes in the latitude of blocking and avoid sensitivity to the choice of CBL'. However, the blocking identified by the two-dimensional indices is not only mid-latitude blocking in the jet stream path, but also blocking at higher latitudes that has different implications for the circulation since it does not block the path of the mid-latitude weather systems.

In this thesis, one-dimensional as well as two-dimensional blocking indices are calculated, both using the geopotential height field. Following Masato et al. (2014) and Gollan et al. (2015), the instantaneous blocking index is defined as

$$BI_{\mathrm{inst}}(\lambda) = \frac{1}{\Delta\varphi}\int_{\varphi_0}^{\varphi_0+\Delta\varphi} z\; d\varphi \quad - \quad \frac{1}{\Delta\varphi}\int_{\varphi_0-\Delta\varphi}^{\varphi_0} z\; d\varphi \tag{2.11}$$

where λ denotes longitude, φ latitude, z is geopotential height, φ_0 is the CBL and $\Delta\varphi = 15°$. As suggested by Pelly and Hoskins (2003), a variable CBL is used for all one-dimensional blocking indices calculated here. The CBL is determined for each experiment separately as the latitude of the maximum spectral power of 300 hPa geopotential height at periods between 2 and 6 days.

In order to separate actual blocking episodes from short and/or localised reversals of the mean flow, a temporal persistence criterion is used as well as a spatial extent criterion. A reversal event is defined as a blocking when the instantaneous blocking index BI_{inst} (Eq. 2.11) is positive for at least four consecutive days and over at least 15° longitude. Many blocking studies have used spatial and temporal criteria that are similar to these (e. g. Tibaldi and Molteni, 1990; Pelly and Hoskins, 2003; and Gollan et al., 2015).

To obtain two-dimensional fields of blocking frequencies, the same geopotential height gradient index is used, but the gradient is calculated across all latitudes φ_0 from 30°N to 75°N (this is comparable to e. g. the two-dimensional geopotential height index used by Scherrer et al., 2006).

For both the one-dimensional and the two-dimensional version of the blocking index, geopotential height on the 300 hPa isobaric surface is used here instead of the usual 500 hPa geopotential height in order to avoid interpolated data in the model fields at the location of the mountain ranges. However, there are no significant changes in the blocking indices when 500 hPa geopotential height fields are used instead.

3. Results

3.1. Mean state in aqua planet setting

When PUMA is run with the basic zonally symmetric setup described in Section 2.2.1, the model circulation and mean state are reasonably realistic for an aqua planet setup and compare well with results from Held and Suarez (1994) and Kunz et al. (2009). The zonal mean temperature and zonal wind climatologies from the zonally symmetric PUMA run are shown in Figure 3.1 (cf. e. g. Held and Suarez, 1994, Figures 1 and 2; and Kunz et al., 2009, Figure 1). Despite the prescribed restoration temperature being constant above the tropopause (see Figure 2.1), PUMA develops a temperature minimum above the equatorial tropopause and a temperature increase with height in the stratosphere. The increase is relatively weak when compared to e. g. Kunz et al. (2009). Otherwise, the temperature field is close to the prescribed restoration temperature field.

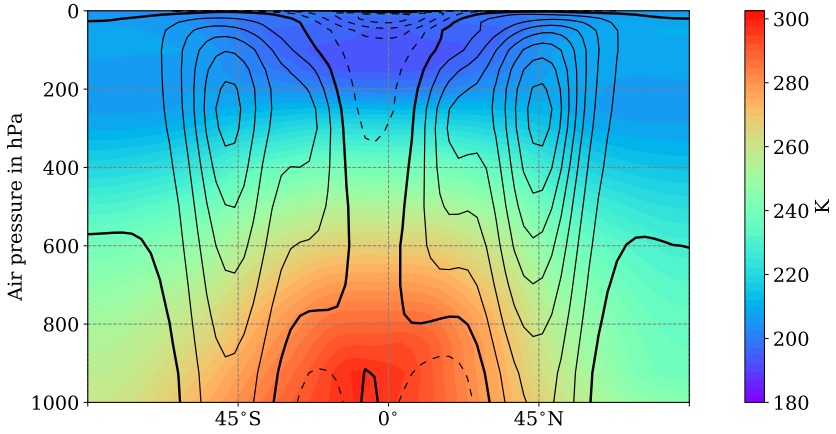

Figure 3.1.: Climatological zonal mean air temperature (colour shading) and zonal wind (black contours) from PUMA when it is run with the zonally symmetric basic setup. Zonal wind contours are drawn every $5\,\mathrm{m\,s^{-1}}$, positive contours are solid and negative contours are dashed. The zero contour is emphasised.

The wind field is characterised by two westerly jets centred at the height of the tropopause and at latitudes of about 45°N/S. At the surface, easterly winds extend

approximately 30° to the north and south from the equator, corresponding to the trade winds. Between 30° and 60°N/S, the surface winds are westerlies, corresponding to the mid-latitude westerlies. The jet as well as the surface westerlies are stronger in the winter (Northern) hemisphere than in the summer hemisphere. Above the equatorial tropopause, an easterly jet is present in the zonally symmetric PUMA run (as in Kunz et al., 2009, Figure 1). Although the model does have levels in the stratosphere, the stratospheric model circulation is less realistic than the tropospheric circulation; there is for example no stratospheric polar vortex included in the model forcing used here and consequently a stratospheric polar vortex is absent in the model.

Although the mean tropospheric circulation features seem to be captured, no blocking occurs in the zonally symmetric PUMA setup due to the strong zonality of the flow field. It has long been recognised that orography and continent-ocean heat contrasts play an important role in establishing the necessary zonal asymmetries for blocking to occur (see Sections 1.1 and 1.1.2). In the following, idealised mountain ranges and heating dipoles as described in Section 2.2 are therefore added to the zonally symmetric setup.

3.2. Sensitivity to configuration of mountain range and heating dipole

For the first series of sensitivity experiments, one mountain range and one heating dipole representing a mid-latitude continent-ocean heat contrast are introduced into the model, to investigate their influence on mid-latitude blocking in a simple model setup. The focus will now lie on the model's Northern Hemisphere only.

3.2.1. Influence of mountain range

In Figure 3.2, results from a model run with one mountain range with a maximum height of 6.5 km and located at 100°E are displayed. The location of the mountain range is indicated by a solid black line in all panels. All fields are shown at 300 hPa, where also blocking indices are calculated in this thesis (see Section 2.3), and in the region of the Northern Hemisphere jet stream. In all fields, a global stationary wave is evident that is forced by the mountain range and leads to strong deviations from zonality of the model's jet stream. Downstream of the mountain, the meridional gradient of climatological 300 hPa geopotential height is strengthened, consistent with very strong climatological westerly winds at 300 hPa, as well as a maximum in the power spectral density of 300 hPa geopotential height integrated over periods of 2–6 days that is taken as a measure of synoptic-scale storm system activity. Further downstream of the mountain, the meridional geopotential height gradient weakens, and consequently also the zonal wind field and the storm track. Directly upstream of

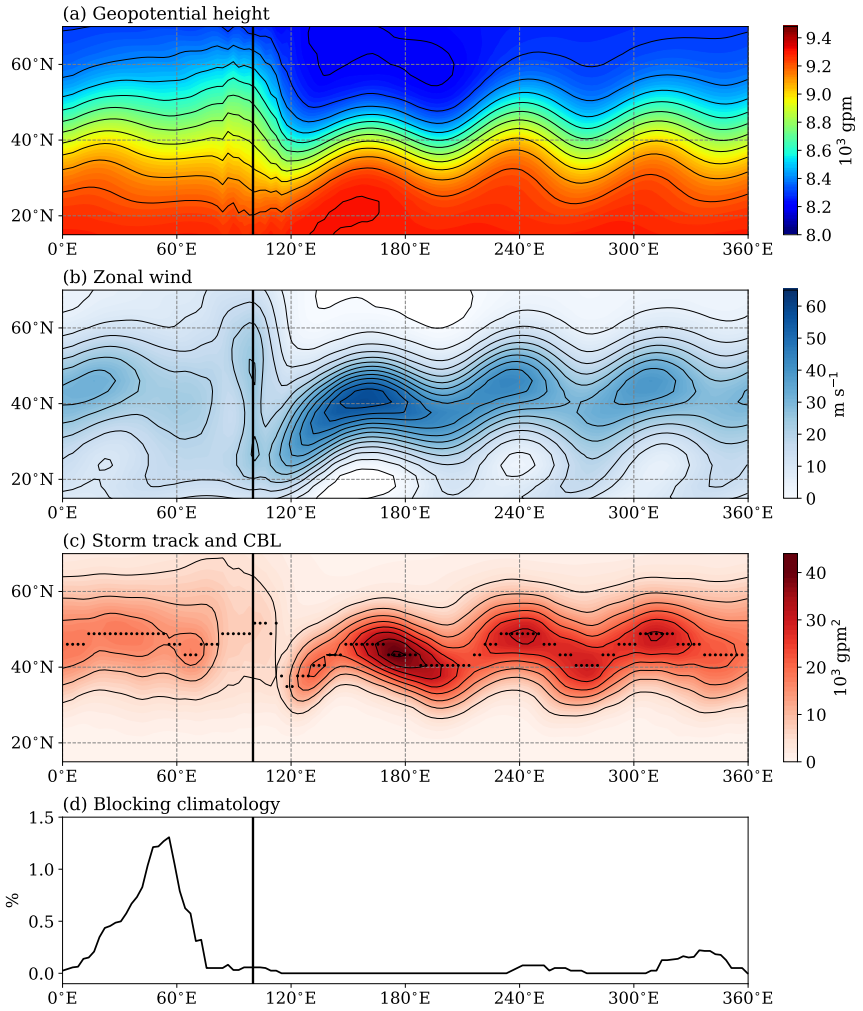

Figure 3.2.: Mean state, storm track and blocking climatology for a model configuration with one mountain range located at 100°E. Panels (a) and (b) show the time mean geopotential height and the time mean zonal wind, both at 300 hPa (black contours every 100 gpm for geopotential height and every $5\,\mathrm{m\,s^{-1}}$ for zonal wind). In panel (c) the power spectral density of 300 hPa geopotential height integrated over periods of 2–6 days is shown as colour shading and black contours (every $5 \cdot 10^3\,\mathrm{gpm}^2$) and the Central Blocking Latitude (CBL) as black dots. The CBL is defined as the location of the storm track, i. e. the latitude where the 2–6 day variability has its maximum. In panel (d) the blocking climatology along the storm track is shown (for details see Chapter 2.3).

the mountain, the geopotential height gradient, zonal wind and storm track become very weak, resembling a jet exit region.

The blocking climatology along the storm track is shown in the bottom panel of Figure 3.2. One blocking frequency peak between 10°E and 70°E stands out. This is of course the jet exit region upstream of the mountain, where the zonal flow weakens

considerably and thus allows quasi-stationary blocking anticyclones to develop. Two minor blocking regions can be seen downstream of the mountain between 240°E and 270°E and between 310°E and 360°E. The locations of both correspond to weakenings of the geopotential height gradient and the zonal wind.

These results agree well with blocking theories that require a widening and deceleration of the jet stream in order for blocking to occur (cf. Section 1.1.2). Moreover, the preferred regions of real Northern Hemisphere winter blocking also coincide with the exit regions of the Atlantic and Pacific jets. The absolute blocking frequency values, however, are considerably smaller than observed values that are as large as 10% at some longitudes (see Figure 3.12).

3.2.2. Influence of continent-ocean heating dipole

In Figure 3.3, results from a model run with one continent-ocean heating dipole located at 100°E can be seen. The dipole has a maximum amplitude of $1.5\,\mathrm{K\,d^{-1}}$. The centre of the dipole is indicated in all panels by a dashed black line. Again, all fields are shown at a height of 300 hPa and in the region of the Northern Hemisphere jet stream. The heating dipole has much less influence on the model circulation than the mountain range. However, it acts to increase the meridional geopotential height gradient as well as the zonal wind directly downstream of the dipole. The synoptic-scale variability of 300 hPa geopotential height is also clearly increased, mostly between 20° and 160° downstream of the heating dipole's centre.

The addition of the heating dipole to the zonally symmetric PUMA setup leads to blocking, but the resulting blocking frequency is extremely low. The blocking climatology along the storm track for the heating dipole experiment is shown in the bottom panel of Figure 3.3. Two regions can be seen where blocking occurs, one of them is slightly more pronounced. The latter is located around 300°E, which is directly downstream of the enhanced storm track variability. The lack of a distinct region with significantly enhanced blocking frequency in the heating dipole experiment is probably due to the strong zonality of the flow field that the heating dipole intensifies rather than disrupts as the mountain range does. There is no jet exit region shaped by the heating dipole, where blocking anticyclones can easily be maintained against zonal advection. The fact that there is some blocking downstream of a stormtrack intensification, despite the enhanced zonal flow, agrees well with blocking theories that highlight the importance of synoptic-scale storm systems for blocking maintenance (cf. Section 1.1.2).

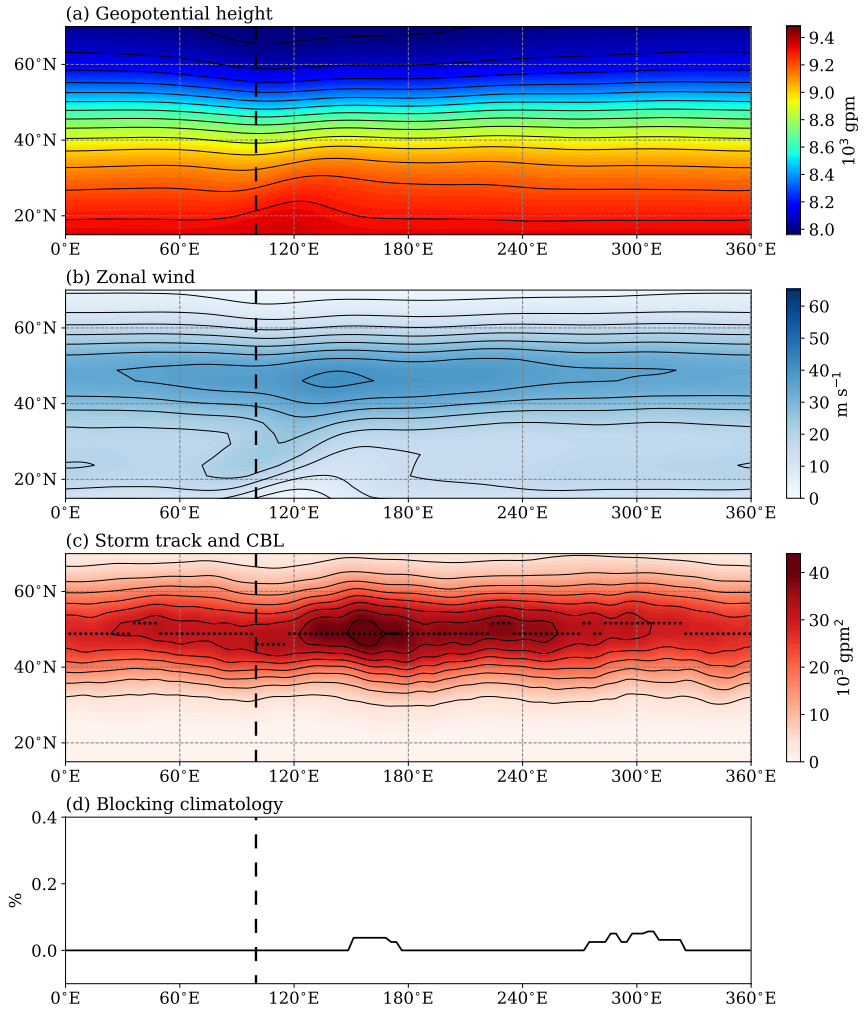

Figure 3.3.: Mean state, storm track and blocking climatology for a model configuration with one land-ocean heating dipole located at 100°E. Panels (a) and (b) show the time mean geopotential height and the time mean zonal wind, both at 300 hPa (black contours every 100 gpm for geopotential height and every 5 $\mathrm{m\,s^{-1}}$ for zonal wind). In panel (c) the power spectral density of 300 hPa geopotential height integrated over periods of 2–6 days is shown as colour shading and black contours (every $5 \cdot 10^3\,\mathrm{gpm^2}$) and the Central Blocking Latitude (CBL) as black dots. The CBL is defined as the location of the storm track, i. e. the latitude where the 2–6 day variability has its maximum. In panel (d) the blocking climatology along the storm track is shown.

3.2.3. Influence of heating dipole location relative to mountain range

In the two experiments shown before, the mountain range emerges as a more efficient source of blocking than the continent-ocean heating dipole, because it disrupts the zonal flow and generates a jet exit region where blocking preferably occurs. Never-

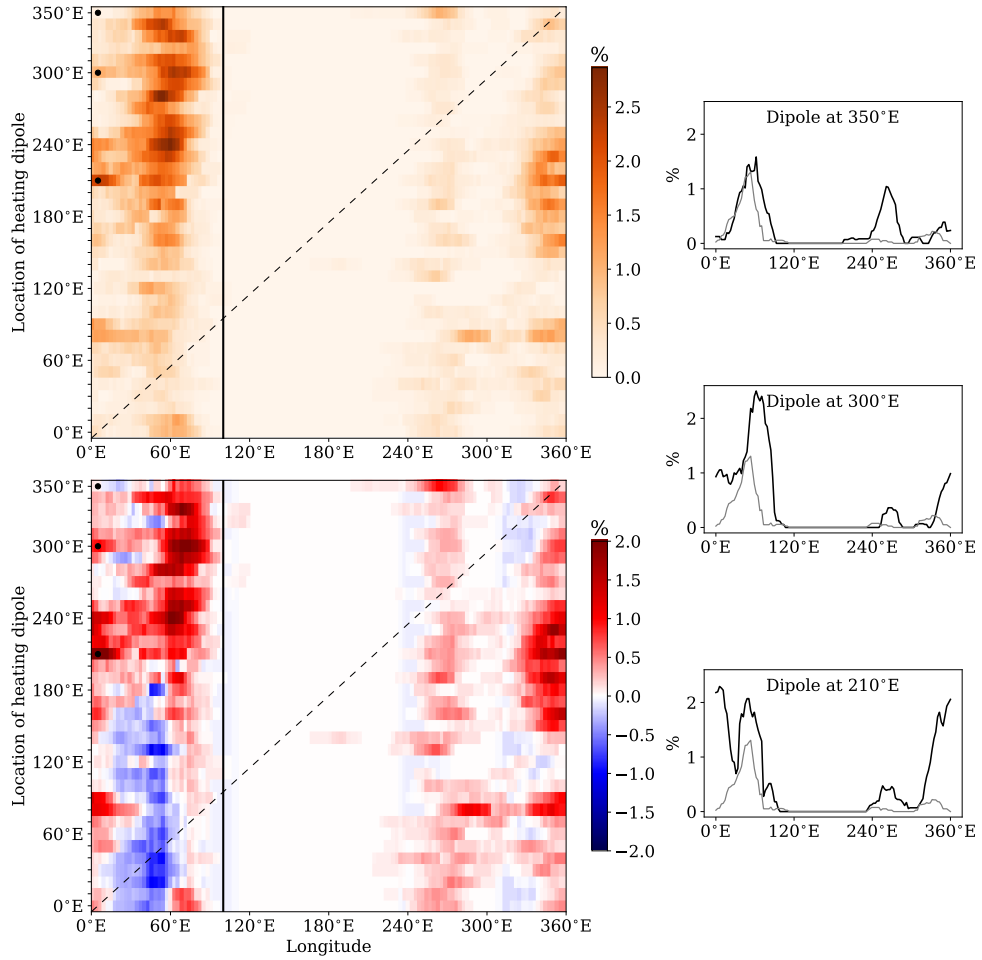

Figure 3.4.: Blocking climatologies for different locations of one land-ocean heating dipole (indicated by the dashed black line in the two panels on the left) relative to one mountain range located at 100°E (indicated by the vertical solid black line in the two panels on the left). In the upper left panel the absolute blocking frequencies are shown as colour shading for the different heating dipole locations. In the lower left panel, the blocking climatology for the only-mountain experiment without a heating dipole (see Figure 3.2) has been subtracted; i. e. red colours show an increase in blocking due to the heating dipole and blue colours show a decrease in blocking due to the heating dipole. The three locations that are chosen for further analysis are marked with a black dot in the left panels. The respective blocking climatologies are shown separately in the three panels on the right (in black), with the blocking climatology from the only-mountain experiment for comparison (in grey).

theless, the heating dipole enhances the synoptic-scale variability in the storm track and generates some blocking downstream of the intensified storm track. Therefore, it seems likely that if the heating dipole is positioned favourably relative to a mountain range, it will act to amplify blocking enabled by the mountain range. In Figure 3.4, the blocking climatologies of 36 different model runs are shown, where one mountain

range is located at 100°E as before and one heating dipole at different longitudes.

Regardless of the heating dipole location, the preferred blocking regions mostly stay at the three locations set by the mountain range. This confirms again the importance of the stationary wave forced by the mountain range in disrupting the zonal flow and thus determining the blocking regions.

However, especially from the lower left panel of Figure 3.4, which shows the difference in climatological blocking frequency between the respective heating dipole location run and the model run without the heating dipole (Figure 3.2), it becomes clear that the heating dipole can indeed amplify the blocking frequency in the blocking regions set by the mountain range. The increase is in some cases as large as 2%, which seems remarkable since the absolute blocking frequency in the only-dipole experiment is everywhere below 0.1% (Figure 3.3) and even in the only-mountain experiment does not exceed 1.5% (Figure 3.2).

The influence of the heating dipole on blocking frequency is different in the three blocking regions. In the first region downstream of the mountain (located around 260°E) the dipole acts slightly amplifying for most locations, but the impact is rather weak. In the second blocking region (located around 350°E) there is strong blocking amplification when the heating dipole is located between 150°E and 240°E, i. e. 110–200° upstream of the blocking region. For the most pronounced blocking region (located around 60°E directly upstream of the mountain range) the impact is strongest. Here the heating dipole strongly amplifies blocking when it is located between 210°E and 340°E, i. e. 80–210° upstream of the blocking region, and it decreases the blocking frequency when it is located between 0°E and 180°E. The amplification of blocking in regions that lie approximately 100–200° east of the heating dipole implies that blocking is indeed favoured by an upstream intensification of the storm track (cf. Figure 3.3).

Of all the model runs shown in Figure 3.4, three model runs are chosen for a more detailed analysis. For each of the three blocking regions, one model run is selected that shows especially strong blocking amplification in the respective region. The selected model runs are marked with a black dot in the left panels of Figure 3.4 and their blocking climatologies are shown separately in the three panels on the right.

3.2.4. Influence of mountain height and heating dipole amplitude

For the three chosen model configurations, the sensitivity of the zonal flow, storm track and blocking frequency to changes in mountain height and heating dipole amplitude is tested. This shall help to clarify the relative importance of mountain range and heating dipole for blocking when both are present in the model.

Mountain height

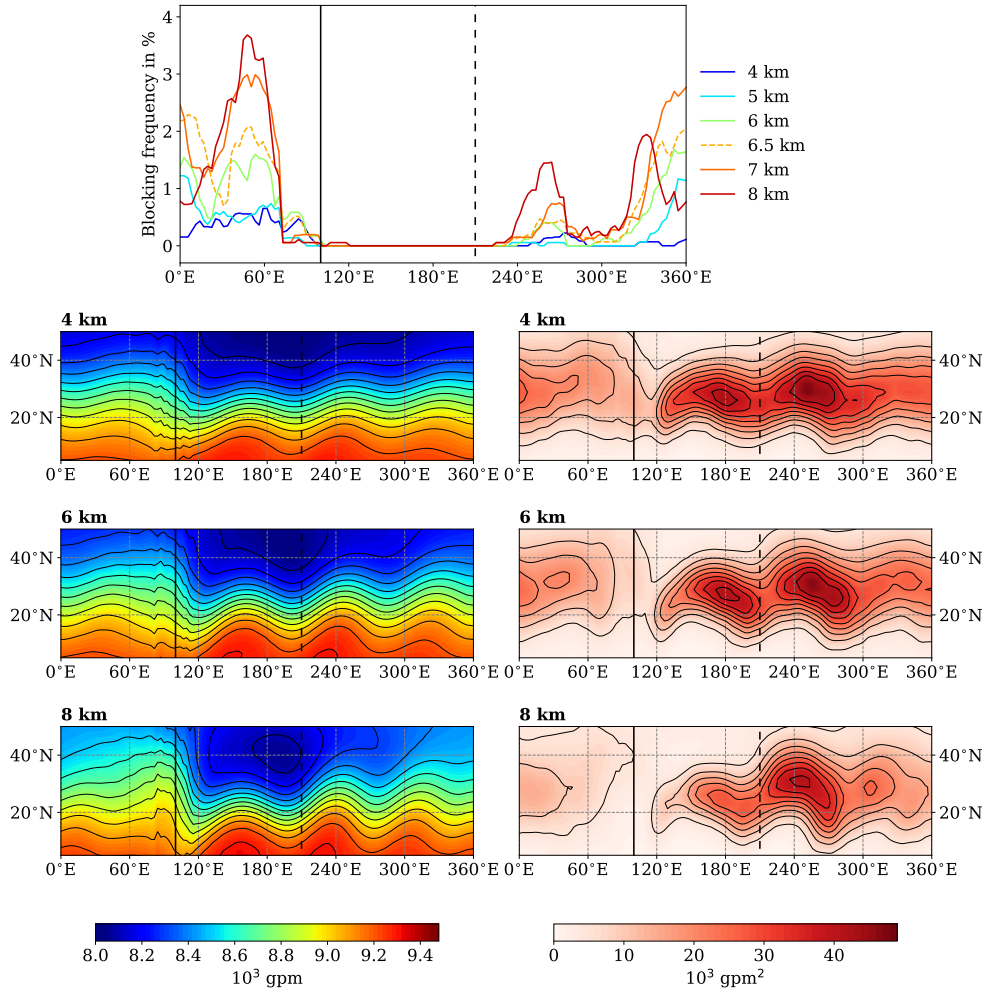

Figure 3.5.: Blocking climatology (top panel) for different mountain heights between 4 km and 8 km, with the mountain range located at 100°E and the heating dipole at 210°E. Because 6.5 km is the mountain height used in all other experiments (e. g. Figure 3.4), the 6.5 km experiment is drawn as a dashed line. In the lower six panels climatologies of the 300 hPa geopotential height (on the left) and of the power spectral density of 300 hPa geopotential height integrated over periods of 2–6 days (on the right) are shown for mountain heights of 4 km, 6 km and 8 km. Black contours are drawn every 100 gpm for geopotential height and every $5 \cdot 10^3$ gpm^2 for the 2–6 day variability. In all panels, the location of the mountain range is indicated by a solid black line, the location of the heating dipole by a dashed black line.

In Figure 3.5 geopotential height, storm track and blocking climatology are shown for different mountain heights; for the experiment with the mountain range at 100°E and the heating dipole at 210°E. Figures 3.6 and 3.7 show the same, but for the heating

dipole at 300°E respectively 350°E. Again, the location of the mountain is indicated by a solid black line in all panels, the location of the heating dipole by a dashed black line.

Generally, the blocking frequency increases with the height of the mountain range, especially in the blocking region directly upstream of the mountain. This is consistent with the weakening of the zonal flow with increasing mountain height especially directly upstream of the mountain, that is also visible for all three configurations. There is a general weakening of the storm track with increasing mountain height, which, however, does not prevent the increase of blocking frequency that is due to the weakening of the mean zonal flow.

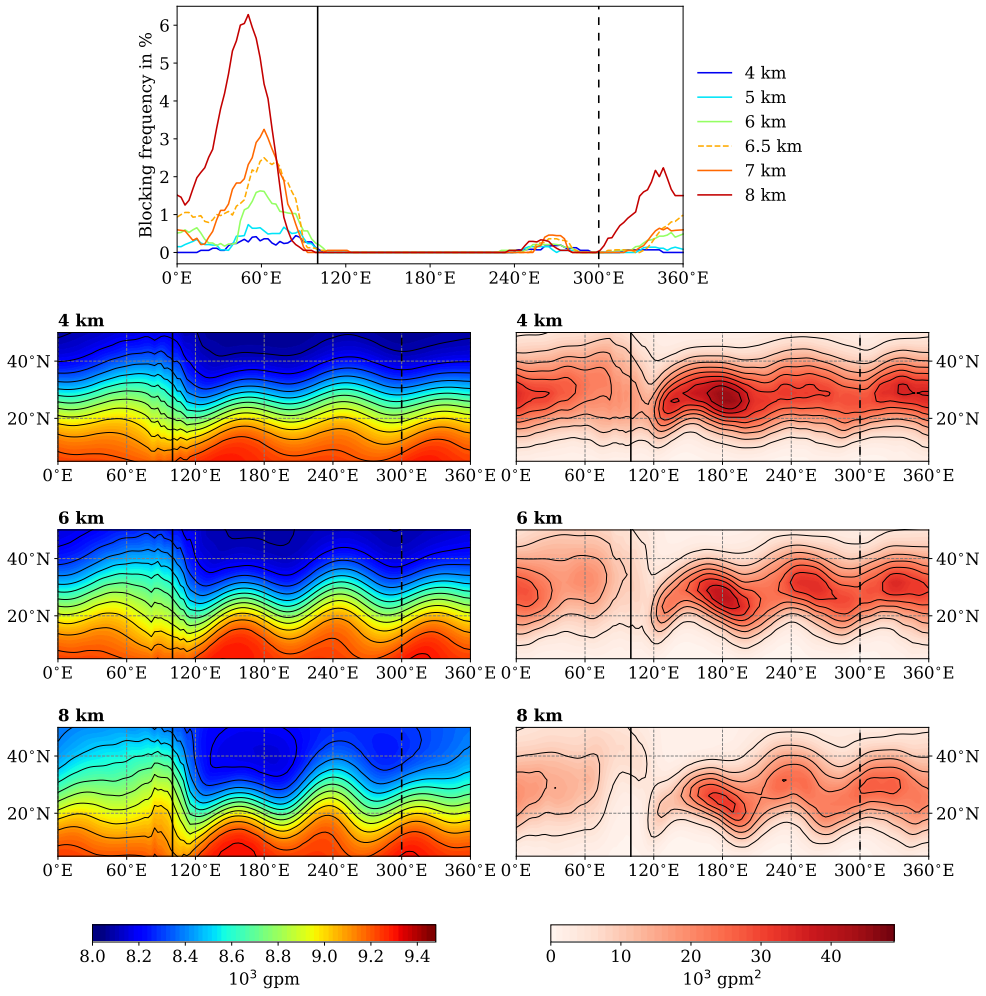

Figure 3.6.: As Figure 3.5, but for the heating dipole located at 300°E.

Between the mountain range and the heating dipole (to the east of the mountain range), there is almost no blocking, because the heating dipole allows for a widening of the jet stream only downstream of its location. Thus, all three blocking regions

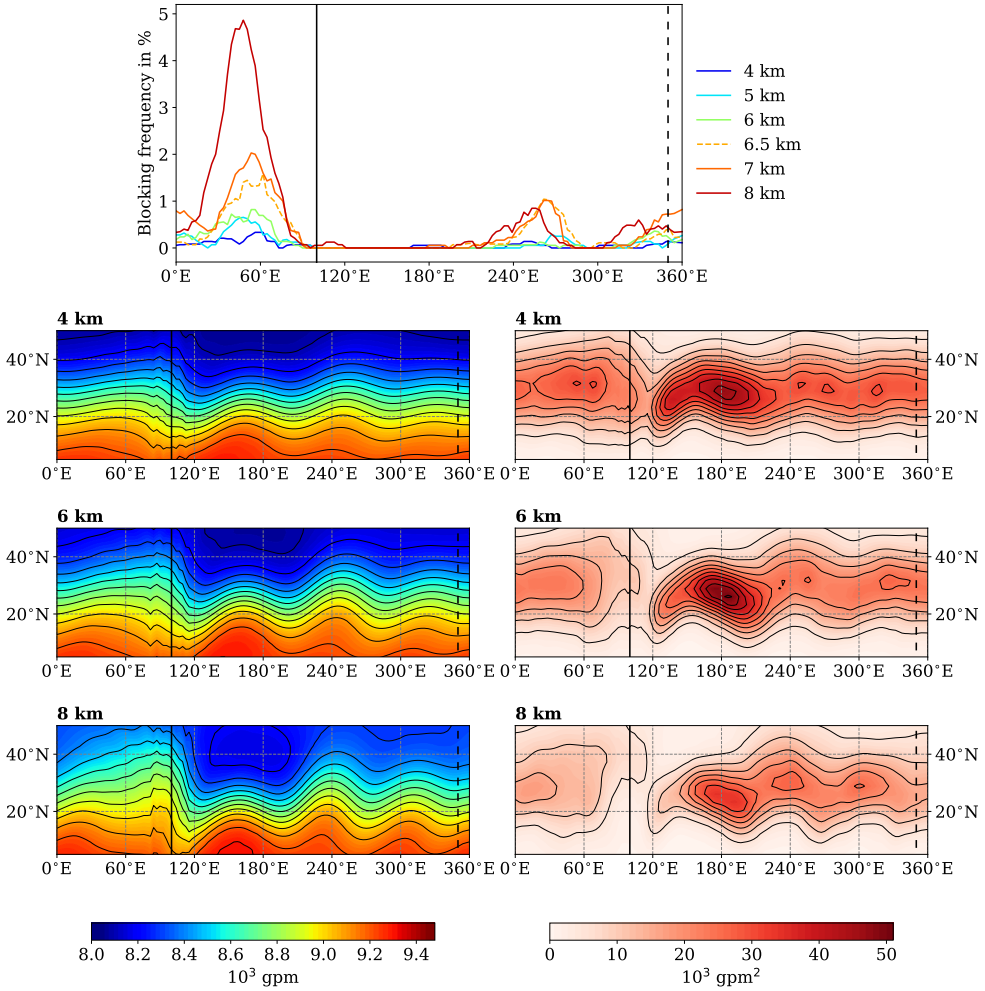

Figure 3.7.: As Figure 3.5, but for the heating dipole located at 350°E.

show an increase of blocking frequency with mountain height when the heating dipole is located at 210°E, whereas for the heating dipole located at 300°E blocking is suppressed and therefore not very sensitive to the mountain height in the blocking region between 240°E and 270°E. When the heating dipole is located at 350°E, blocking is additionally suppressed in the blocking region between 310°E and 360°E.

Interestingly, the dependence of blocking frequency on mountain height is much less strong for the configuration with the heating dipole at 210°E (Figure 3.5) than for the other two configurations.

Heating dipole amplitude

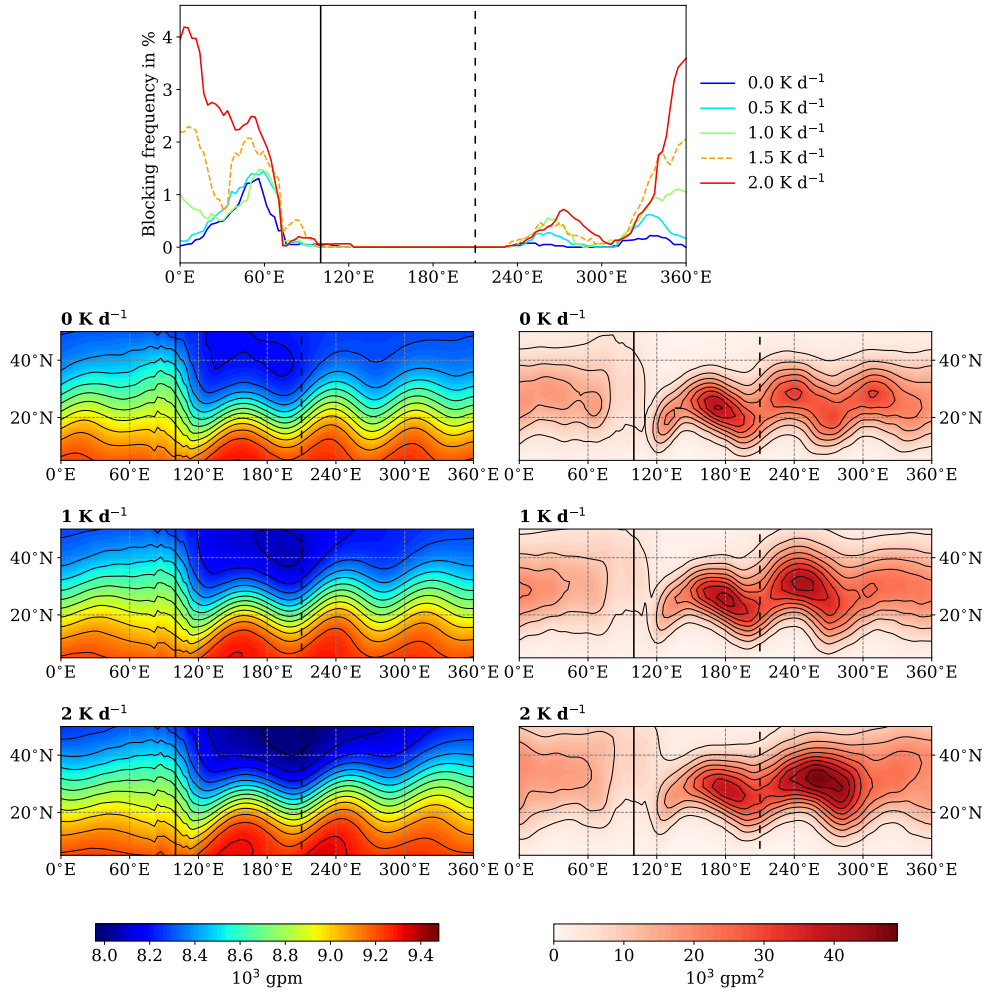

Figure 3.8.: Blocking climatology (top panel) for different heating dipole amplitudes between $0\,\mathrm{K\,d^{-1}}$ and $2\,\mathrm{K\,d^{-1}}$, with the mountain range located at 100°E and the heating dipole at 210°E. Because $1.5\,\mathrm{K\,d^{-1}}$ is the heating dipole amplitude used in all other experiments (e. g. Figure 3.4), the $1.5\,\mathrm{K\,d^{-1}}$ experiment is drawn as a dashed line. In the lower six panels climatologies of the 300 hPa geopotential height (on the left) and of the power spectral density of 300 hPa geopotential height integrated over periods of 2–6 days (on the right) are shown for heating dipole amplitudes of $0\,\mathrm{K\,d^{-1}}$, $1\,\mathrm{K\,d^{-1}}$ and $2\,\mathrm{K\,d^{-1}}$. Black contours are drawn every 100 gpm for geopotential height and every $5 \cdot 10^3\,\mathrm{gpm^2}$ for the 2–6 day variability. In all panels, the location of the mountain range is indicated by a solid black line, the location of the heating dipole by a dashed black line.

In Figure 3.8 geopotential height, storm track and blocking climatology are shown for different heating dipole amplitudes for the experiment with the mountain range at 100°E and the heating dipole at 210°E. Figures 3.9 and 3.10 show the same, but for the

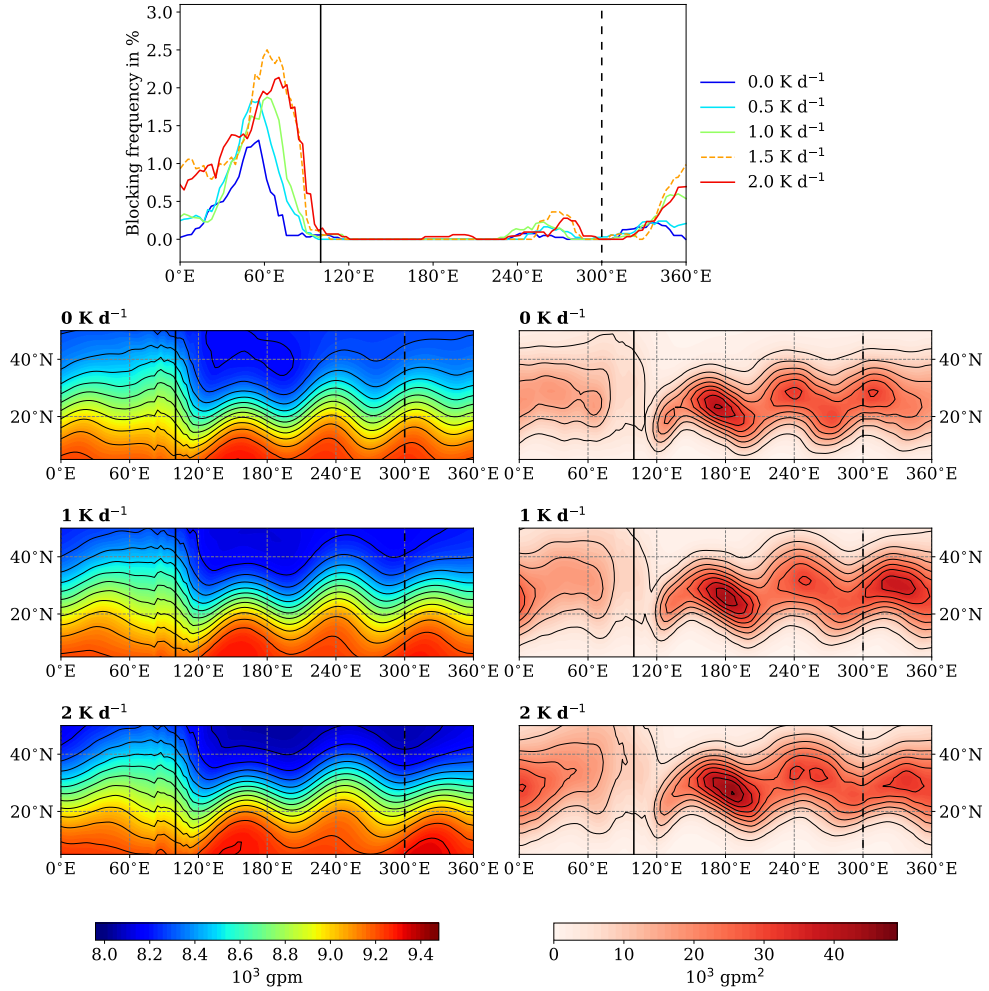

Figure 3.9.: As Figure 3.8, but for the heating dipole located at 300°E.

heating dipole at 300°E respectively 350°E. Here, the differences between the three configurations are much more notable than for the mountain height experiments.

The extent to which the heating dipole amplitude influences blocking frequency seems to be closely connected to the dipole's influence on the storm track. When the heating dipole is located at 210°E, there is a strong increase in blocking frequency with increasing amplitude of the heating dipole. With increasing amplitude there is also a strong intensification of the storm track branch downstream of the heating dipole (see Figure 3.8). For the configuration with the heating dipole at 300°E the increase in both storm track variability and blocking is reduced (see Figure 3.9), and when the dipole is located at 350°E there is no clear dependence of blocking frequency on the heating dipole amplitude, and only a weak dependence of the storm track variability on the amplitude (see Figure 3.10). The latter configuration was chosen because of the apparent blocking amplification around 260°E, but from Figure 3.10 it now becomes

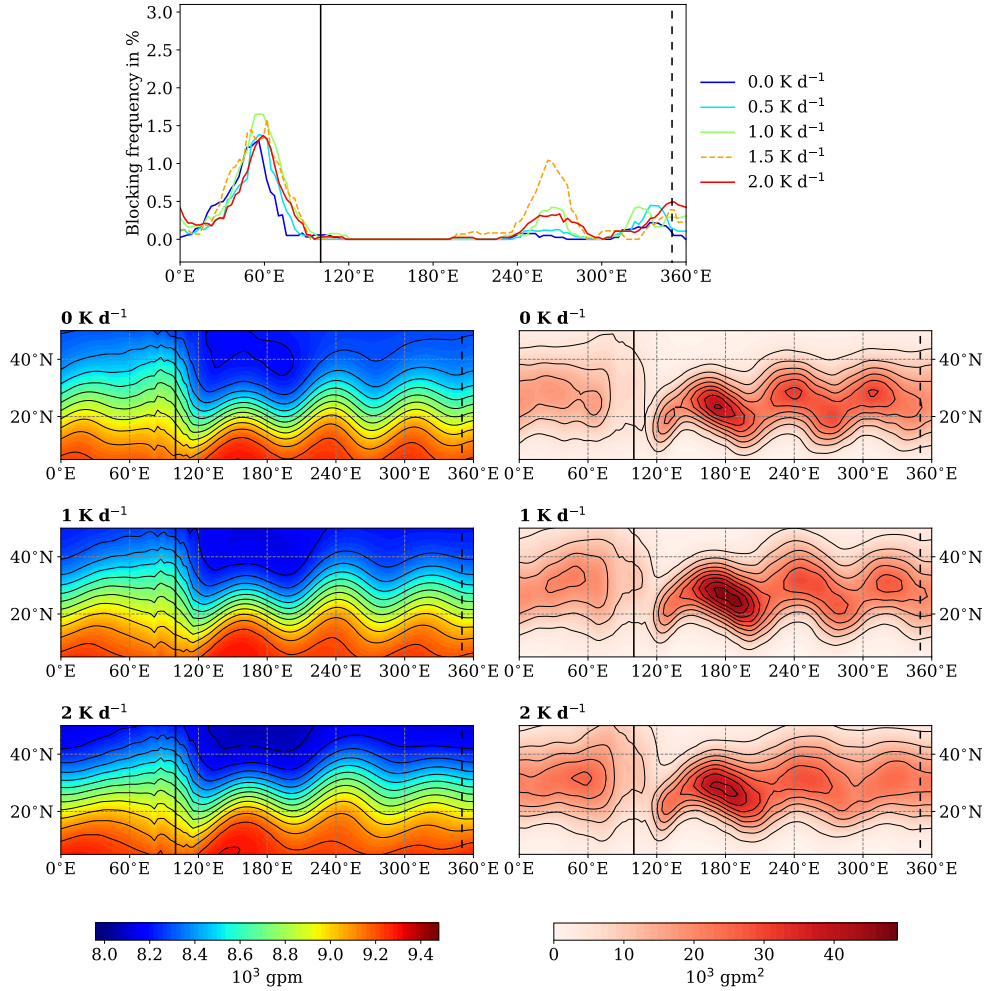

Figure 3.10.: As Figure 3.8, but for the heating dipole located at 350°E.

clear that the blocking frequency increase seen in the 1.5 K d^{-1} run is an outlier and does not appear in the runs with different heating dipole amplitudes.

The results from the runs with different heating dipole amplitudes confirm the earlier impression from Figure 3.4 that the heating dipole can have a strongly amplifying effect on blocking, but only if the heating dipole is located such that it can intensify the storm track upstream of the blocking region.

3.3. Influence of tropical heating anomalies

3.3.1. Reference run

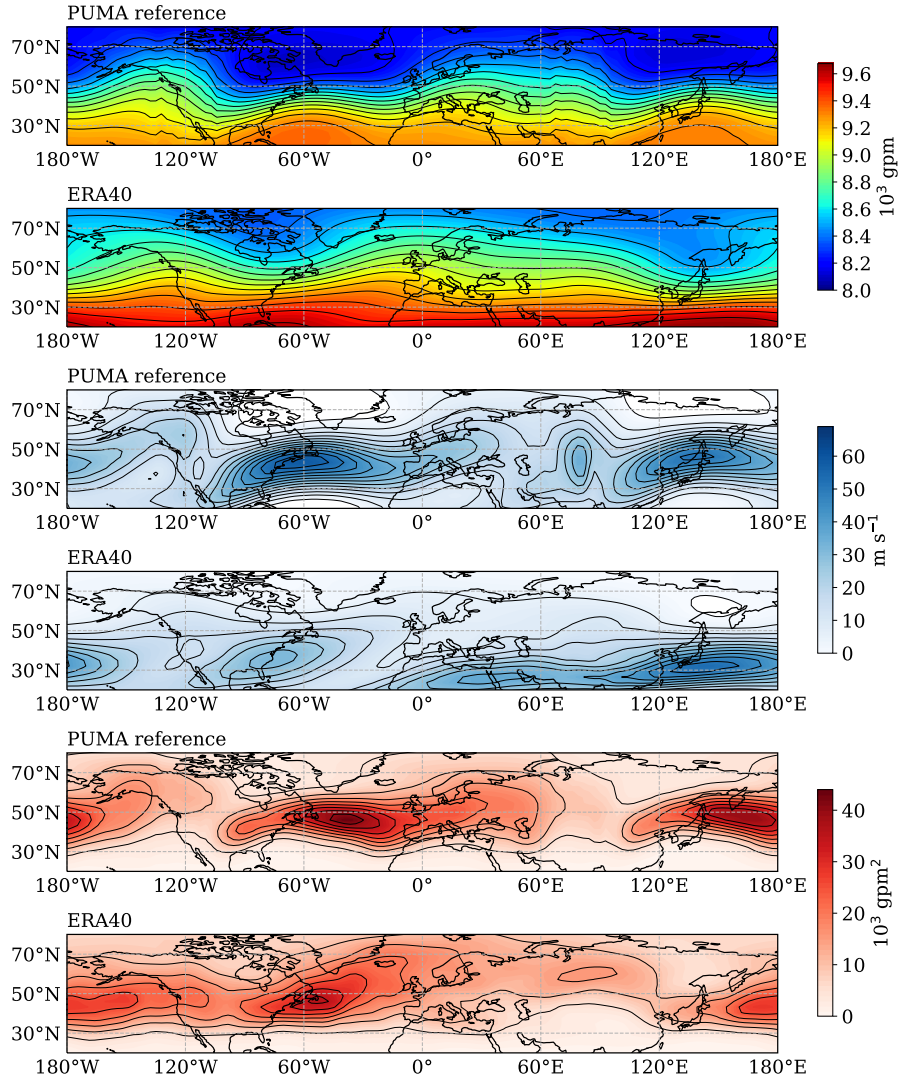

Figure 3.11.: Comparison between the PUMA reference run for the tropical heating sensitivity experiments and DJF ERA-40 reanalysis data (Kållberg et al., 2004). In the uppermost two panels, time mean geopotential height at 300 hPa is shown (black contours every 100 gpm) for respectively PUMA and ERA-40. In the third and fourth panel, time mean zonal wind at 300 hPa is shown (black contours every $5\,\mathrm{m\,s^{-1}}$). In the fifth and sixth panel, the power spectral density of 300 hPa geopotential height integrated over periods of 2–6 days is shown (black contours every $5 \cdot 10^3\,\mathrm{gpm}^2$). The continents in the PUMA panels are only drawn for comparison.

The reference run for the tropical heating sensitivity experiments is designed to re-

semble the Northern Hemisphere winter circulation. Therefore, a comparison of the reference run's geopotential height, zonal wind and storm track to ERA-40 data from December, January and February (DJF) is shown in Figure 3.11. Since PUMA is run without realistic continents, but instead with certain idealised features that deviate from the otherwise zonally symmetric configuration, it cannot be expected that the PUMA fields correspond exactly to the reanalysis fields. Generally, the main features are captured by the PUMA reference run: the two regions of a widening and decelerating jet stream over North America and Europe, the intensified jet cores over the Atlantic and the Pacific and the Atlantic and Pacific storm tracks. However, the jet exit region over the Atlantic is shifted to the east in the PUMA fields (where it is located rather over eastern Europe), and consequently the Atlantic jet stream and storm track are too strong and extend too far east as well. The Pacific storm track is shifted to the northwest in the PUMA reference run compared to ERA-40. These differences have to be kept in mind when results from the idealised PUMA experiments are compared to other blocking studies.

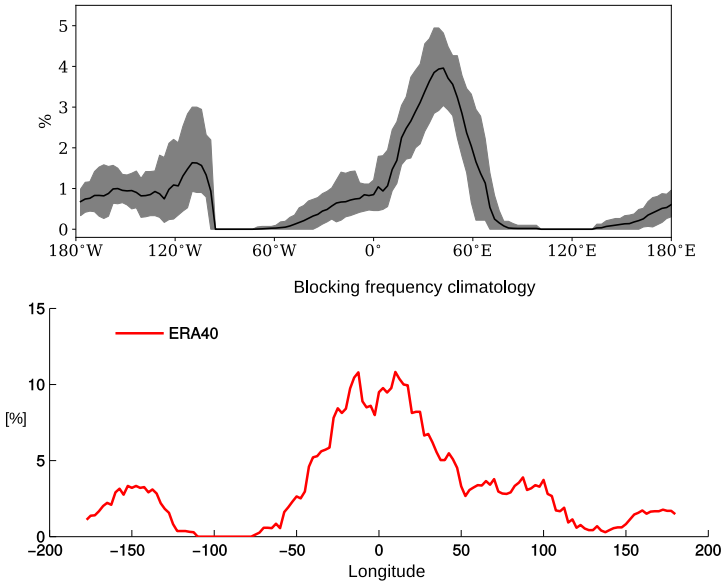

Figure 3.12.: Time mean Northern Hemisphere winter blocking frequency along the storm track, in black for the PUMA reference run (upper panel) and in red for ERA-40 (lower panel, DJF data only, figure from G. Gollan, cf. Gollan et al., 2015). The grey shading in the upper panel indicates a 95% confidence interval for 20-year blocking frequency means obtained by Monte Carlo simulations.

In Figure 3.12 the blocking climatology along the storm track is displayed for the PUMA reference experiment and for ERA-40 winter data. There is a large difference in the total values; the PUMA blocking frequencies are about half as high as those from ERA-40. The general shape is reasonably similar, though: both climatologies exhibit a large maximum over Europe and a smaller maximum over the Pacific. The European

maximum is shifted to the east in the PUMA climatology, which is consistent with the eastward shift of the jet exit region (cf. Figure 3.11). The grey shading around the PUMA blocking climatology indicates the 95% confidence interval for 20-year blocking frequency means, obtained by Monte Carlo simulations. (Multiple 20-year means were taken from the reference run that is in total 270 years long, assuming that the blocking frequency in one year is sufficiently independent from the blocking frequency in the adjacent years, and the upper and lower 2.5% of the obtained values for each latitude were excluded from the range to get the 95% confidence interval. The same method was applied to the two-dimensional blocking frequencies – see Figure 3.14.)

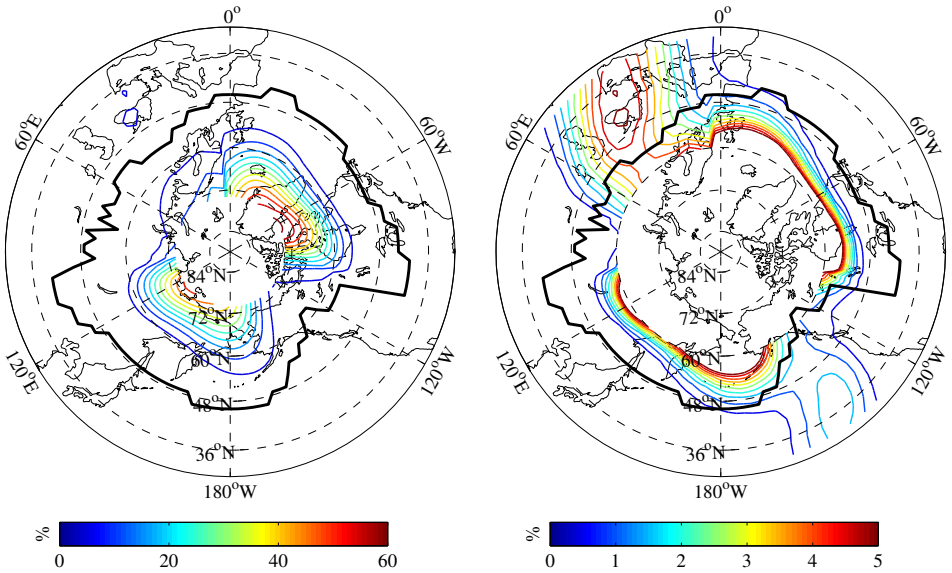

Figure 3.13.: Two-dimensional blocking climatology from the reference run. The right panel shows the blocking climatology only in mid-latitudes with a different colour scale because of the much smaller values of mid-latitude blocking frequency. Contours are drawn every 5% (left panel) and every 0.5% (right panel). The thick black line shows the location of the CBL. Realistic continents are only drawn for better orientation.

To get a more detailed picture of tropical influence on blocking, as well as to facilitate comparison with other studies that have examined the influence of tropical heating on blocking (e. g. Henderson et al., 2016; and Gollan and Greatbatch, 2017), a two-dimensional blocking index is used for the following sensitivity experiments. The one-dimensional index along the storm track is always shown additionally, to ensure consistency. In Figure 3.13 the two-dimensional blocking climatology from the PUMA reference experiment is shown. The high-latitude blocking exhibits two maxima over Greenland and Siberia that correspond well to winter high-latitude blocking from ERA reanalysis data (cf. Figure 1.1 and Gollan and Greatbatch, 2017), except that the Greenland blocking peak is overestimated and the Siberian peak is underestimated by PUMA. The mid-latitude blocking climatology (right panel) shows the two maxima

over Europe and the Pacific that are also visible in the one-dimensional climatology along the storm track (Figure 3.12).

The width of the 95% confidence interval for the two-dimensional reference blocking climatology is shown in Figure 3.14.

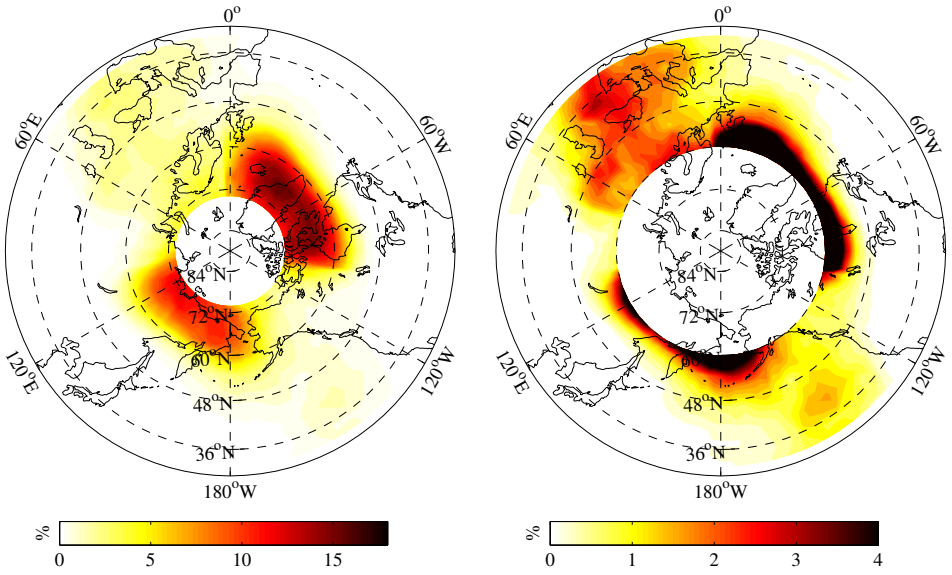

Figure 3.14.: Width of the 95% confidence interval for the two-dimensional blocking climatology from the reference run. The right panel shows only mid-latitude values with a different colour scale for clarity. Realistic continents are only drawn for better orientation.

3.3.2. Location of equatorial heating anomaly

In the first series of experiments, the general influence of a tropical heating anomaly on blocking depending on the heating's location is examined. This is done for a positive and a negative equatorial heating anomaly (corresponding to e. g. anomalous, enhanced convective precipitation, respectively an anomalous lack of precipitation). Due to the large number of experiments, only one-dimensional blocking along the storm track is analysed.

Positive equatorial heating anomaly

In Figure 3.15, blocking climatologies for 36 model runs with a positive heating anomaly centred at different longitudes above the equator are shown. Black dots indicate where the difference to the reference run is significant, i. e. the climatology lies outside the 95% confidence interval for the reference run (see Figure 3.12). The largest change can be seen for European blocking that is strongly decreased when the

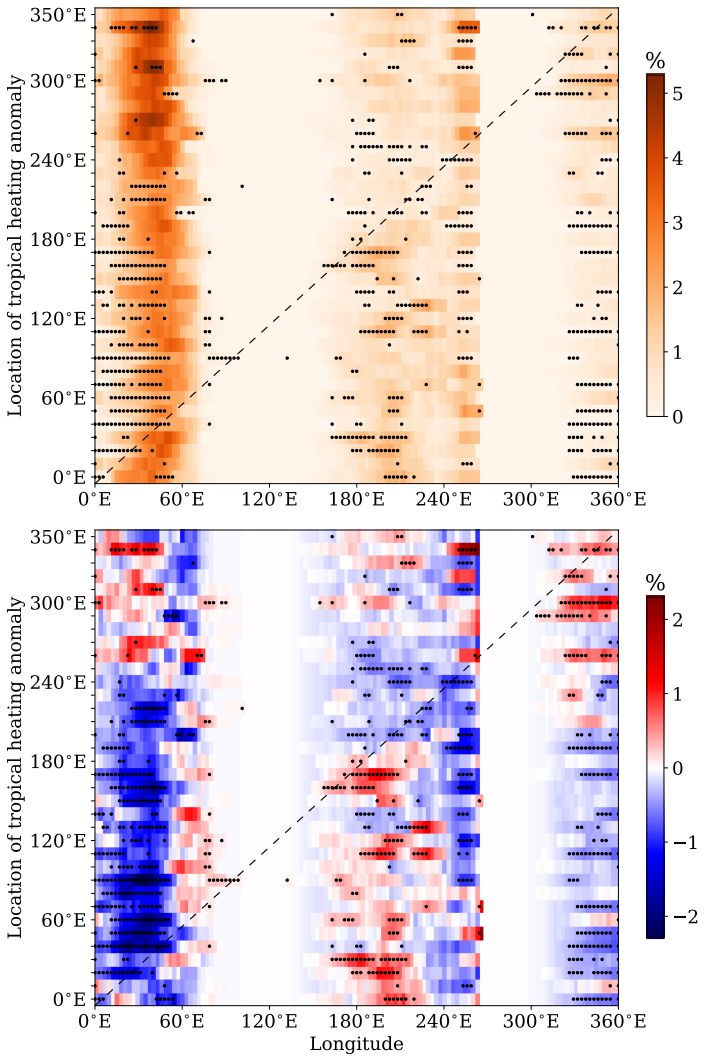

Figure 3.15.: Blocking climatologies for different locations of a positive equatorial heating anomaly. In the upper panel, the absolute blocking frequency is shown. In the lower panel, the blocking frequency of the reference run has been subtracted; i. e. blue colours indicate a decrease in blocking frequency due to the equatorial heating anomaly and red colours indicate an increase in blocking frequency due to the heating anomaly. The location of the equatorial heating anomaly is in both panels indicated by the dashed line. Black dots are drawn where the difference to the reference climatology exceeds the 95% confidence interval (cf. Figure 3.12).

positive equatorial heating anomaly is located between 20°E and 220°E, i. e. over the Indian Ocean, the Maritime Continent or the western Pacific. There seems to be an increase in European blocking when the heating anomaly is located between 260°E and 340°E, i. e. over the eastern Pacific or western Atlantic, but this is not as clear. The changes in Pacific blocking frequency are not very clear either, but there seems to be an increase in blocking when the equatorial heating anomaly is located between

0°E and 170°E, i. e. over Africa, the Indian Ocean or the Maritime Continent, and a decrease in Pacific blocking for the heating anomaly located between 200°E and 270°E, i. e. over the eastern Pacific.

Negative equatorial heating anomaly

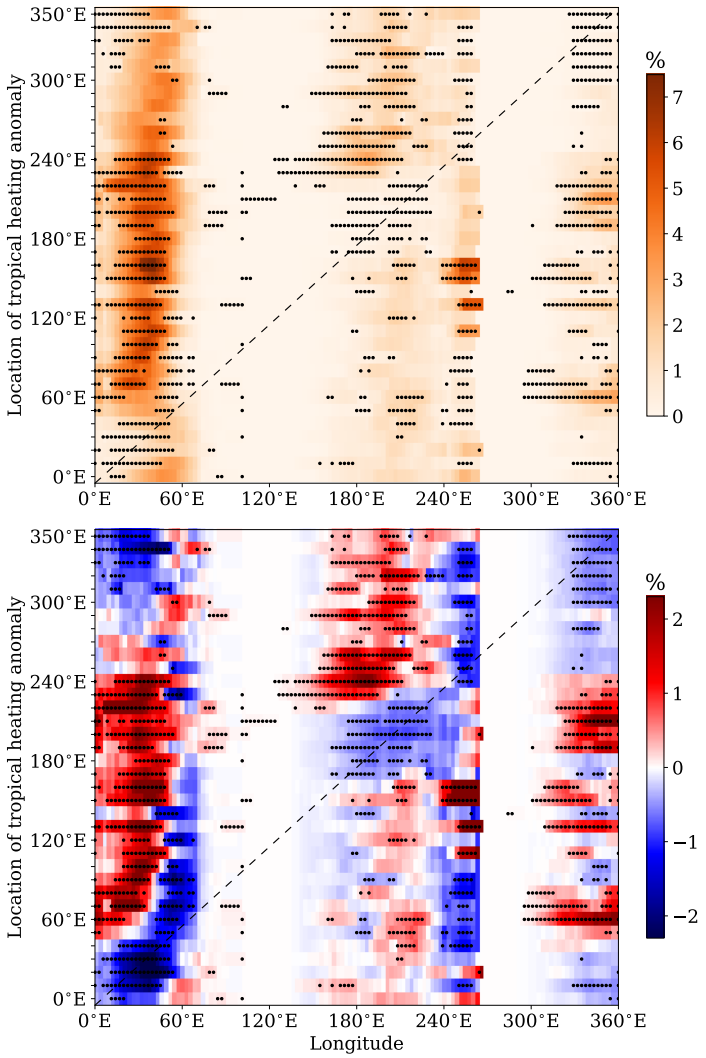

Figure 3.16.: As Figure 3.15, but for a negative equatorial heating anomaly.

In Figure 3.16, blocking climatologies are shown for a negative heating anomaly centred at different longitudes above the equator. Interestingly, the changes in blocking frequency due to the negative equatorial heating anomaly are larger and more clear than the changes due to the positive anomaly in Figure 3.15. The negative heating anomaly leads to an increase in Atlantic blocking frequency when it is located between 60°E and 240°E, i. e. over the Indian Ocean, the Maritime Continent, the

western or central Pacific, and to a decrease in Atlantic blocking when it is located between 310°E and 40°E, i. e. over the Atlantic or Africa. Pacific blocking frequency is increased when the negative equatorial anomaly is located between 230°E and 350°E, i. e. over the eastern Pacific, South America or the Atlantic, and it is decreased when the anomaly is located between 170°E and 220°E, i. e. over the central Pacific.

Apart from these distinct influences, a larger pattern can be seen in Figure 3.16: the negative equatorial heating anomaly leads to a decrease in mid-latitude blocking at its own longitude and to an increase in mid-latitude blocking west of its location.

In the following, the influence of tropical heating anomalies on blocking in the simplified PUMA setup is analysed in more detail. This is done with the help of experiments that are based on ENSO and the MJO as important modes of tropical variability, and on the multi-model tropical precipitation bias of the CMIP5 general circulation models.

3.3.3. ENSO-like anomaly

In Figure 3.17 the one-dimensional blocking climatology along the storm track, geopotential height and storm track are shown for different model runs with a tropical Pacific heating anomaly based on El Niño respectively La Niña. Although the heating anomaly now has a larger zonal extent than that described in the last section, there is good agreement between the blocking climatologies for the La Niña experiments and the results described in Section 3.3.2 (the ENSO anomalies are centred at 190°E, for comparison with Figure 3.16). There is a significant increase in European blocking frequency and a significant decrease in Pacific blocking frequency in the La Niña experiments, which is consistent with the change in blocking frequency for a negative Pacific equatorial heating anomaly in Figure 3.16. The increase in European blocking frequency associated with La Niña becomes larger with increasing (negative) amplitude, which enhances confidence in the result.

For El Niño, the change in blocking frequency is much smaller. For both Pacific and Atlantic blocking there seems to be a small decrease in blocking frequency, which is, however, mostly not significant. This supports the impression from Section 3.3.2 that the influence of equatorial heating on blocking is not linear, but that a positive equatorial heating anomaly generally has less influence on blocking than a negative heating anomaly.

An El Niño anomaly is accompanied by a stronger meridional geopotential height gradient in the PUMA fields, whereas for La Niña the gradient is weakened. Consistent with this, the storm tracks are generally stronger with an El Niño anomaly than with a La Niña anomaly. Over Europe, the jet stream decelerates and widens in the La Niña runs, which can explain the increase in European mid-latitude blocking frequency.

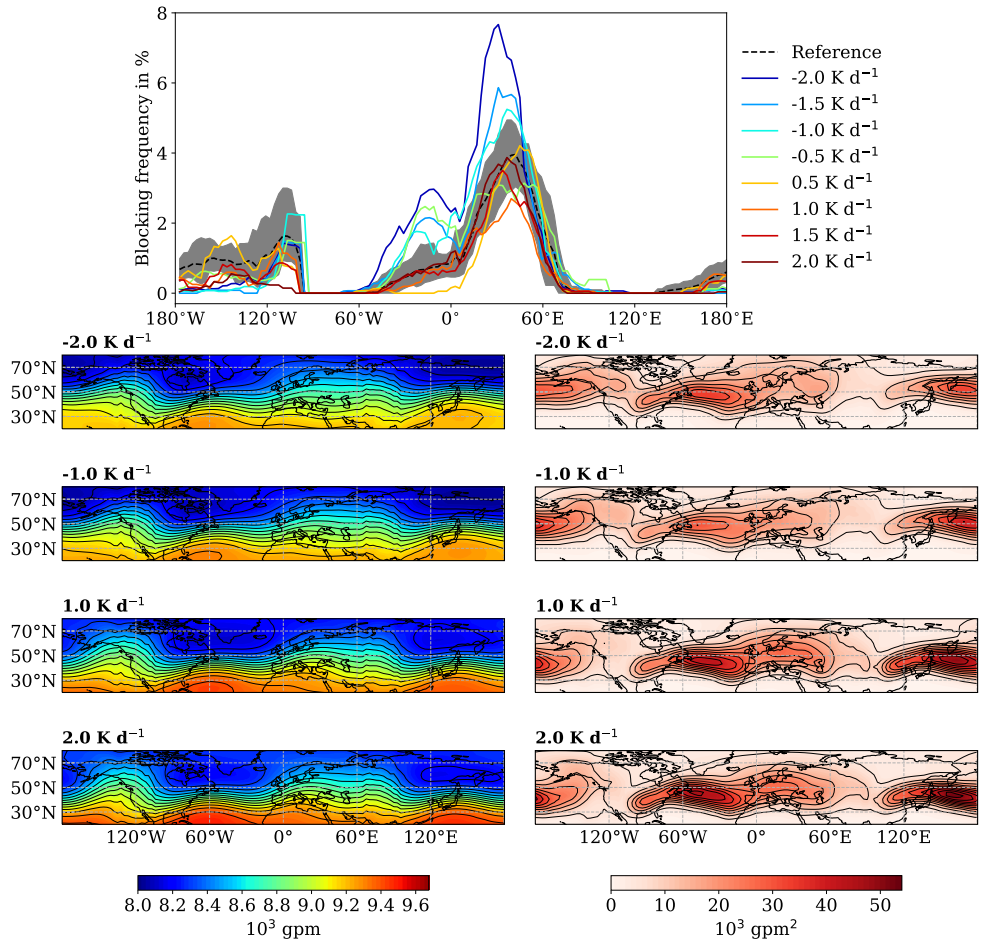

Figure 3.17.: Blocking climatology along the storm track, climatological geopotential height and storm tracks for El Niño and La Niña experiments with different amplitudes. In the top panel, blocking climatologies for the different experiments are shown in colour (blue to green colours correspond to La Niña, orange to red colours to El Niño). The reference blocking climatology is drawn as a dashed black line, with the 95% confidence interval as grey shading. In the lower panels, 300 hPa time mean geopotential height is shown on the left (black contours every 100 gpm), and the time mean power spectral density of 300 hPa geopotential height integrated over periods of 2–6 days on the right (black contours every $5 \cdot 10^3$ gpm^2). Realistic continents are only drawn for better orientation.

Positive heating anomaly (El Niño)

Two-dimensional blocking frequency fields are now examined for selected ENSO model runs, to obtain a more detailed impression of the blocking changes also at higher latitudes. Additionally for the selected model runs, geopotential height anomalies relative to the reference run are shown for the extratropical Northern Hemisphere to detect changes in the mean state also outside of the storm track region that was the

main focus before. In the following analysis, the El Niño run with a heating anomaly amplitude of 1.5 $\mathrm{K\,d^{-1}}$ is used.

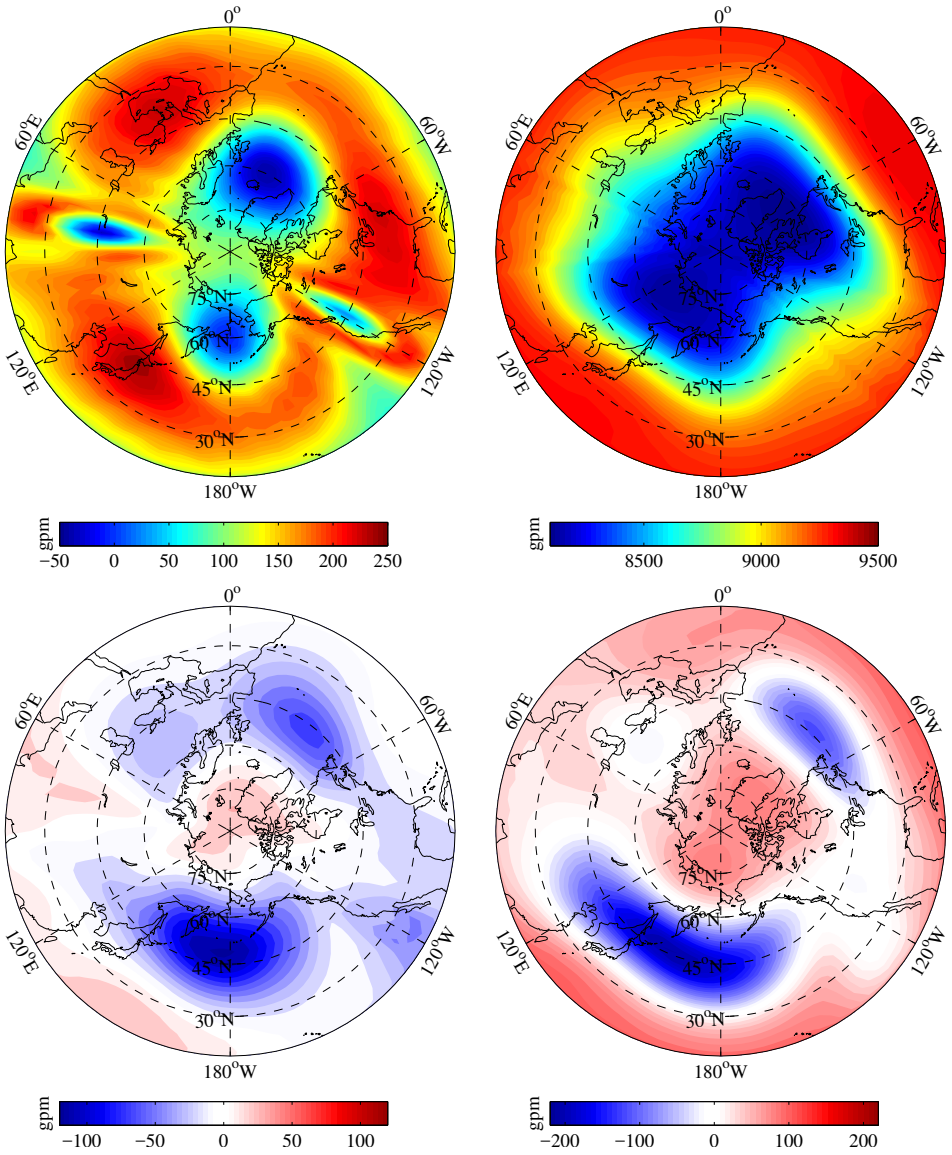

Figure 3.18.: Time mean geopotential height at 1000 hPa (left panels) and 300 hPa (right panels), with absolute fields from the reference run (top panels), and difference between the 1.5 $\mathrm{K\,d^{-1}}$ El Niño and the reference run (bottom panels). Realistic continents are only drawn for better orientation.

Figure 3.18 shows the climatological geopotential height field from the reference run at 1000 hPa (top left panel) and 300 hPa (top right panel). All geopotential height anomalies shown in the following are calculated relative to these fields. Displayed in the bottom panels of Figure 3.18 are the climatological geopotential height anomalies of the El Niño run relative to the reference run. The most dominant features of the 1000 hPa anomaly field are negative anomalies over the northern parts of both Pacific

and Atlantic. These patches of reduced geopotential height also appear in the 300 hPa anomaly field, where they are accompanied by positive anomalies to the north and south that are not as clear in the 1000 hPa anomaly field. The deepened Aleutian low, together with the positive geopotential height anomaly to the south, are the Pacific part of the positive Pacific North American (PNA) pattern that is usually associated with El Niño (cf. e. g. Philander, 1990, pp. 48–50). In PUMA, however, the wave train does not bend southward over the North American continent as for the real PNA pattern, but instead continues towards the North Atlantic. Due to this, the pattern in the model is also reminiscent of the Northern Annular Mode (NAM) or Arctic Oscillation (AO) in its negative phase (cf. e. g. Thompson and Wallace, 1998; and Wallace and Thompson, 2002).

In the climatological 1000 hPa geopotential height field of the reference run, small-amplitude wavelike features can be seen especially over the Pacific, but also over the eastern part of North America (see the upper left panel of Figure 3.18). These features are 'spectral ripples' or 'Gibbs ripples' (cf. Hoskins, 1980; Lindberg and Broccoli, 1996), spurious maxima and minima that appear in spectral models as soon as topography is introduced. The ripples appear over regions where the topography is flat (e. g. oceans), because of the truncation of the spherical harmonics – in order to represent both regions with topography and entirely flat regions, the number of spherical harmonics included in the approximation would need to approach infinity (see also Randall, 2015). The spectral ripples are present in all PUMA runs with mountain ranges, but are usually sufficiently small compared to physically meaningful variability.

In Figure 3.19, the change in two-dimensional blocking frequency in the El Niño run relative to the reference run is shown. When an El Niño-like positive heating anomaly is present in the equatorial Pacific, high-latitude blocking is increased in PUMA, both over Greenland and over Siberia. In mid-latitudes, the positive Pacific heating anomaly leads to significantly reduced blocking frequency over eastern Europe and the eastern Pacific, although the latter change is located south of the climatological storm track. Similar to high-latitude blocking, blocking events south of the storm track are not necessarily 'classical' blocking events in the sense that they block the westerly jet stream and the progression of the embedded storm systems (cf. e. g. Woollings et al., 2008; and Tibaldi and Molteni, 2018), except in cases when the storm track departs from its climatological position far enough.

The changes in blocking frequency in the PUMA simulations due to an El Niño-like positive heating anomaly in the tropical Pacific show some similarities to blocking changes found by Gollan and Greatbatch (2017), which can be seen in the left panels of Figure 3.22. The most striking similarity is the enhanced blocking frequency over the northern Pacific and Siberia. However, other features of the El Niño influence on blocking that are visible in Figure 3.22 are not captured by the PUMA run at all; most prominently the large decrease in blocking frequency over northern Canada

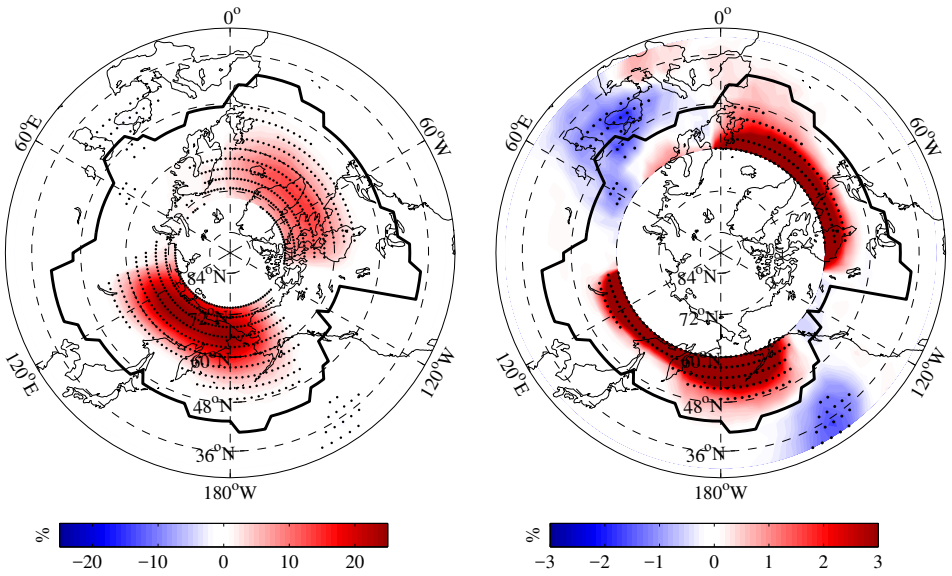

Figure 3.19.: Difference in two-dimensional blocking climatology between the $1.5\,\mathrm{K\,d^{-1}}$ El Niño run and the reference run. The right panel shows only mid-latitude values with a different colour scale for clarity. Black dots indicate significant differences from the reference run, i. e. values that lie outside the 95% confidence interval shown in Figure 3.14. The thick black line shows the location of the CBL. Realistic continents are only drawn for better orientation.

and the somewhat smaller blocking frequency decrease over the central/eastern Asian continent. The change over northern Canada is even reversed in the PUMA run, which exhibits a significant blocking increase that extends over the entire northern Atlantic. Possible causes for this large difference are discussed in Chapter 4. Over Europe, the blocking changes found by Gollan and Greatbatch (2017) are not significant and rather opposite in model (shown in the lower left panel of Figure 3.22) and reanalysis data. In the model simulations of Gollan and Greatbatch (2017) there seems to be a decrease in European blocking associated with El Niño (Figure 3.22, lower left panel) that could correspond to the European blocking decrease found in the PUMA experiment (Figure 3.19). This is, however, not confirmed by the analysis of the ERA data that shows a weak increase in European blocking (Figure 3.22, upper left panel).

Negative heating anomaly (La Niña)

From the negative ENSO runs, the run with a heating anomaly amplitude of -1.5 $\mathrm{K\,d^{-1}}$ has been selected for further analysis.

Figure 3.20 shows the climatological difference in geopotential height between the La Niña run and the reference run. In the 1000 hPa field, a wave train emerges, consisting

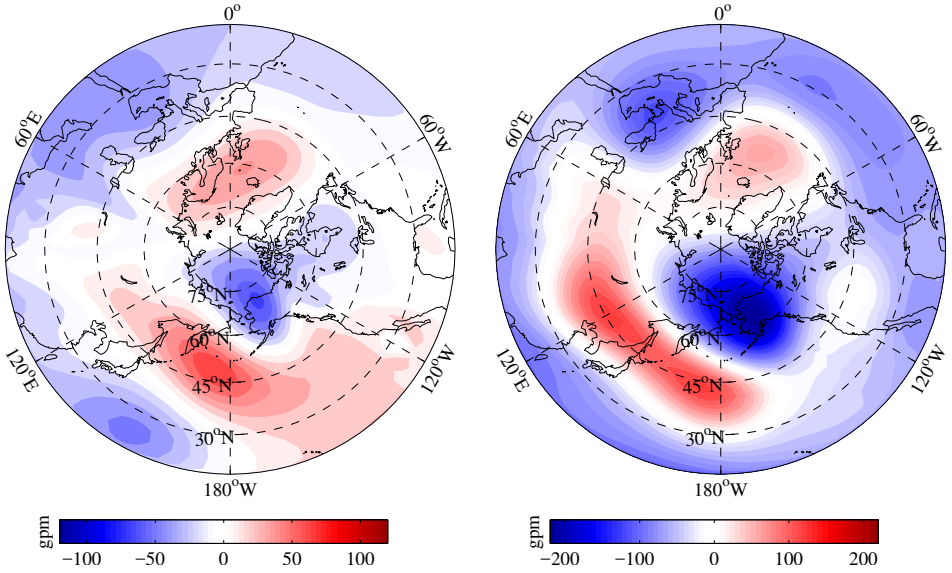

Figure 3.20.: Time mean geopotential height difference at 1000 hPa (left panel) and 300 hPa (right panel) between the 1.5 K d^{-1} La Niña run and the reference run. Realistic continents are only drawn for better orientation.

of alternating negative and positive anomalies that extend from the eastern tropical Pacific over Alaska and northern Europe until the Mediterranean. The wave train is also visible in the 300 hPa field, where it is accompanied by a negative anomaly present at all longitudes in the tropics that is probably the direct effect of the negative tropical heating. Over the Pacific and Alaska, the wave train is reminiscent of the Pacific North American (PNA) pattern in its negative phase (cf. Wallace and Gutzler, 1981), but it is shifted towards the west, and a positive anomaly over the southern part of North America, that usually constitutes the fourth center of action of the PNA, is absent. Instead, the wave train bends towards northern Europe in the PUMA fields. When the climatological location of the jet stream is taken into account (see Figure 3.21, where the CBL is shown), the 300 hPa geopotential height field implies a strengthening of the westerly jet over the central Pacific, and a weakening of the westerly jet over the Atlantic, which is consistent with the blocking increase over Europe and the blocking decrease over the Pacific visible in Figures 3.17 and 3.21.

The change in two-dimensional blocking frequency due to the negative heating anomaly in the tropical Pacific is shown in Figure 3.21. As already visible in Figure 3.17, there is a significant increase in European and Atlantic blocking frequency and a significant decrease in eastern Pacific blocking frequency along the storm track. At higher latitudes, there is a large blocking frequency decrease over the northern Pacific and Siberia that is, apart from its opposite sign, very similar in both shape and amplitude to the high-latitude Asian/Pacific blocking anomaly due to El Niño (Figure 3.19). Over the northern Atlantic and Greenland, however, the blocking changes are not opposite to those visible in Figure 3.19; instead, there is a decrease in blocking frequency

north of about 70°N and a blocking increase south of that, the latter extending from eastern Canada to eastern Europe. From Figures 3.19 and 3.21, it thus seems that in the case of the ENSO experiments the afore-noted nonlinearity of the tropical heating impact on blocking is primarily true for Atlantic blocking.

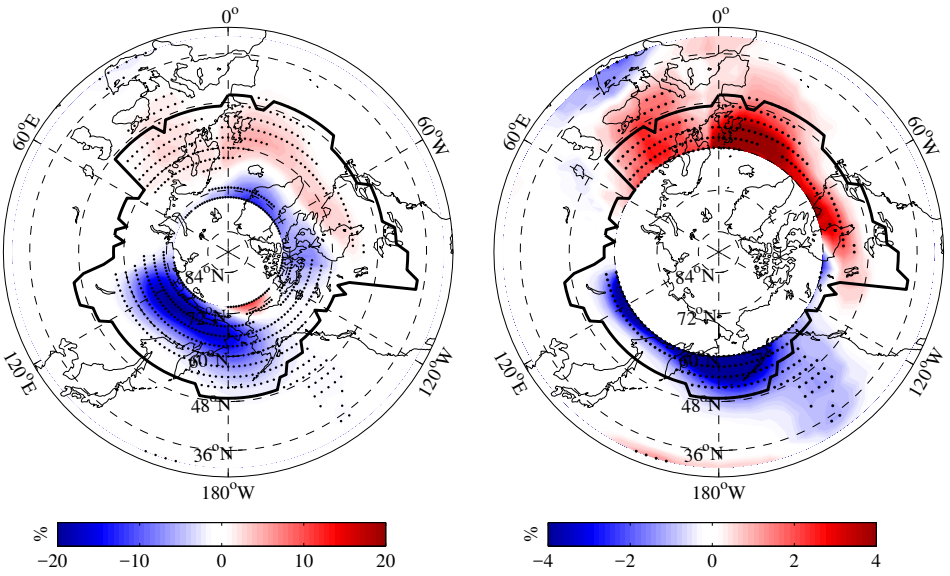

Figure 3.21.: Difference in two-dimensional blocking climatology between the $1.5\,\mathrm{K\,d^{-1}}$ La Niña run and the reference run. The right panel shows only mid-latitude values with a different colour scale for clarity. Black dots indicate significant differences from the reference run, i. e. values that lie outside the 95% confidence interval shown in Figure 3.14. The thick black line shows the location of the CBL. Realistic continents are only drawn for better orientation.

Overall, the blocking changes in the La Niña PUMA run correspond better to the results from Gollan and Greatbatch (2017) than for the El Niño case. The changes in Northern Hemisphere winter blocking frequency associated with La Niña that were found by Gollan and Greatbatch (2017) are shown in the right panels of Figure 3.22. In both model and reanalysis data they find a large decrease in north Pacific blocking frequency that is very similar to the north Pacific blocking decrease in PUMA except that the latter is slightly westward shifted. The small region of significantly enhanced blocking frequency north of Alaska that is present in the PUMA run (Figure 3.21) also appears in the reanalysis data of Gollan and Greatbatch (2017), although not very clearly in their model data (Figure 3.22). There is some increase of European blocking in both model and reanalysis visible in Figure 3.22, but it is not as significant as in the PUMA run. The overall pattern of increased blocking over central Europe and reduced blocking to the north is also visible in the results of Gollan and Greatbatch (2017), but the pattern is located further south in the reanalysis data than in their model and the PUMA run. The largest difference between the PUMA run and the Gollan and Greatbatch (2017) results can be seen over the Atlantic, where a significant

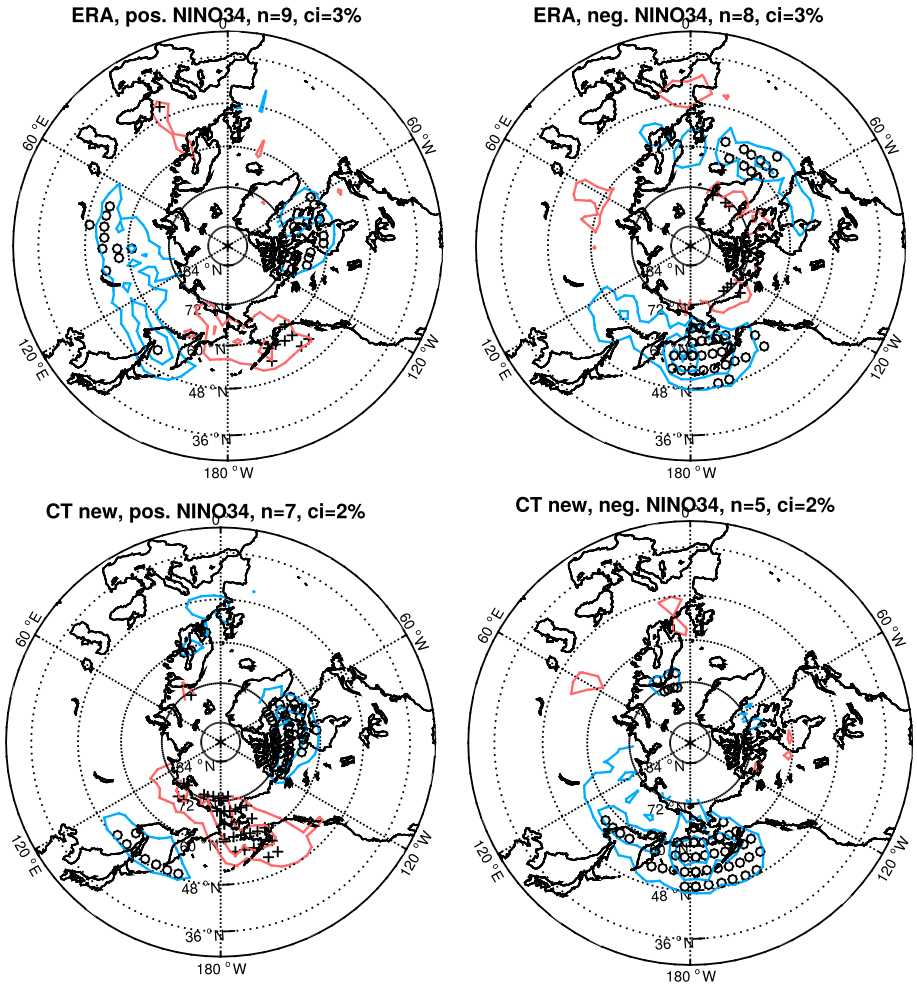

Figure 3.22.: Composites of anomalous DJF blocking frequency in combined ERA-40/ERA-Interim data (top panels) and in model simulations performed by Gollan and Greatbatch (2017) with the ECMWF Integrated Forecast System (bottom panels). The figure is taken from Gollan and Greatbatch (2017). The composites are calculated with respect to the Niño-3.4 index; composites for positive events (i. e. El Niño) are shown in the left panels, composites for negative events (i. e. La Niña) in the right panels. Contours are drawn every 4% for the ERA data and every 2% for the model data, the zero contour is omitted. Red contours indicate enhanced blocking, blue contours indicate decreased blocking; crosses or circles are drawn where the changes are significant. For more details see Gollan and Greatbatch (2017).

increase in blocking frequency appears in the PUMA run, whereas the reanalysis data exhibits a significant decrease in blocking frequency. For a discussion of possible reasons for this difference see Chapter 4.

3.3.4. MJO-like anomaly

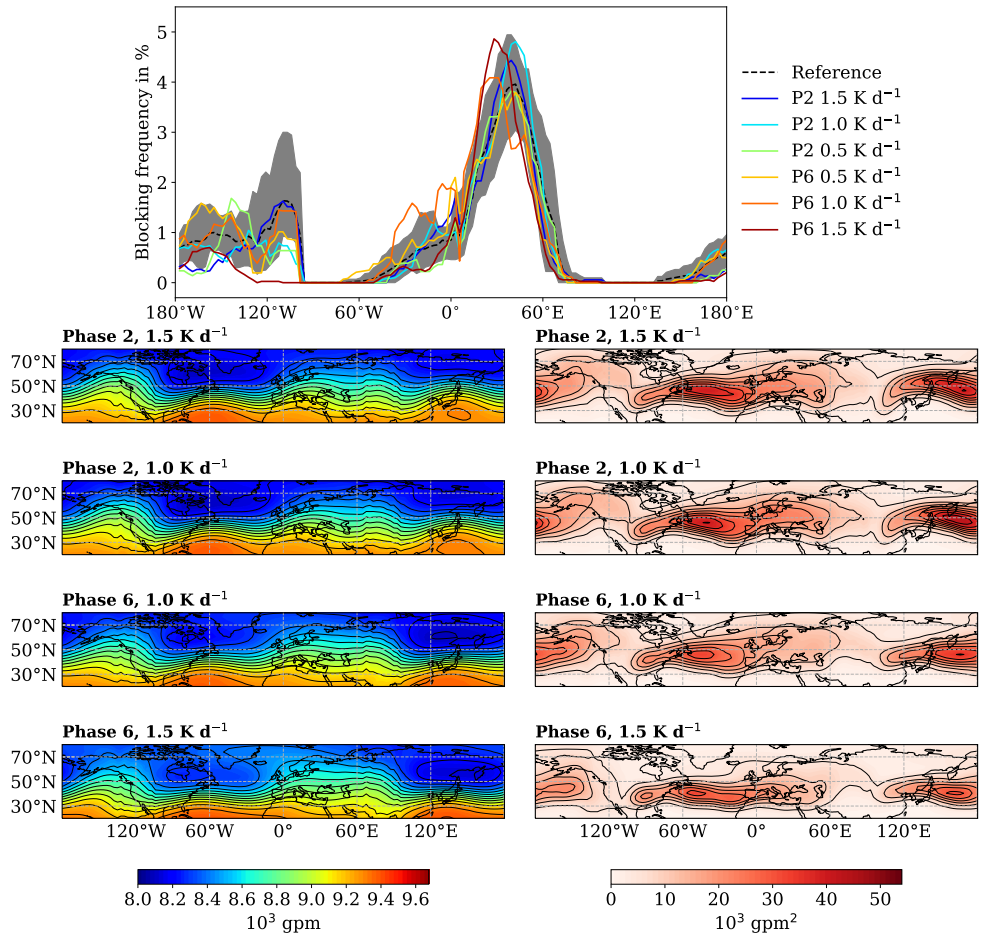

Figure 3.23.: Blocking climatology along the storm track, climatological geopotential height and storm tracks for MJO phase 2 and 6 experiments with different amplitudes. In the top panel, blocking climatologies for the different experiments are shown in colour (blue to green colours correspond to MJO phase 2, orange to red colours to MJO phase 6). The reference blocking climatology is drawn as a dashed black line, with the 95% confidence interval as grey shading. In the lower panels, 300 hPa time mean geopotential height is shown on the left (black contours every 100 gpm), and the time mean power spectral density of 300 hPa geopotential height integrated over periods of 2–6 days on the right (black contours every $5 \cdot 10^3$ gpm^2). Realistic continents are only drawn for better orientation.

In Figure 3.23 the one-dimensional blocking climatology along the storm track, climatological geopotential height and storm track are displayed for different model runs with idealised tropical heating anomalies resembling MJO phases 2 and 6. The changes in blocking frequency along the storm track are for both phases rather small and not as clear as for example the changes associated with La Niña. However, especially over the Atlantic and Europe some significant changes emerge. Both MJO

phases seem to be associated with increased blocking frequency around the peak of the blocking climatology at about 50°E. This increase is accompanied by a slight shift of the blocking peak; eastward for phase 2 and westward for phase 6. For phase 2, the blocking increase is fairly narrowly confined, whereas for phase 6 the blocking increase extends westward over the Atlantic. In the Pacific region, the picture is not very clear, but there seems to be a blocking decrease associated with phase 2 over the central Pacific.

Also the impact of the MJO heating anomalies on the mean state is less obvious than for the ENSO experiments. There is an eastward shift of the jet exit over Europe for phase 6 compared to phase 2, which coincides with the eastward shift of the blocking peak. Additionally, the jet stream widens considerably more over Europe for phase 6 than for phase 2; in the phase 6 $1.5\,\mathrm{K\,d^{-1}}$ run there is even a climatological reversal of the meridional geopotential height gradient west of Iceland. The storm track is weaker for phase 6 than for phase 2, both over the Pacific and the Atlantic, and shifted towards the south.

Phase 2

For a more detailed analysis of the MJO influence on blocking, the experiment with a heating anomaly amplitude of $1\,\mathrm{K\,d^{-1}}$ is chosen for each of the two phases. In Figure 3.24 the climatological geopotential height anomaly of the MJO phase 2 run is shown. Neither at 1000 hPa nor at 300 hPa, the differences to the reference run are large (the colour scale is chosen to match the colour scale of the phase 6 geopotential height anomaly shown in Figure 3.28 that is much stronger). There is a broad but weak negative anomaly over the Atlantic and Europe at both heights, and a weak positive anomaly over eastern Asia at 300 hPa that is almost absent at 1000 hPa.

The difference in two-dimensional blocking climatology between the MJO phase 2 run and the reference run is shown in Figure 3.25. In the model run including the phase 2 heating dipole anomaly, there is increased high-latitude blocking over the northern Atlantic and Greenland, and decreased high-latitude blocking over Siberia. Along the storm track there is not much change in blocking frequency, except over eastern Europe where a small but significant blocking increase is visible as in Figure 3.23. South of the storm track there is reduced blocking over the Mediterranean and enhanced blocking over the eastern Pacific, but this is, as mentioned before, probably not associated with classical blocking events.

The changes in PUMA blocking frequency due to the MJO phase 2 heating dipole anomaly compare well with model results from Gollan and Greatbatch (2017) that are shown in the right panel of Figure 3.26. They also find enhanced high-latitude blocking over the northern Atlantic and Greenland and decreased high-latitude blocking over the northern Pacific and Siberia, as well as decreased blocking frequency over

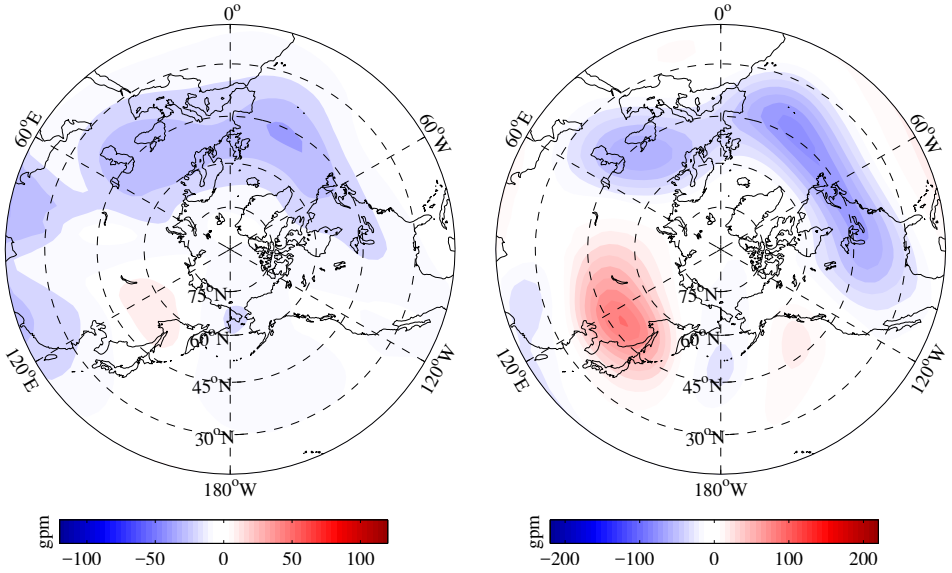

Figure 3.24.: Time mean geopotential height difference at 1000 hPa (left panel) and 300 hPa (right panel) between the 1.0 K d^{-1} MJO phase 2 run and the reference run. Realistic continents are only drawn for better orientation.

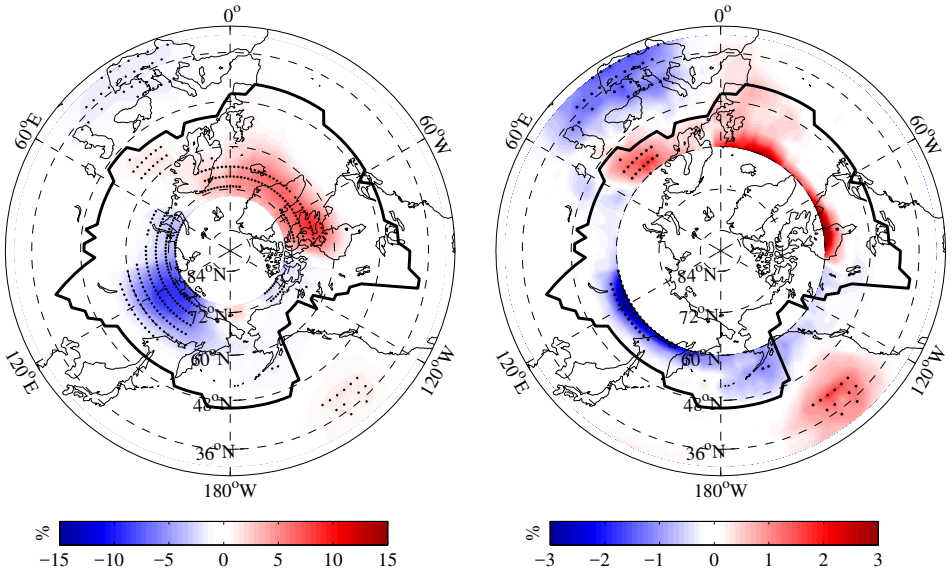

Figure 3.25.: Difference in two-dimensional blocking climatology between the 1.0 K d^{-1} MJO phase 2 run and the reference run. The right panel shows only mid-latitude values with a different colour scale for clarity. Black dots indicate significant differences from the reference run, i. e. values that lie outside the 95% confidence interval shown in Figure 3.14. The thick black line shows the location of the CBL. Realistic continents are only drawn for better orientation.

southern Europe, although this is located further west than in the PUMA run probably because of the high degree of idealisation in the latter. Only the enhanced blocking frequency over the Asian continent that is visible in the right panel of Figure 3.26 does not appear in the PUMA results in Figure 3.25. However, the investigation of reanalysis data by Gollan and Greatbatch (2017) gives blocking changes associated with MJO phase 2 that are less clear and somewhat different than in their model and in the PUMA run. There rather emerges the impression of an almost hemispheric decrease of blocking from the left panel of Figure 3.26, where the reanalysis results are shown, although the change is not everywhere significant.

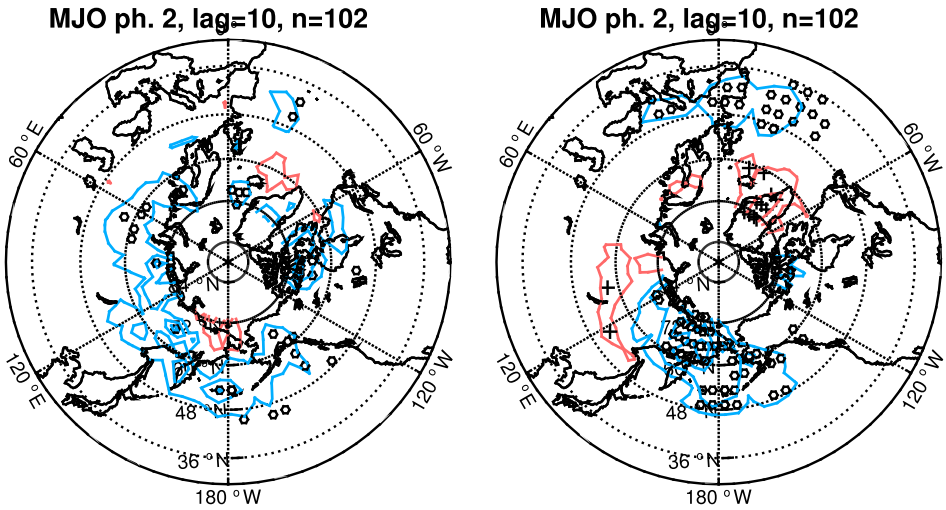

Figure 3.26.: Composites of anomalous DJF blocking frequency in combined ERA-40/ERA-Interim data (left panel) and in model simulations performed by Gollan and Greatbatch (2017) with the ECMWF Integrated Forecast System (right panel). The figure is taken from Gollan and Greatbatch (2017). The composites are calculated with respect to the Wheeler and Hendon (2004) MJO index for MJO phase 2. Contours are drawn every 4% for the ERA data and every 2% for the model data, the zero contour is omitted. Red contours indicate enhanced blocking, blue contours indicate decreased blocking; crosses or circles are drawn where the changes are significant. For more details see Gollan and Greatbatch (2017).

Henderson et al. (2016), who also investigated blocking changes due to the MJO in ERA-Interim reanalysis data, find a similar almost hemispherical decrease in mid-latitude blocking frequency associated with MJO phase 2. This can be seen in Figure 3.27 that depicts blocking climatology composites for different lags relative to the occurrence of MJO phase 2. Apart from this general blocking decrease, there is one region of slightly enhanced blocking for the larger lags: the Atlantic/European blocking peak around 0°E is enhanced and shifted to the west 10 to 15 days after the occurrence of MJO phase 2. This corresponds well with the mid-latitude blocking changes found in the PUMA run (Figure 3.23), where the European blocking peak

is generally located further east than in the reanalysis data but experiences a very similar increase and westward shift due to the MJO phase 2 heating.

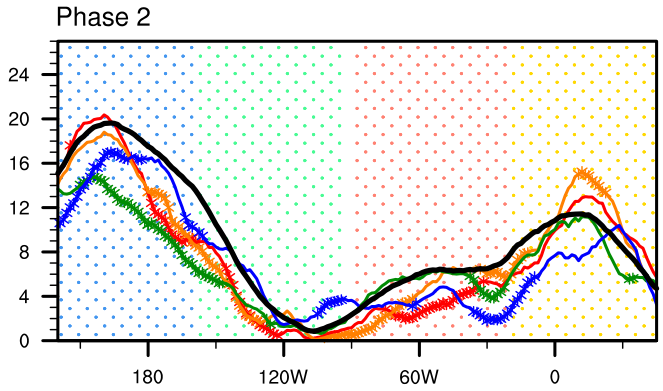

Figure 3.27.: Mid-latitude DJF blocking climatology from ERA-Interim reanalysis data, averaged between 40°N and 60°N. The figure is taken from Henderson et al. (2016). The vertical axis shows the climatological blocking frequency in %. Drawn in black is the mean winter blocking frequency, in colour the composite blocking climatologies for different lags relative to MJO phase 2 (blue – 0 days; green – 5 days; orange – 10 days; red – 15 days after the MJO phase). Asterisks are drawn where the coloured lines deviate significantly from the black winter mean curve. The coloured dots in the background indicate the following regions: West-Central Pacific (blue), East Pacific (green), Atlantic (red) and Europe (yellow). For more details see Henderson et al. (2016).

Phase 6

The climatological geopotential height anomaly relative to the reference run for the MJO phase 6 run is shown in Figure 3.28; at 1000 hPa in the left panel and at 300 hPa in the right panel. The fields at both heights exhibit similar features, most prominently a positive anomaly over the Arctic and northern Atlantic that is surrounded by negative anomalies over the western and eastern Pacific, the Atlantic and Europe. A clear signal of a negative North Atlantic Oscillation (NAO) is visible, consisting of the positive geopotential height anomaly over Iceland together with the Atlantic negative anomaly towards the south. The entire pattern together with the Pacific negative anomalies resembles the negative phase of the Arctic Oscillation or Northern Annular Mode (cf. Thompson and Wallace, 1998). The negative NAO pattern weakens the meridional geopotential height gradient and is therefore associated with a weakened westerly jet over the Atlantic. This in turn is favourable for blocking over Europe.

The anomalous geopotential height pattern that appears in the MJO phase 6 PUMA run is remarkably similar to the composite geopotential height pattern that Henderson et al. (2016) find for phase 6 in ERA-Interim reanalysis data; albeit only for lags

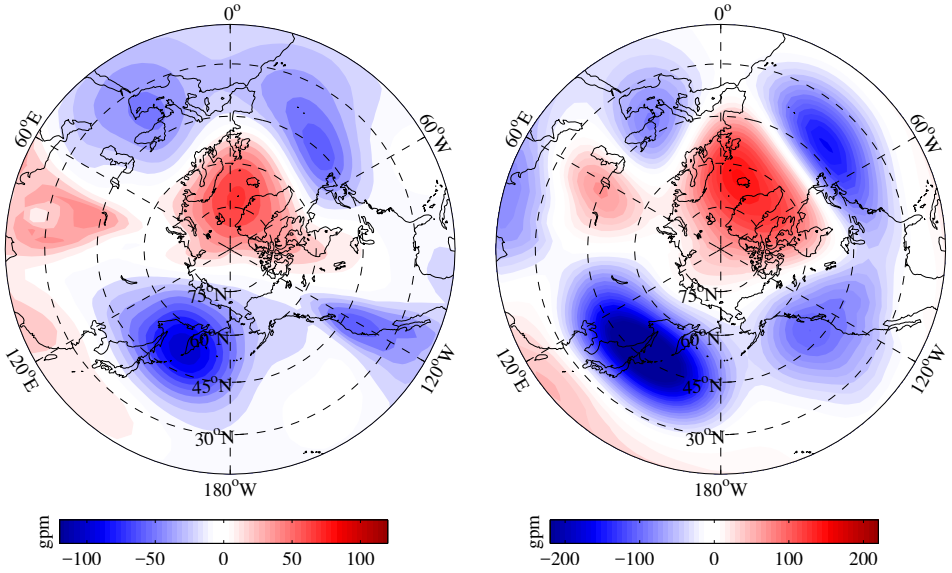

Figure 3.28.: Time mean geopotential height difference at 1000 hPa (left panel) and 300 hPa (right panel) between the 1.0 K d^{-1} MJO phase 6 run and the reference run. Realistic continents are only drawn for better orientation.

between 10 and 20 days after the occurrence of the MJO phase and not for smaller lags. Their composite geopotential height anomaly averaged between 15 and 19 days after MJO phase 6 can be seen in Figure 3.29. Because the PUMA experiments do not include any variation in the tropical MJO forcing, they represent an atmospheric state that has already adjusted to the tropical heating. Hence, it is not surprising that the extratropical response to the MJO phase 6 heating that is found in PUMA corresponds to a lagged response in reanalysis data as examined by Henderson et al. (2016). The details and time scales of this relation are further elaborated in Chapter 4.

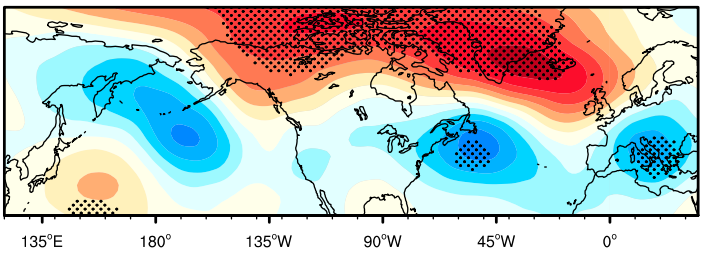

Figure 3.29.: Composite geopotential height anomaly at 500 hPa 15–19 days after MJO phase 6, in ERA-Interim reanalysis data. The figure is taken from Henderson et al. (2016). Blue colours indicate negative, red colours positive anomalies, contours are drawn every 10 m. Black dots are drawn where the anomalies are significant. For more details see Henderson et al. (2016).

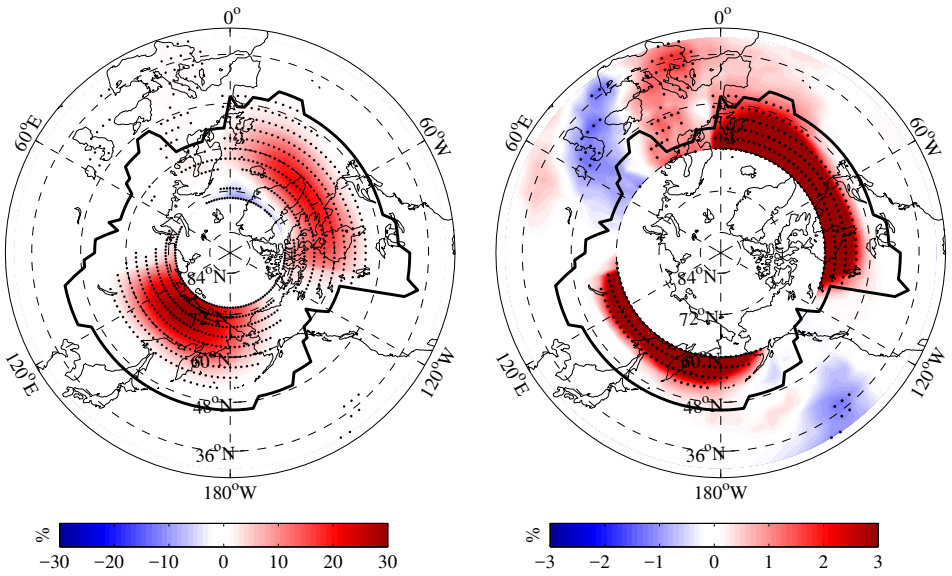

Figure 3.30.: Difference in two-dimensional blocking climatology between the $1.0\,\mathrm{K\,d^{-1}}$ MJO phase 6 run and the reference run. The right panel shows only mid-latitude values with a different colour scale for clarity. Black dots indicate significant differences from the reference run, i. e. values that lie outside the 95% confidence interval shown in Figure 3.14. The thick black line shows the location of the CBL. Realistic continents are only drawn for better orientation.

In Figure 3.30 the change in two-dimensional blocking frequency in the PUMA MJO phase 6 run relative to the reference run is displayed. At high latitudes, blocking is strongly enhanced in the two climatological blocking regions over the northern Atlantic and the northern Pacific/Siberia. Apart from this general increase in high-latitude blocking, there is a small region of significantly decreased blocking frequency over northern Greenland and north of Scandinavia. Along the storm track, the shift in the European blocking maximum towards the west that appeared in Figure 3.23 can be seen again. This shift, consisting of blocking decrease over eastern Europe and blocking increase over central Europe, extends southward as far as to the Mediterranean and is thus insensitive to the exact location of the storm track and CBL, which enhances confidence in the result. The blocking increase over the Atlantic does not only cover high latitudes, but extends into the vicinity of the storm track especially over the eastern Atlantic. A small decrease in blocking frequency is visible over the southeastern Pacific, although this is rather far away from the climatological storm track position and thus arguably not very influential.

The blocking changes found by Gollan and Greatbatch (2017) following MJO phase 6 are shown in Figure 3.31. Overall, they agree quite well with the results from the PUMA run. In both reanalysis and model data, Gollan and Greatbatch (2017) also find enhanced high-latitude blocking over the northern Pacific and north of Canada, and decreased high-latitude blocking in a small region north of Scandinavia. In the

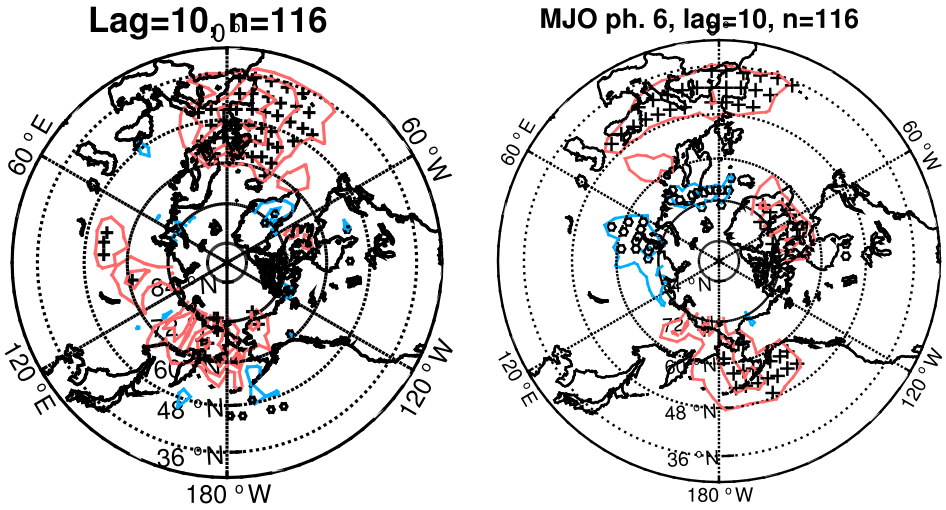

Figure 3.31.: Composites of anomalous DJF blocking frequency in combined ERA-40/ERA-Interim data (left panel) and in model simulations performed by Gollan and Greatbatch (2017) with the ECMWF Integrated Forecast System (right panel). The figure is taken from Gollan and Greatbatch (2017). The composites are calculated with respect to the Wheeler and Hendon (2004) MJO index for MJO phase 6. Contours are drawn every 4% for the ERA data and every 2% for the model data, the zero contour is omitted. Red contours indicate enhanced blocking, blue contours indicate decreased blocking; crosses or circles are drawn where the changes are significant. For more details see Gollan and Greatbatch (2017).

ERA reanalysis data, a large blocking increase in mid-latitudes over the eastern Atlantic and Europe is visible, as well as a small but not significant decrease over eastern Europe. This pattern matches the Atlantic and European blocking changes from the PUMA run quite well. Also in their model experiments Gollan and Greatbatch (2017) found a large blocking increase over Europe and the Atlantic, but is is confined to southern Europe. Their model also has decreased blocking over northern central Russia, which does not appear in the reanalysis data or in the PUMA run.

The change in blocking frequency in the PUMA MJO phase 6 run also agrees quite well with the results from Henderson et al. (2016). In Figure 3.32 mid-latitude blocking climatology composites for different lags relative to MJO phase 6 are shown that Henderson et al. (2016) calculated for ERA-Interim reanalysis data. Again, as seen in the geopotential height fields in Figures 3.28 and 3.29, the composites for lags smaller than 10 days show little agreement with the PUMA results, whereas the composites for 10 and 15 days after MJO phase 6 fit the PUMA results better. The composite blocking climatologies for the latter two lags feature a very similar increase over the Atlantic and Europe as the PUMA phase 6 blocking climatology in mid-latitudes, including the slight westward shift of the European blocking peak (Figures 3.23 and 3.30).

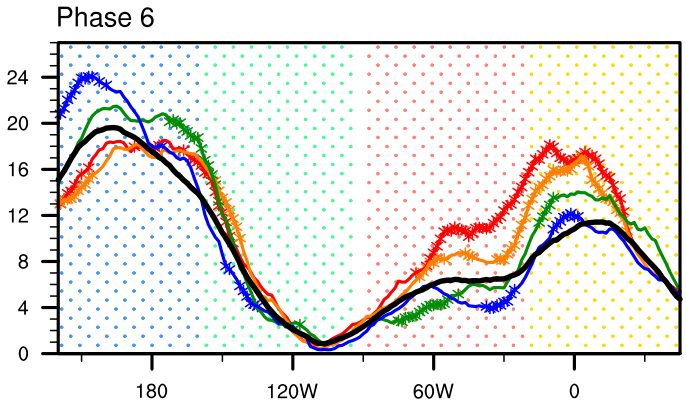

Figure 3.32.: Mid-latitude DJF blocking climatology from ERA-Interim reanalysis data, averaged between 40°N and 60°N. The figure is taken from Henderson et al. (2016). The vertical axis shows the climatological blocking frequency in %. Drawn in black is the mean winter blocking frequency, in colour the composite blocking climatologies for different lags relative to MJO phase 6 (blue – 0 days; green – 5 days; orange – 10 days; red – 15 days after the MJO phase). Asterisks are drawn where the coloured lines deviate significantly from the black winter mean curve. The coloured dots in the background indicate the following regions: West-Central Pacific (blue), East Pacific (green), Atlantic (red) and Europe (yellow). For more details see Henderson et al. (2016).

3.3.5. CMIP5 equatorial precipitation bias anomaly

Figure 3.33 shows the one-dimensional blocking climatology along the storm track, the climatological geopotential height at 300 hPa, and the climatological storm track for different PUMA runs with a tropical heating anomaly that is based on the multi-model mean precipitation bias of the CMIP5 models. Because now both the spatial extent and the amplitude of the heating anomalies is relatively large compared to the heating anomalies based on ENSO and MJO, it is not surprising that also the influence on blocking is much larger for the CMIP5 precipitation bias anomaly. For all three amplitudes, the mid-latitude blocking frequency is everywhere largely and significantly reduced. The blocking frequency seems to decrease approximately linearly with increasing amplitude of the tropical heating, which gives increased confidence in the result.

In the geopotential height fields, an intensification of the jet stream and an increase in the meridional geopotential height gradient with increasing amplitude of the tropical heating anomaly can be seen. This is primarily due to increased geopotential height in the tropics, due to the large positive tropical heating anomalies around the globe. Along with the strengthening of the meridional geopotential height gradient and the jet stream, there is a shift of the jet exit regions towards the east. These changes are also visible in the storm tracks, which become stronger as the amplitude of the tropical heating anomaly increases and the jet stream intensifies. Apparently, the

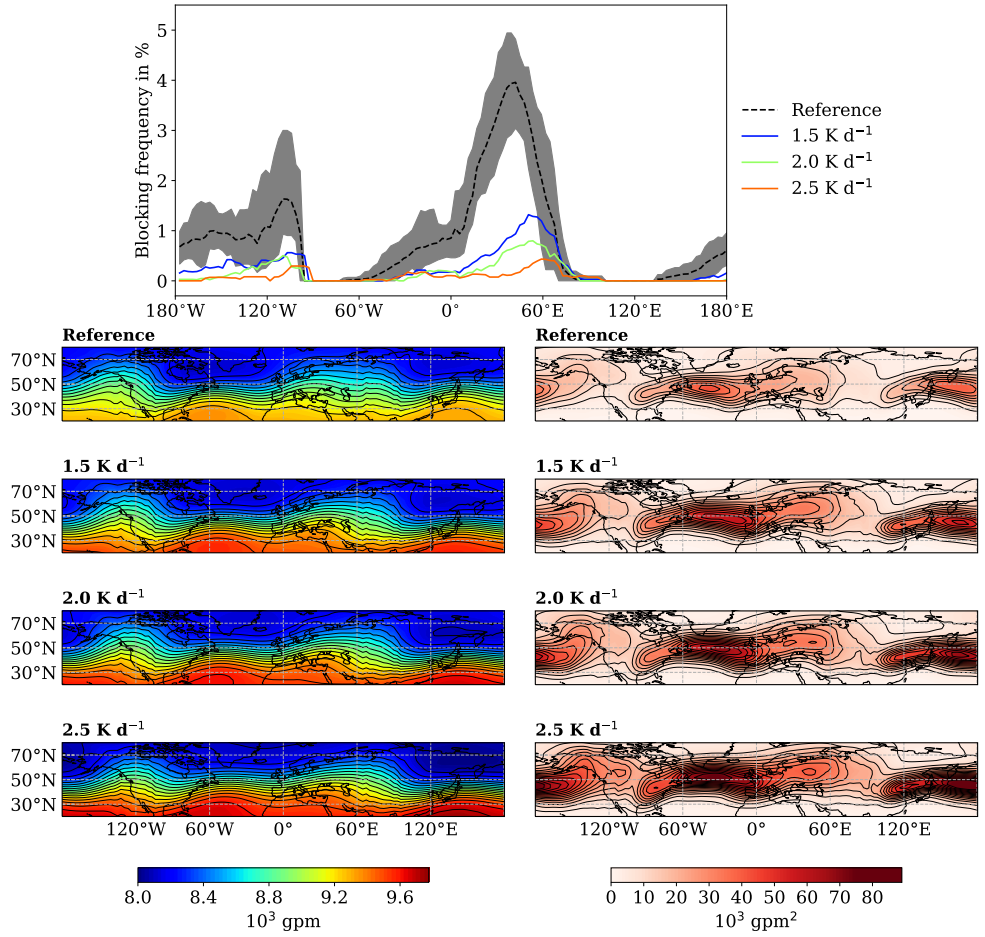

Figure 3.33.: Blocking climatology along the storm track, climatological geopotential height and storm tracks for CMIP5 precipitation bias experiments with different amplitudes. In the top panel, blocking climatologies for the different experiments are shown in colour. The reference blocking climatology is drawn as a dashed black line, with the 95% confidence interval as grey shading. In the lower panels, 300 hPa time mean geopotential height is shown on the left (black contours every 100 gpm), and the time mean power spectral density of 300 hPa geopotential height integrated over periods of 2–6 days on the right (black contours every $5 \cdot 10^3$ gpm^2). Realistic continents are only drawn for better orientation.

decrease in blocking frequency and the shift of the blocking peaks towards the east are primarily a consequence of the strengthened westerly mean flow and shifting jet exit regions; whereas the strengthening of storm track activity seems to have only minor influence and cannot sufficiently counteract these blocking-decreasing factors. This is in accordance with the earlier sensitivity experiments in Section 3.2, where the distribution of the westerly mean flow emerged as the primary factor determining blocking frequency, and storm track intensity only as a secondary modulating factor.

For further more detailed analysis, the CMIP5 precipitation bias run with an anomaly

amplitude of $2\,\mathrm{K\,d^{-1}}$ has been chosen. In Figure 3.34 the climatological geopotential height anomaly of that run relative to the reference run is displayed. At 1000 hPa, the field is dominated by a large negative anomaly over the northern Pacific, together with a smaller negative anomaly over Scandinavia and the northern Atlantic. Small positive anomalies are visible over western Asia and western North America. The pattern at 300 hPa is relatively similar, but the positive anomalies are much more pronounced. South of about 30°N, the anomalous 300 hPa geopotential height is positive at all longitudes, as a direct consequence of the large positive equatorial heating anomalies in the middle troposphere.

The extratropical geopotential height anomaly pattern that emerges in the CMIP5 precipitation bias run is, at high latitudes, very similar to the Cold Ocean-Warm Land (COWL) pattern that is described in e. g. Wallace et al. (1996) and Lu et al. (2004). It is characterised by a simultaneous deepening of the Aleutian and the Icelandic lows and positive geopotential height anomalies over North America and Asia. Lu et al. (2004) showed that tropical heating in the Indo-Pacific region, as it is also present in the CMIP5 precipitation bias run, is responsible for the COWL pattern development.

Over Europe, the geopotential height anomaly could also be a reversed blocking pattern; with the negative anomaly in the north where the anomalously high pressure of the blocking anticyclone would be located for a European blocking event, and a positive anomaly to the south. As Henderson et al. (2016) stated, the cause-and-effect relationship between the climatological mean state and changes in the blocking climatology is not always easy to determine and sometimes reversed: in the case of the CMIP5 precipitation bias run the reversed blocking pattern in the geopotential height could be a direct reflection of the strong blocking reduction over Europe (see Figure 3.35).

The change in two-dimensional blocking frequency in the CMIP5 precipitation bias run relative to the reference run is shown in Figure 3.35. The only increase in blocking is visible at high latitudes over the northern Pacific and Siberia. Apart from this, there is a general decrease of blocking frequency, in the high-latitude blocking region over the northern Atlantic as well as in mid-latitudes over the eastern Pacific and over Europe. The blocking decrease along the storm track that seems very robust already in the one-dimensional blocking climatologies shown in Figure 3.33, is significant in relatively large areas in the two-dimensional field, and at least over Europe insensitive to the location of the CBL.

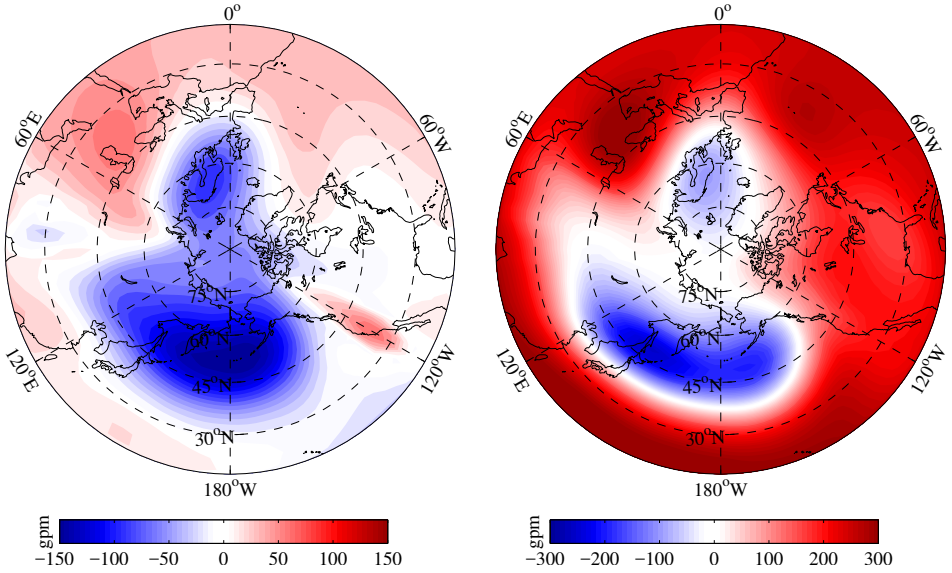

Figure 3.34.: Time mean geopotential height difference at 1000 hPa (left panel) and 300 hPa (right panel) between the 2.0 K d^{-1} CMIP5 precipitation bias run and the reference run. Realistic continents are only drawn for better orientation.

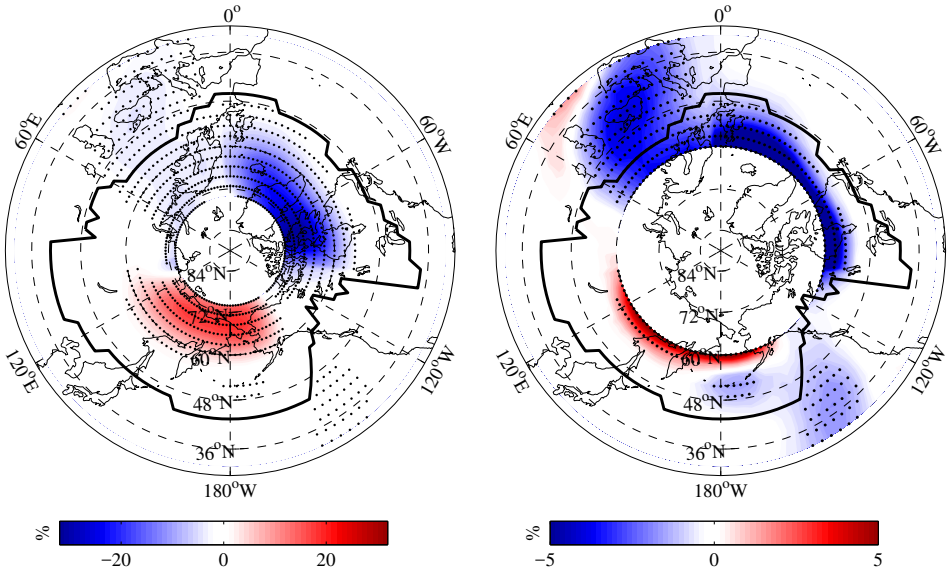

Figure 3.35.: Difference in two-dimensional blocking climatology between the 2.0 K d^{-1} CMIP5 precipitation bias run and the reference run. The right panel shows only mid-latitude values with a different colour scale for clarity. Black dots indicate significant differences from the reference run, i. e. values that lie outside the 95% confidence interval shown in Figure 3.14. The thick black line shows the location of the CBL. Realistic continents are only drawn for better orientation.

4. Discussion

Before the results of the different experiments presented in Chapter 3 are separately discussed, two general remarks on the comparability to other studies follow.

First, the comparison between studies that investigate blocking is very often complicated by the fact that it is not always discriminated clearly between blocking along the storm track (i. e. classical mid-latitude blocking) and high-latitude blocking that has a very different impact on the circulation. Here, it has therefore been attempted to distinguish between blocking along the storm track and high-latitude blocking very clearly, to facilitate both the interpretation of the results and the comparison with different studies. When a one-dimensional blocking index has been used, it has always been calculated along the climatological position of the storm track. Additionally, in the cases where a two-dimensional blocking index was employed, the climatological location of the storm track has always been marked in the figures.

Second, all experiments described in this thesis have been conducted with a highly idealised model setup, even in the second part where the configuration was chosen based on the geography of the Northern Hemisphere. It is thus not trivially evident that the results can be meaningfully compared to other studies that have used reanalysis data or more realistic model setups. Nevertheless, there is a surprisingly large degree of agreement between the PUMA results and realistic data, e. g. in the cases of forcing by ENSO and the MJO, which conveys the impression that the performed experiments can indeed give insights into the relationship between observed blocking and individual atmospheric phenomena.

In the following sections, the results that were obtained with PUMA and presented in Chapter 3 are discussed. Section 4.1 deals with the influence of mid-latitude orography and continent-ocean heating contrasts, and in Section 4.2 the relationship between blocking and the different tropical heating anomalies are addressed.

4.1. Sensitivity to configuration of mountain range and heating dipole

Consistent with many earlier studies, orography emerges to be an essential factor of the Northern Hemisphere geography for the establishment of stationary planetary waves in the jet stream and hence the occurrence of mid-latitude blocking in

the PUMA experiments. Its main effect seems to be the generation of regions with a weakened climatological meridional geopotential height gradient, where poleward advection of subtropical low potential vorticity air is facilitated and a thus created blocking anticyclone can be more easily maintained against zonal advection. This is in accordance with for example Luo (2005), who stated that eastward moving blocking-like anticyclones can also be excited by synoptic scale eddies alone, but that orography is necessary to fix their geographical location. Also e. g. Masato et al. (2009) stressed the importance of regions where the climatological mid-latitude meridional gradients are weak as preferred regions of blocking.

In addition to the importance of orography for mid-latitude blocking, the PUMA experiments show that, when such blocking-favourable regions of weakened westerly flow are present due to orography, the blocking frequency can be significantly increased by land-ocean heating contrasts that enhance the synoptic-scale variability through increasing baroclinicity (cf. Hoskins and Valdes, 1990). In order to increase blocking, the heating dipole must lie between 100° and 200° upstream of the respective blocking region, such that it can amplify the storm track activity upstream of the blocking region. The blocking frequency can be more than doubled by the enhanced synoptic activity compared to the case with only orography, which emphasises the importance of the transient storm systems in blocking generation and maintenance that has been shown by many earlier studies (cf. e. g. Illari and Marshall, 1983; Shutts, 1983; Haines and Marshall, 1987; Vautard and Legras, 1988; Masato et al., 2009).

Generally, the mid-latitude blocking frequency increases with mountain height in the PUMA experiments. The minimum height for the mountain range to allow for blocking in the model is about 4 km. This increase of blocking with mountain height is in accordance with studies that have tested the sensitivity of blocking to model resolution, e. g. Jung et al. (2012) and Berckmans et al. (2013), who found that coarse model resolution leads to reduced blocking partly because of the associated lower model orography.

4.2. Influence of tropical heating anomalies

The influence of diabatic heating in the tropics on blocking, both along the storm track and at high latitudes, has been found to be quite substantial in the idealised PUMA experiments. As Horel and Wallace (1981) and Wallace and Gutzler (1981) have first shown, the extratropical teleconnection patterns that are associated with tropical heating have an almost barotropic structure, which can also be seen in the PUMA geopotential height fields that agree quite well at 1000 hPa and at 300 hPa. Hoskins and Karoly (1981) showed that subtropical heating excites a stationary Rossby wave response that can explain large parts of the extratropical circulation anomalies associated with the subtropical heating. They could not, however, conclusively explain how

such a wave response could also be generated by heating located on the equator, because waves should then be trapped along the equatorial waveguide. This issue was solved by Sardeshmukh and Hoskins (1988) who showed that the 'effective Rossby wave source' due to equatorial heating is actually located in the region of upper tropospheric convergence north and south of the divergent flow above the heat source. This region of upper level convergence is often located in the subtropical westerly jet streams where vorticity anomalies are easy to generate due to the large meridional vorticity gradients, and Rossby waves can thus easily be excited. From the subtropics, the generated waves can then propagate poleward and affect the extratropics as shown by Hoskins and Karoly (1981). In the PUMA results, the stationary Rossby wave response to the equatorial heating is sometimes clearly visible, most prominently in the geopotential height anomaly from the La Niña run that is displayed in Figure 3.20. The pattern resembles the model results for Northern Hemisphere winter from Sardeshmukh and Hoskins (1988) quite closely (see their Figure 4).

In the following sections, the influence on blocking of the different tropical heating anomalies that have been added to the PUMA reference setup will be discussed.

4.2.1. Location of equatorial heating anomaly

There are two results that stand out from the tropical anomaly location experiments. First, the apparent nonlinearity in the extratropical response to tropical heating that is also confirmed in the ENSO experiments: the changes in mid-latitude blocking associated with the negative equatorial heating anomaly are much more pronounced than the changes associated with the positive heating anomaly. Second, the relatively clear pattern of blocking frequency changes: for the negative equatorial heating anomaly, the mid-latitude blocking frequency is decreased at the longitude of the anomalous heating and increased approximately between 60° and 180° west of its location. For the positive heating anomaly, this pattern is approximately reversed (i. e. there is increased blocking north of the heating and decreased blocking to the west), though not as strong in amplitude as stated before.

The nonlinearity in the strength of the extratropical response to positive or negative tropical heating has also been noted by e. g. Hoerling et al. (1997) for SST anomalies associated with El Niño or La Niña. They attributed the nonlinearity of the extratropical response partly to asymmetries in tropical rainfall associated with positive or negative SST anomalies; an explanation which is not valid for the PUMA results because the mid-tropospheric anomalous tropical heating is chosen to be symmetric for El Niño and La Niña. However, Hoerling et al. (1997) also stated that part of the asymmetry in the extratropical response could arise from changes in the mean circulation due to the heating that in turn influence the propagation of the wave response into the extratropics, or from feedbacks with the transient eddies in the storm tracks.

The changes in mid-latitude blocking frequency associated with the equatorial heating in PUMA can be understood by considering the extratropical circulation anomalies that develop as a stationary Rossby wave response to the anomalous heating. Sardeshmukh and Hoskins (1988) modelled the stationary wave response to tropical heating in a Northern Hemisphere winter background flow. In their Figure 4 g) it can be seen that north of the anomalous positive heating, the westerly mean flow at mid-latitudes is weakened, whereas about 100° to 200° west of the heating, the mid-latitude westerly flow is slightly strengthened. This strengthening of the westerly mean flow approximately corresponds to the decrease in mid-latitude blocking west of a positive equatorial heating anomaly that can be seen in PUMA (the weakening of the mean flow north of the heating would match a blocking increase although the latter is not very clearly apparent in the PUMA results). To the northeast of the anomalous heating, however, where Sardeshmukh and Hoskins (1988) also find a weakening of the mid-latitude westerly flow, there is no clear change in blocking frequency visible in the PUMA results. For a negative heating anomaly, the relation seems to be reversed and stronger in amplitude.

4.2.2. ENSO

Concerning the influence of ENSO on Northern Hemisphere winter blocking, there have been somewhat contradictory findings in the past, as already described in Section 1.2. In some cases, these differences arise from inconsistent blocking definitions (e. g. lacking discrimination between blocking along the storm track and high-latitude blocking) or from differences in the ENSO representation (most studies have used composite techniques based on ENSO indices that capture all components of El Niño or La Niña events, whereas some studies, e. g. Hinton et al. (2009), have focused on the impact of certain idealised features of ENSO). The approach that is taken in this thesis follows Hinton et al. (2009) rather than e. g. Renwick and Wallace (1996), Barriopedro et al. (2006) or Gollan and Greatbatch (2017): here, ENSO is represented by a very idealised, monopole heating anomaly over the tropical Pacific that is based on the maximum of anomalous convective precipitation during El Niño.

In the northern Pacific, the disagreement about the influence of ENSO on winter blocking has probably been strongest. Some earlier studies found enhanced north Pacific winter blocking during La Niña and decreased blocking during El Niño, e. g. Renwick and Wallace (1996) and Barriopedro et al. (2006). In both of these studies, observational or reanalysis data was used. Renwick and Wallace (1996), however, only considered blocking events over Alaska, whereas Barriopedro et al. (2006) used a two-dimensional blocking detection method in the entire Northern Hemisphere. In contrast to this, the results of Gollan and Greatbatch (2017) and from the PUMA experiments presented in this thesis show a significant increase of high-latitude blocking over the northern Pacific during El Niño, and a significant decrease of the high-latitude north Pacific blocking frequency during La Niña. It has been suggested by Hinton

et al. (2009) that such controversial results might be due to the counteracting influences from different components of an ENSO event: they found that opposite heating anomalies over the Maritime Continent and the eastern Pacific, that are often present at the same time during an ENSO event, also have an opposing impact on north Pacific blocking, and that the overall impact of ENSO on blocking over the northern Pacific thus depends on the relative magnitude of these two heating anomalies. This is certainly an important point to keep in mind when comparing the PUMA experiments with their idealised monopole heating anomalies to previous studies using realistic ENSO data. However, it is striking that also Gollan and Greatbatch (2017) found increased north Pacific blocking for El Niño and decreased blocking for La Niña in both reanalysis data and model simulations, despite their realistic representation of ENSO. The large degree of conformity between the north Pacific blocking changes due to ENSO found by Gollan and Greatbatch (2017) and with PUMA enhances confidence in the results and rather suggests that different blocking detection and analysis techniques might be responsible for the discrepancy with earlier studies.

Over Europe and the Atlantic, the PUMA results show a significant increase in mid-latitude blocking along the storm track associated with La Niña. Most studies have focused on northern Pacific blocking changes connected with ENSO, but Barriopedro et al. (2006) also investigated European and Atlantic blocking and found a similar increase during La Niña winters compared to El Niño winters (compare their Figure 9 e) to Figure 3.17).

Despite the relatively good agreement between the PUMA results and those of Gollan and Greatbatch (2017), the strong idealisation of the PUMA configuration obviously impacts the outcome. The PNA pattern, for example, that is in reality closely linked to ENSO (cf. e. g. Philander, 1990, pp. 48–50), is only partly recognisable in the geopotential height anomalies. The Pacific part of the positive PNA pattern, with a deep Aleutian low and a positive geopotential height anomaly to the south, is visible in the El Niño experiment; likewise an approximately reversed Pacific pattern for La Niña. From the northern Pacific, however, the stationary wave train does not bend southwards over the North American continent as for the PNA pattern, but crosses the Arctic and continues towards the Atlantic instead. This change in the stationary wave response to the idealised ENSO heating compared to the usual PNA response could be due to the lack of realistic Northern Hemisphere geography in the PUMA configuration. The misrepresentation of the PNA response to ENSO in other regions than the Pacific could explain why the blocking changes found in PUMA agree much better to the results from Gollan and Greatbatch (2017) over the northern Pacific than over Europe and the Atlantic.

From the PUMA results it is obvious that neither the changes in geopotential height nor the changes in blocking are exactly opposite in the El Niño, respectively La Niña, experiments. Over the Atlantic, for example, the blocking frequency is increased for both El Niño and La Niña. The high-latitude Pacific is the region where the induced

changes are most symmetric. As mentioned in Section 4.2.1, the nonlinearity in the extratropical response to ENSO has also been noted in other studies, e. g. by Renwick and Wallace (1996) and Barriopedro et al. (2006), and has been investigated in some detail by Hoerling et al. (1997). They generally found larger changes in the geopotential height field over Europe during La Niña than during El Niño, which agrees well with the PUMA results that show a much larger influence of the negative ENSO anomaly on European mid-latitude blocking than of the positive ENSO anomaly. As brought up before, the existence of this asymmetry in the idealised, symmetric PUMA experiments suggests that the nonlinearity is at least partly inherent in the evolution of the extratropical response, and does not only originate from asymmetries between the cold and warm ENSO phases themselves.

4.2.3. MJO

Only two of the eight MJO phases have been investigated here with respect to their influence on Northern Hemisphere winter blocking, unlike in for example Henderson et al. (2016) and Gollan and Greatbatch (2017) who extensively documented the MJO impact on blocking. Nevertheless, the results obtained with the simplified PUMA setup give some additional information on the blocking change due to MJO phase 6.

Generally, the blocking changes in the idealised PUMA experiments confirm most of the changes found by Cassou (2008), Henderson et al. (2016) and Gollan and Greatbatch (2017) for MJO phases 2 and 6. The impact of the phase 2 heating anomalies is not very large in the PUMA run, neither in the geopotential height field nor in the blocking frequency. Along the storm track, there are almost no significant blocking changes, but the pattern at high latitudes and over southern Europe matches the blocking changes after phase 2 found in model experiments by Gollan and Greatbatch (2017) very closely. For phase 6, the PUMA run shows more pronounced anomalies, both in the geopotential height field and the blocking frequency. Also these changes are mostly in accordance with earlier findings. In particular, the strong increase in European and Atlantic mid-latitude blocking frequency after phase 6 that has been noted by Cassou (2008), Henderson et al. (2016) and Gollan and Greatbatch (2017) can be reproduced with the simple PUMA MJO phase 6 configuration. The latter result is interesting, because there has been some doubt concerning the origin of this European/Atlantic blocking frequency increase after MJO phase 6: lagged influence from earlier MJO phases has been suggested to be the cause. The PUMA experiments add some new information here, because PUMA is run with a constant tropical heat source that does not change its phases like the real MJO. The implications of this, and the conclusions that arise from the PUMA results concerning the reasons for the MJO phase 6 blocking change, are discussed in the following paragraphs.

In the PUMA run with the MJO phase 6 heating anomaly, a negative NAO (as part of a pattern reminiscent of the negative NAM) is distinctly visible in the anoma-

lous geopotential height field. The negative NAO pattern leads to a weakening of the meridional geopotential height gradient over the Atlantic, which in turn favours mid-latitude blocking over the Atlantic and Europe. This connection between MJO phase 6, a negative NAO and enhanced European/Atlantic mid-latitude blocking is consistent with several earlier studies (see e. g. Cassou, 2008; Woollings et al., 2008; Gollan and Greatbatch, 2017). However, as mentioned above, there has been some discussion about whether or not the negative NAO and the enhanced European blocking are really due to the MJO phase 6 heating, or rather consequences of earlier MJO phases that just coincide with phase 6. Cassou (2008) proposed that the negative NAO regime following phase 6 could originate from phase 3 forcing, but also directly from phase 6 forcing. Henderson et al. (2016) additionally suggested that there is more to the MJO phase 6/European blocking relationship than the connection through the NAO as identified by the other studies. According to their theory, a negative PNA pattern, which develops due to earlier MJO phases, acts as a Rossby wave pathway over North America towards Europe and thus increases European and Atlantic blocking after phase 6.

The fact that the PUMA run with the idealised, invariant MJO phase 6 heating can reproduce a large part of the blocking change that has been found by Henderson et al. (2016) and Gollan and Greatbatch (2017), shows that MJO phase 6 heating can directly induce both a negative NAO pattern and a European/Atlantic blocking increase. This does, of course, not rule out the possibility that either of the proposed mechanisms for an influence of earlier MJO phases can also contribute to the MJO-blocking relationship during phase 6, but these contributions seem minor compared to the direct influence of the phase 6 heating.

This result becomes even more plausible when the time evolution of the extratropical response to MJO phase 6, as shown by Henderson et al. (2016), is taken into account. Their Figure 5 shows the geopotential height anomalies for different lags after MJO phase 6; their Figure 12 the mid-latitude blocking frequency for different lags after phase 6 (both figures have been partly shown in Chapter 3, see Figures 3.29 and 3.32). The geopotential height as well as the blocking frequency from the reanalysis data become very similar to the PUMA results for lags of 10 days or more after the occurrence of phase 6. This is consistent with the time that a stationary Rossby wave response to tropical heating needs to fully develop, as shown by Hoskins and Karoly (1981) who investigated the extratropical response to tropical heating in an idealised model and stated that 'a[f]ter 10 days the solution changes little with time'. The similarity of the PUMA results and the 10-day (and 15-day) lagged responses found by both Henderson et al. (2016) and Gollan and Greatbatch (2017) thus gives strong confidence in the hypothesis that the anomalous tropical heating during MJO phase 6 directly causes a negative NAO pattern and increased mid-latitude blocking frequency over the Atlantic and Europe.

4.2.4. CMIP5 precipitation bias

There is strong agreement throughout studies concerned with the CMIP5 models' blocking bias that almost all of the models significantly underestimate winter blocking over Europe and the Atlantic, consistent with the strong European/Atlantic decrease of blocking in the PUMA experiment. Over the Pacific, the picture is less clear; there are models with positive as well as negative blocking biases in that region (cf. e. g. Anstey et al., 2013; Masato et al., 2013; Davini and D'Andrea, 2016). The CMIP5 multi-model mean winter blocking bias is shown for example in Figure 1 of Masato et al. (2013) in the two-dimensional version, and in their Figure 2 in the one-dimensional version along the storm track. Both of these are, over Europe and the Atlantic, quite similar to the changes found in the PUMA experiment (see Figures 3.33 and 3.35). Also over Siberia, the PUMA blocking change agrees well with the multi-model mean CMIP5 blocking bias; both are positive. However, over the high-latitude Pacific, the CMIP5 multi-model mean blocking bias is negative unlike in the PUMA experiment. Along the storm track, again the change in blocking in the CMIP5 models and the PUMA experiment is very similar over the Atlantic and rather different over the Pacific, where the multi-model mean blocking frequency in the CMIP5 models is slightly increased instead of decreased as in the PUMA run. Depending on the number of models included and the blocking detection method used in the studies, the CMIP5 winter blocking bias is a little different in Anstey et al. (2013) and Davini and D'Andrea (2016), but especially over Europe and the Atlantic, they agree on the main features (see Figure 2 in Anstey et al., 2013; and Figure 4 in Davini and D'Andrea, 2016).

Due to the complexity of the blocking phenomenon, there are a large number of model biases and simplifications that could play a role in creating the blocking bias. As mentioned in Section 1.3, both higher horizontal resolution and reduced mean state biases have been shown to reduce climate models' blocking biases, although the role of the former is subject to debate: higher horizontal resolution could improve blocking simulation because of improved simulation of synoptic-scale activity and the associated positive feedbacks on blocking persistence, or simply because of an improvement in the mean state simulation (cf. e. g. Scaife et al., 2010; Jung et al., 2012; or Berckmans et al., 2013). It is very likely that both explanations are valid, although probably the ratio of their relative importance is different over the Atlantic and the Pacific. Some studies have suggested that the role of improved synoptic eddy simulation due to increased horizontal resolution is more important over the Atlantic and Europe than over the Pacific (cf. e. g. Vial and Osborn, 2012; and Berckmans et al., 2013). The PUMA runs have all been carried out with a rather coarse horizontal resolution (T42) that has not been varied throughout the experiments. Here, no statement about the importance of resolution for blocking simulation can therefore be made. However, interesting conclusions about the role of tropical mean state biases for blocking simulation emerge from the PUMA experiments. It can be shown

that, particularly for the simulation of Atlantic and European blocking, the correct representation of tropical precipitation is an important factor.

The reason for the blocking changes in the CMIP5 bias PUMA experiment is the development of a climatological geopotential height anomaly that is reminiscent of the COWL pattern. This pattern leads to a strengthening of the Atlantic and Pacific jet streams, due to the negative geopotential height anomalies to the north and the positive anomalies to the south that enhance the meridional gradient (see Figure 3.34). The mid-latitude blocking reduction that occurs in the PUMA run is probably a direct consequence of this jet stream intensification over the oceans. Lu et al. (2004) have shown that the appearance of the COWL pattern is due to anomalously enhanced heating in the Indo-Pacific region, a feature that is also an important component of the CMIP5 precipitation bias. Hence, from the results obtained with the idealised PUMA simulations, the hypothesis arises that the excess heating in the tropics due to the CMIP5 models' precipitation bias is responsible for a large part of the models' blocking bias, especially the lack of blocking over Europe and the Atlantic, through driving extratropical geopotential height anomalies that strengthen the westerly mean flow over the oceans.

Of course, the large degree of variation between the CMIP5 models makes it difficult to extract a message concerning model bias reduction only from investigation of the multi-model mean. Nevertheless, it is striking that in the simple PUMA model setup, a heating anomaly based on the CMIP5 multi-model mean precipitation bias can induce blocking changes that so closely resemble the multi-model mean blocking bias. This result certainly points to the importance of tropical precipitation biases in impeding the correct simulation of atmospheric blocking in global climate models, especially over Europe and the Atlantic. Although this was beyond the scope of this thesis, it would surely be very useful to conduct similar experiments based on the tropical precipitation biases of single models instead of the multi-model mean.

5. Summary

In this thesis, the dry, spectral atmospheric model PUMA has been employed to investigate Northern Hemisphere winter blocking in a simplified setting. The model has been run in a basic aqua planet configuration with a zonally symmetric distribution of the radiative equilibrium temperature. To this basic setting, idealised Gaussian-shaped orography and heating anomalies have been added to test their influence on blocking in several sensitivity experiments.

With the aqua planet configuration, the model develops a reasonably realistic, although zonally symmetric, tropospheric circulation with a westerly jet stream and storm track centred at about 45°N and 250 hPa. However, no blocking occurs in the model with the basic setup; this happens only when a mountain range or a continent-ocean heating dipole is added at mid-latitudes.

An idealised mountain range that lies in the path of the westerly flow forces a stationary planetary wave which causes the jet stream to depart from its formerly purely zonal path. Additionally, the climatological meridional geopotential height gradient (and consequently also the jet stream) is weakened at some longitudes, most prominently directly upstream of the mountain range where a jet exit region forms. Consistent with earlier studies and observations, blocking occurs at the locations where the geopotential height gradient and the westerly mean flow are weakened. A heating dipole, based on Northern Hemisphere winter land-ocean heating contrasts, leads to a stronger jet stream and enhanced synoptic variability downstream of its location. When only the heating dipole is added to the zonally symmetric setup, there is some blocking downstream of the enhanced storm track activity, but the frequency amounts to only a fraction of the value that is reached with the mountain range.

The influence of the heating dipole on blocking becomes much larger, however, when a mountain range is also present in the model setup. In this case, the regions where blocking preferably occurs are still set by the mountain range, but the heating dipole can more than double the peak blocking frequency if it is located favourably, i. e. between 100° and 200° upstream of the respective blocking region, confirming previous studies that showed the importance of transient synoptic eddies in blocking amplification and maintenance. Blocking frequencies generally increase both with increasing mountain height and increasing heating dipole amplitude.

In order to get a reference configuration for sensitivity experiments with tropical heating anomalies, two idealised mountain ranges have been added to the zonally

symmetric basic setup at the approximate locations of the Rocky Mountains and the Himalayas, as well as two continent-ocean heating dipoles at the locations of the eastern coasts of Asia and North America. With this configuration, the model's blocking climatology approaches the observed Northern Hemisphere winter blocking climatology, although the absolute values are lower in PUMA. Several tropical heating anomalies have then been added to the reference configuration to investigate their influence on blocking.

Generally, a negative heating anomaly over the equator is found to have a larger impact on mid-latitude blocking than a positive heating anomaly of the same amplitude. The negative equatorial heating anomaly entails significantly reduced mid-latitude blocking frequency at the longitude of the heating, and significantly increased mid-latitude blocking frequency between 60° and 180° west of the longitude of the heating. For a positive tropical heating anomaly, the changes in mid-latitude blocking frequency are approximately reversed, but weaker.

Consistent with this, a heating anomaly over the tropical Pacific, based on anomalous convection associated with ENSO, leads to reduced mid-latitude blocking over the Pacific and increased mid-latitude blocking over Europe and the Atlantic when it is negative (i. e. representing La Niña), and to slightly reduced mid-latitude blocking over Europe when it is positive (i. e. representing El Niño). At high latitudes, the blocking frequency in PUMA significantly increases over Siberia and the northern Pacific due to El Niño, and decreases due to La Niña, which corroborates previous results from Gollan and Greatbatch (2017).

For a tropical heating anomaly based on MJO phase 2, the changes in blocking frequency found with PUMA are rather small, and at mid-latitudes mostly not significant. For a heating anomaly based on MJO phase 6, however, blocking frequencies are much increased in PUMA, both at high latitudes over Siberia and Greenland, which is consistent with changes found by Gollan and Greatbatch (2017), and at mid-latitudes over the Atlantic and Europe, which has also been previously found by Cassou (2008), Henderson et al. (2016) and Gollan and Greatbatch (2017). A negative NAO pattern appears in PUMA as a result of the tropical MJO phase 6 heating, which weakens the westerly mean flow over the Atlantic and thus favours the occurrence of European and Atlantic mid-latitude blocking. It has been speculated that both the negative NAO and the increase in European and Atlantic blocking are not due to MJO phase 6, but are rather consequences of earlier MJO phases. This is, however, disproved by the PUMA results that were obtained with a constant phase 6 forcing.

A tropical heating anomaly that is based on the multi-model mean tropical precipitation bias of the CMIP5 models leads to strongly decreased mid-latitude blocking frequencies. The reason for this large mid-latitude blocking reduction in PUMA is the development of the COWL pattern due to the anomalous tropical heating over the Indian and Pacific Oceans, with negative geopotential height anomalies over the northern parts of the oceans and positive geopotential height anomalies over the

continents, that leads to strengthened westerly mean flow over the oceans and thus prohibits mid-latitude blocking. The changes in blocking frequency that emerge in PUMA as a response to the CMIP5 precipitation bias heating are very similar to the CMIP5 multi-model mean blocking bias found by previous studies, which implies that the general overestimation of tropical precipitation in the CMIP5 models contributes greatly to their deficiencies in blocking simulation.

References

Altenhoff, A. M., Martius, O., Croci-Maspoli, M., Schwierz, C., and Davies, H. C., 2008: Linkage of atmospheric blocks and synoptic-scale Rossby waves: a climatological analysis. *Tellus*, 60A, 1053–1063.

Anstey, J. A., Davini, P., Gray, L. J., Woollings, T. J., Butchart, N., Cagnazzo, C., Christiansen, B., Hardiman, S. C., Osprey, S. M., and Yang, S., 2013: Multi-model analysis of Northern Hemisphere winter blocking: Model biases and the role of resolution. *Journal of Geophysical Research*, 118, 3956–3971.

Antokhina, O. Y., Antokhin, P. N., Devyatova, E. V., and Martynova, Y. V., 2018: 2004–2016 Wintertime Atmospheric Blocking Events over Western Siberia and Their Effect on Surface Temperature Anomalies. *Atmosphere*, 9, 72.

Barnes, E. A., Slingo, J., and Woollings, T., 2012: A methodology for the comparison of blocking climatologies across indices, models and climate scenarios. *Climate Dynamics*, 38, 2467–2481.

Barriopedro, D., García-Herrera, R., Lupo, A. R., and Hernández, E., 2006: A Climatology of Northern Hemisphere Blocking. *Journal of Climate*, 19, 1042–1063.

Berckmans, J., Woollings, T., Demory, M.-E., Vidale, P.-L., and Roberts, M., 2013: Atmospheric blocking in a high resolution climate model: influences of mean state, orography and eddy forcing. *Atmospheric Science Letters*, 14, 34–40.

Berggren, R., Bolin, B., and Rossby, C.-G., 1949: An Aerological Study of Zonal Motion, its Perturbations and Break-down. *Tellus*, 1, 14–37.

Black, E., Blackburn, M., Harrison, G., Hoskins, B., and Methven, J., 2004: Factors contributing to the summer 2003 European heatwave. *Weather*, 59, 217–223.

Buehler, T., Raible, C. C., and Stocker, T. F., 2011: The relationship of winter season North Atlantic blocking frequencies to extreme cold or dry spells in the ERA-40. *Tellus*, 63A, 212–222.

Cassou, C., 2008: Intraseasonal interaction between the Madden-Julian Oscillation and the North Atlantic Oscillation. *Nature*, 455, 523–527.

Cassou, C., Terray, L., and Phillips, A. S., 2005: Tropical Atlantic Influence on European Heat Waves. *Journal of Climate*, 18, 2805–2811.

D'Andrea, F., Tibaldi, S., Blackburn, M., Boer, G., Déqué, M., Dix, M. R., Dugas, B., Ferranti, L., Iwasaki, T., Kitoh, A., Pope, V., Randall, D., Roeckner, E., Straus, D., Stern, W., Van den Dool, H., and Williamson, D., 1998: Northern Hemisphere atmospheric blocking as simulated by 15 atmospheric general circulation models in the period 1979–1988. *Climate Dynamics*, 14, 385–407.

Davini, P. and D'Andrea, F., 2016: Northern Hemisphere Atmospheric Blocking Representation in Global Climate Models: Twenty Years of Improvements?. *Journal of Climate*, 29, 8823–8840.

Dent, J., 2013: The 1962/1963 winter as observed at Belstead Hall (Suffolk) and through investigation of the synoptic charts. *Weather*, 68, 18–23.

Dole, R., Hoerling, M., Perlwitz, J., Eischeid, J., Pegion, P., Zhang, T., Quan, X.-W., Xu, T., and Murray, D., 2011: Was there a basis for anticipating the 2010 Russian heat wave?. *Geophysical Research Letters*, 38.

Dunn-Sigouin, E. and Son, S.-W., 2013: Northern Hemisphere blocking frequency and duration in the CMIP5 models. *Journal of Geophysical Research*, 118, 1179–1188.

Flato, G., Marotzke, J., Abiodun, B., Braconnot, P., Chou, S., Collins, W., Cox, P., Driouech, F., Emori, S., Eyring, V., Forest, C., Gleckler, P., Guilyardi, E., Jakob, C., Kattsov, V., Reason, C., and Rummukainen, M.: Evaluation of Climate Models, in: Climate Change 2013: The Physical Science Basis. Contribution of Working Group I to the Fifth Assessment Report of the Intergovernmental Panel on Climate Change, edited by Stocker, T. F., Qin, D., Plattner, G.-K., Tignor, M., Allen, S. K., Boschung, J., Nauels, A., Xia, Y., Bex, V., and Midgley, P. M., pp. 741–866, Cambridge University Press, Cambridge, United Kingdom and New York, NY, USA, 2013.

Fraedrich, K., Kirk, E., and Lunkeit, F., 1998: PUMA: Portable University Model of the Atmosphere. *DKRZ Technical Report*.

Fraedrich, K., Blessing, S., Borth, H., Kirk, E., Kunz, T., Lunkeit, F., McDonald, A., Schubert, S., and Sielmann, F., 2017: PUMA User's Guide Version 16, published by the Theoretical Meteorology at the Meteorological Institute of the University of Hamburg.

Franzke, C., Fraedrich, K., and Lunkeit, F., 2000: Low-frequency variability in a simplified atmospheric global circulation model: Storm-track induced 'spatial resonance'. *Quarterly Journal of the Royal Meteorological Society*, 126, 2691–2708.

Gangoiti, G., Alonso, L., Navazo, M., Albizuri, A., Perez-Landa, G., Matabuena, M., Valdenebro, V., Maruri, M., García, J. A., and Millán, M. M., 2002: Regional transport of pollutants over the Bay of Biscay: analysis of an ozone episode under a blocking anticyclone in west-central Europe. *Atmospheric Environment*, 36, 1349–1361.

Gill, A. E., 1982: Atmosphere-Ocean Dynamics, vol. 30 of *International Geophysics Series*, Academic Press.

Gollan, G. and Greatbatch, R. J., 2017: The Relationship between Northern Hemisphere Winter Blocking and Tropical Modes of Variability. *Journal of Climate*, 30, 9321–9337.

Gollan, G., Greatbatch, R. J., and Jung, T., 2015: Origin of variability in Northern Hemisphere winter blocking on interannual to decadal timescales. *Geophysical Research Letters*, 42, 10,037–10,046.

Greatbatch, R. J., Gollan, G., Jung, T., and Kunz, T., 2015: Tropical origin of the severe European winter of 1962/1963. *Quarterly Journal of the Royal Meteorological Society*, 141, 153–165.

Haines, K. and Marshall, J., 1987: Eddy-forced coherent structures as a prototype of atmospheric blocking. *Quarterly Journal of the Royal Meteorological Society*, 113, 681–704.

Held, I. M. and Suarez, M. J., 1994: A Proposal for the Intercomparison of the Dynamical Cores of Atmospheric General Circulation Models. *Bulletin of the American Meteorological Society*, 75, 1825–1830.

Henderson, S. A., Maloney, E. D., and Barnes, E. A., 2016: The Influence of the Madden-Julian Oscillation on Northern Hemisphere Winter Blocking. *Journal of Climate*, 29, 4597–4616.

Hinton, T. J., Hoskins, B. J., and Martin, G. M., 2009: The influence of tropical sea surface temperatures and precipitation on north Pacific atmospheric blocking. *Climate Dynamics*, 33, 549–563.

Hoerling, M. P., Kumar, A., and Zhong, M., 1997: El Niño, La Niña, and the Nonlinearity of Their Teleconnections. *Journal of Climate*, 10, 1769–1786.

Holton, J. R., 1992: An introduction to dynamic meteorology, vol. 48 of *International Geophysics Series*, Academic Press, 3rd edn.

Horel, J. D. and Wallace, J. M., 1981: Planetary-Scale Atmospheric Phenomena Associated with the Southern Oscillation. *Monthly Weather Review*, 109, 813–829.

Hoskins, B. J., 1980: Representation of the Earth Topography Using Spherical Harmonics. *Monthly Weather Review*, 108, 111–115.

Hoskins, B. J. and Karoly, D. J., 1981: The Steady Linear Response of a Spherical Atmosphere to Thermal and Orographic Forcing. *Journal of the Atmospheric Sciences*, 38, 1179–1196.

Hoskins, B. J. and Simmons, A. J., 1975: A multi-layer spectral model and the semi-implicit method. *Quarterly Journal of the Royal Meteorological Society*, 101, 637–655.

Hoskins, B. J. and Valdes, P. J., 1990: On the Existence of Storm-Tracks. *Journal of the Atmospheric Sciences*, 47, 1854–1864.

Hoskins, B. J., McIntyre, M. E., and Robertson, A. W., 1985: On the use and significance of isentropic potential vorticity maps. *Quarterly Journal of the Royal Meteorological Society*, 111, 877–946.

Illari, L. and Marshall, J. C., 1983: On the Interpretation of Eddy Fluxes During a Blocking Episode. *Journal of the Atmospheric Sciences*, 40, 2232–2242.

James, I. N. and Gray, L. J., 1986: Concerning the effect of surface drag on the circulation of a baroclinic planetary atmosphere. *Quarterly Journal of the Royal Meteorological Society*, 112, 1231–1250.

Johnson, N. C. and Kosaka, Y., 2016: The impact of eastern equatorial Pacific convection on the diversity of boreal winter El Niño teleconnection patterns. *Climate Dynamics*, 47, 3737–3765.

Jung, T., Miller, M. J., Palmer, T. N., Towers, P., Wedi, N., Achuthavarier, D., Adams, J. M., Altshuler, E. L., Cash, B. A., Kinter, J. L., Marx, L., Stan, C., and Hodges, K. I., 2012: High-Resolution Global Climate Simulations with the ECMWF Model in Project Athena: Experimental Design, Model Climate, and Seasonal Forecast Skill. *Journal of Climate*, 25, 3155–3172.

Kållberg, P., Simmons, A., Uppala, S., and Fuentes, M., 2004: The ERA-40 Archive. ERA-40 Project Report Series No. 17, published by ECMWF, revised October 2007.

Kalnay, E., Kanamitsu, M., Kistler, R., Collins, W., Deaven, D., Gandin, L., Iredell, M., Saha, S., White, G., Woollen, J., Zhu, Y., Chelliah, M., Ebisuzaki, W., Higgins, W., Janowiak, J., Mo, K. C., Ropelewski, C., Wang, J., Leetmaa, A., Reynolds, R., Jenne, R., and Joseph, D., 1996: The NCEP/NCAR 40-Year Reanalysis Project. *Bulletin of the American Meteorological Society*, 77, 437–471.

Kistler, R., Kalnay, E., Collins, W., Saha, S., White, G., Woollen, J., Chelliah, M., Ebisuzaki, W., Kanamitsu, M., Kousky, V., van den Dool, H., Jenne, R., and Fiorino, M., 2001: The NCEP/NCAR 50-Year Reanalysis: Monthly Means CD-ROM and Documentation. *Bulletin of the American Meteorological Society*, 82, 247–268.

Kunz, T., Fraedrich, K., and Lunkeit, F., 2009: Synoptic scale wave breaking and its potential to drive NAO-like circulation dipoles: A simplified GCM approach. *Quarterly Journal of the Royal Meteorological Society*, 135, 1–19.

Lau, N.-C., 1979: The Observed Structure of Tropospheric Stationary Waves and the Local Balances of Vorticity and Heat. *Journal of the Atmospheric Sciences*, 36, 996–1016.

Lejenäs, H. and Økland, H., 1983: Characteristics of northern hemisphere blocking as determined from a long time series of observational data. *Tellus*, 35A, 350–362.

Lindberg, C. and Broccoli, A. J., 1996: Representation of Topography in Spectral Climate Models and Its Effect on Simulated Precipitation. *Journal of Climate*, 9, 2641–2659.

Lohmann, U., Lüönd, F., and Mahrt, F., 2016: An Introduction to Clouds – From the Microscale to Climate, Cambridge University Press, 1st edn.

Lu, J., Greatbatch, R. J., and Peterson, K. A., 2004: Trend in Northern Hemisphere Winter Atmospheric Circulation during the Last Half of the Twentieth Century. *Journal of Climate*, 17, 3745–3760.

Luo, D., 2005: A Barotropic Envelope Rossby Soliton Model for Block-Eddy Interaction. Part I: Effect of Topography. *Journal of the Atmospheric Sciences*, 62, 5–21.

MacVean, M. K., 1983: The effects of horizontal diffusion on baroclinic development in a spectral model. *Quarterly Journal of the Royal Meteorological Society*, 109, 771–783.

Masato, G., Hoskins, B. J., and Woollings, T., 2009: Can the Frequency of Blocking Be Described by a Red Noise Process?. *Journal of the Atmospheric Sciences*, 66, 2143–2149.

Masato, G., Hoskins, B. J., and Woollings, T., 2013: Winter and Summer Northern Hemisphere Blocking in CMIP5 Models. *Journal of Climate*, 26, 7044–7059.

Masato, G., Woollings, T., and Hoskins, B. J., 2014: Structure and impact of atmospheric blocking over the Euro-Atlantic region in present-day and future simulations. *Geophysical Research Letters*, 41, 1051–1058.

Matsueda, M., 2011: Predictability of Euro-Russian blocking in summer of 2010. *Geophysical Research Letters*, 38, L06 801.

Meehl, G. A., Boer, G. J., Covey, C., Latif, M., and Stouffer, R. J., 2000: The Coupled Model Intercomparison Project (CMIP). *Bulletin of the American Meteorological Society*, 81, 313–318.

Morita, J., Takayabu, Y. N., Shige, S., and Kodama, Y., 2006: Analysis of rainfall characteristics of the Madden-Julian oscillation using TRMM satellite data. *Dynamics of Atmospheres and Oceans*, 42, 107–126.

Namias, J., 1947: Characteristics of the general circulation over the Northern Hemisphere during the abnormal winter 1946-47. *Monthly Weather Review*, 75, 145–152.

Pelly, J. L. and Hoskins, B. J., 2003: A New Perspective on Blocking. *Journal of the Atmospheric Sciences*, 60, 743–755.

Philander, S. G., 1990: El Niño, La Niña, and the Southern Oscillation, vol. 46 of *International Geophysics Series*, Academic Press.

Polvani, L. M. and Kushner, P. J., 2002: Tropospheric response to stratospheric perturbations in a relatively simple general circulation model. *Geophysical Research Letters*, 29, 18–1–18–4.

Randall, D. A., 2015: An Introduction to Numerical Modelling of the Atmosphere. Chapter 13: Spectral Methods, URL `http://kiwi.atmos.colostate.edu/group/dave/at604pdf/AT604_LaTeX_Book.pdf`, downloaded on January 25, 2018.

Renwick, J. A. and Wallace, J. M., 1996: Relationships between North Pacific Wintertime Blocking, El Niño, and the PNA Pattern. *Monthly Weather Review*, 124, 2071–2076.

Rex, D. F., 1950a: Blocking Action in the Middle Troposphere and its Effect upon Regional Climate – Part I: An Aerological Study of Blocking Action. *Tellus*, 2, 196–211.

Rex, D. F., 1950b: Blocking Action in the Middle Troposphere and its Effect upon Regional Climate – Part II: The Climatology of Blocking Action. *Tellus*, 2, 275–301.

Rossby, C.-G., 1950: On the dynamics of certain types of blocking waves. *Journal of the Chinese Geophysical Society*, 2, 2–13.

Sardeshmukh, P. D. and Hoskins, B. J., 1988: The Generation of Global Rotational Flow by Steady Idealized Tropical Divergence. *Journal of the Atmospheric Sciences*, 45, 1228–1251.

Scaife, A. A., Woollings, T., Knight, J., Martin, G., and Hinton, T., 2010: Atmospheric Blocking and Mean Biases in Climate Models. *Journal of Climate*, 23, 6143–6152.

Scherrer, S. C., Croci-Maspoli, M., Schwierz, C., and Appenzeller, C., 2006: Two-dimensional indices of atmospheric blocking and their statistical relationship with winter climate patterns in the Euro-Atlantic region. *International Journal of Climatology*, 26, 233–249.

Scinocca, J. F. and Haynes, P. H., 1998: Dynamical Forcing of Stratospheric Planetary Waves by Tropospheric Baroclinic Eddies. *Journal of the Atmospheric Sciences*, 55, 2361–2392.

Shutts, G. J., 1983: The propagation of eddies in diffluent jetstreams: eddy vorticity forcing of 'blocking' flow fields. *Quarterly Journal of the Royal Meteorological Society*, 109, 737–761.

Sillmann, J., Croci-Maspoli, M., Kallache, M., and Katz, R. W., 2011: Extreme Cold Winter Temperatures in Europe under the Influence of North Atlantic Atmospheric Blocking. *Journal of Climate*, 24, 5899–5913.

Stevens, B., Giorgetta, M., Esch, M., Mauritsen, T., Crueger, T., Rast, S., Salzmann, M., Schmidt, H., Bader, J., Block, K., Brokopf, R., Fast, I., Kinne, S., Kornblueh, L., Lohmann, U., Pincus, R., Reichler, T., and Roeckner, E., 2013: Atmospheric component of the MPI-M Earth System Model: ECHAM6. *Journal of Advances in Modeling Earth Systems*, 5, 146–172.

Thompson, D. W. J. and Wallace, J. M., 1998: The Arctic Oscillation signature in the wintertime geopotential height and temperature fields. *Geophysical Research Letters*, 25, 1297–1300.

Tibaldi, S. and Molteni, F., 1990: On the operational predictability of blocking. *Tellus*, 42A, 343–365.

Tibaldi, S. and Molteni, F., 2018: Atmospheric Blocking in Observation and Models. *Oxford Research Encyclopedia of Climate Science*.

Tyrlis, E. and Hoskins, B. J., 2008: The Morphology of Northern Hemisphere Blocking. *Journal of the Atmospheric Sciences*, 65, 1653–1665.

Vautard, R. and Legras, B., 1988: On the Source of Midlatitude Low-Frequency Variability. Part II: Nonlinear Equilibration of Weather Regimes. *Journal of the Atmospheric Sciences*, 45, 2845–2867.

Vial, J. and Osborn, T. J., 2012: Assessment of atmosphere-ocean general circulation model simulations of winter northern hemisphere atmospheric blocking. *Climate Dynamics*, 39, 95–112.

Wallace, J. M. and Gutzler, D. S., 1981: Teleconnections in the Geopotential Height Field during the Northern Hemisphere Winter. *Monthly Weather Review*, 109, 784–812.

Wallace, J. M. and Thompson, D. W. J., 2002: The Pacific Center of Action of the Northern Hemisphere Annular Mode: Real or Artifact?. *Journal of Climate*, 15, 1987–1991.

Wallace, J. M., Zhang, Y., and Bajuk, L., 1996: Interpretation of Interdecadal Trends in Northern Hemisphere Surface Air Temperature. *Journal of Climate*, 9, 249–259.

Weijenborg, C., de Vries, H., and Haarsma, R. J., 2012: On the direction of Rossby wave breaking in blocking. *Climate Dynamics*, 39, 2823–2831.

Wheeler, M. C. and Hendon, H. H., 2004: An All-Season Real-Time Multivariate MJO Index: Development of an Index for Monitoring and Prediction. *Monthly Weather Review*, 132, 1917–1932.

Woollings, T., Hoskins, B., Blackburn, M., and Berrisford, P., 2008: A New Rossby Wave-Breaking Interpretation of the North Atlantic Oscillation. *Journal of the Atmospheric Sciences*, 65, 609–626.

List of figures

List of tables

Acknowledgements

All model experiments described in this work have been conducted with version 17.0 of the Portable University Model of the Atmosphere that is developed by scientists at the University of Hamburg, Germany. The model code is open source and available through the website of the University of Hamburg. I am very grateful to PUMA's developers for freely providing this well-documented and comprehensible atmospheric model. Additionally, I am obliged to the University of Kiel for providing the necessary computing facilities.

Other open source software that has been used for this thesis includes LaTeX, Python, the Anaconda distribution and m_map.

I thank my supervisors Richard Greatbatch and Gereon Gollan for their ideas, their support and helpful comments. Many thanks also to Martin Claus who helped to solve some technical problems with the PUMA model. I am also very grateful to Michael Gloyer for his extensive proofreading.

A. Appendix

Table A.1.: **Variables**

λ	longitude	φ	latitude
μ	$\sin(\varphi)$		
σ	vertical coordinate	w	vertical velocity
u	zonal wind	v	meridional wind
p	pressure	p_*	surface pressure
ζ	absolute vorticity	ξ	relative vorticity
D	divergence	Φ	geopotential
K	hyperdiffusion coefficient	h	hyperdiffusion order
τ_F	Rayleigh friction timescale	τ_R	Newtonian cooling timescale
T	temperature	κ	adiabatic coefficient
T_R	restoration temperature		

Table A.2.: **Abbreviations**

AGCM	Atmospheric General Circulation Model
AO	Arctic Oscillation
CBL	Central Blocking Latitude
CGCM	Coupled General Circulation Model
CMIP	Coupled Model Intercomparison Project
COWL	Cold Ocean-Warm Land pattern
DJF	December, January, February
ECHAM	AGCM of the ECMWF and the Max-Planck Institute for Meteorology in Hamburg
ECMWF	European Centre for Medium Range Weather Forecasts
ENSO	El Niño/Southern Oscillation
ERA-40	Reanalysis dataset of the ECMWF (1957–2002)
ERA-Interim	Reanalysis dataset of the ECMWF (1979–present)
GFS	Global Forecast System (NOAA model)
HadGEM1	Hadley Centre Global Environmental Model version 1
IFS	Integrated Forecast System (ECMWF model)
MJO	Madden-Julian Oscillation
MPI-OM	Ocean model of the Max-Planck Institute for Meteorology in Hamburg
NAM	Northern Annular Mode
NAO	North Atlantic Oscillation
NCAR	National Center for Atmospheric Research
NCEP	National Centers for Environmental Prediction
NOAA	National Oceanic and Atmospheric Administration
OLR	Outgoing Longwave Radiation
PNA	Pacific North American pattern
PUMA	Portable University Model of the Atmosphere
PV	Potential Vorticity
SST	Sea Surface Temperature
UTC	Coordinated Universal Time

Erklärung

Hiermit erkläre ich, dass ich die vorliegende Arbeit selbstständig und ohne fremde Hilfe angefertigt und keine anderen als die angegebenen Quellen und Hilfsmittel verwendet habe. Die eingereichte schriftliche Fassung der Arbeit entspricht der auf dem elektronischen Speichermedium. (Name der Datei: Master-Arbeit-1005538.pdf)

Weiterhin versichere ich, dass diese Arbeit noch nicht als Abschlussarbeit an anderer Stelle vorgelegen hat.

30.04.2018, Swantje Bastin